Mr.sci. Adnan Bosović, dipl.ing.el.

Optimal Placement of Voltage Quality Monitoring Devices

DOCTORAL THESIS

to achieve the university degree of

Doktor der technischen Wissenschaften

submitted to

Graz University of Technology

Supervisor

Ao.Univ.-Prof. Dipl.-Ing. Dr.techn. Herwig Renner

Institute of Electrical Power Systems

Graz, April 2022

AFFIDAVIT

I declare that I have authored this thesis independently, that I have not used other than the declared sources/resources, and that I have explicitly indicated all material which has been quoted either literally or by content from the sources used. The text document uploaded to TUGRAZonline is identical to the present doctoral thesis.

Date

Signature

i) ACKNOWLEDGMENTS

First of all, I want to thank God Almighty, without Whose will and power nothing happens in this Universe, for grating me the opportunity, motivation, time, resources, energy and persistence to finish this PhD thesis.

I would like to especially thank prof. Herwig Renner for his invaluable guidance and all the knowledge and advice he provided. During my many visits from Sarajevo where I live to Graz, Austria, prof. Renner always found as much time as it was needed for our PhD consultation meetings. His professionalism and full devotion during these meetings will be a role model for me during the rest of my career.

I would also like to thank prof. Mustafa Music, my superior and head of the Department of strategic development in JP Elektroprivreda BiH d.d. – Sarajevo, where I work. He has provided a constant and full support for my PhD study, and has always been like a strong gust of wind in my back for all my achievements, both in professional and academic career.

My special thanks go also to prof. Lothar Fickert, who has been a link between me and TU Graz and my mentor prof. Herwig Renner, and without his efforts this PhD study would not be possible. I am grateful for the opportunity to study at a prestigious university as TU Graz.

This PhD thesis would not be possible without the help from Netz OÖ GmbH, who provided network model data as well as the measurement data for networks we analysed. Special thanks go to dr. Andreas Abart and Ewald Traxler, for their efforts in providing the data.

Also, I need to thank the team from TU Dresden, who provided measurement data essential for developing methodology in this research. My thanks go to prof. Jan Meyer and his team members Max Domagk, Friedemann Möller, Sascha Müller and Ana Maria Blanco. I especially thank prof. Jan Meyer for his devotion in commenting in detail the results of our work, which helped us a lot.

Also, I would like to thank DIgSILENT GmbH for providing a thesis license of DIgSILENT PowerFactory software tool.

I would like to heartfully thank my parents for supporting me during my whole life of studying through different schools and faculties. They have always sacrificed themselves so I can achieve.

Thanks also go to my younger sister, who has been a support for my academic career. I wish her lots of success in her academic career.

I would like also to thank to my wife Amela Bambur Bosović for her emotional support, patience and understanding of the sacrifice needed to finish a PhD study program.

At the end, I would like to thank to all other professors and colleagues, who have provided their contributions and comments to the thesis.

ii) ABSTRACT

Power quality (PQ) is being regulated in most of the EU countries and distribution system operators are obliged to supply the electricity according to European norm EN 50160. The information about actual levels of PQ is the first prerequisite for supplying electricity according to the norm. Many distribution system operators are therefore installing PQ monitoring systems in their networks. The problems are that distribution networks have many nodes and the power quality monitors (PQM) are rather expensive. Therefore, the optimisation of number and locations of these measurement devices is needed in order to install the system while minimising cost and maximising effect. Research done so far has mostly optimised the location and number of PQMs only from the aspect of monitoring voltage dips or harmonic voltages. There is therefore much space for research in optimisation from the point of monitoring other PQ parameters. Also, almost all research works optimised the locations from the point of only one PQ parameter, while PQ monitors measure several PQ parameters simultaneously and it is economical only to put them in locations optimal from the standpoint of several PQ parameters.

The focus of this thesis is the problem of optimal placement of voltage quality monitoring devices in medium voltage distribution networks. The focus of this research is on several key PQ parameters chosen from the list of parameters defined in EN 50160 (harmonic voltages, voltage flicker, voltage unbalance and voltage dips). For the chosen parameters, novel modelling methodologies were applied in order to model longer time-series (e.g. week or month) of PQ parameter behaviour in a large real medium voltage distribution network. All the model were performed on a large real medium voltage distribution network from Austria. Real customer, consumption, load profile and network data were used. Models of PQ parameters were validated by measurements. Multivariable regression (MVR) was applied to obtain PQM locations, while the R^2 coefficient of determination was choice criteria, representing variability explained by the regression model. All the calculations were performed using commercial software tools: DIgSILENT PowerFactory, MATLAB and Microsoft Excel. The results have shown that only two PQMs are needed to monitor the analysed network.

This thesis is the first research work to optimize the locations of PQMs from the point of several PQ parameters, using real data to develop the models. The methodology is relatively straightforward and easy to apply, and therefore can be applied to numerous other networks.

iii) ABSTRAKT

Spannungsqualität ist in den meisten EU-Ländern reglementiert und Verteilnetzbetreiber sind verpflichtet die Versorgungsspannung gemäß der europäischen Norm EN 50160 zur Verfügung zu stellen. Die Informationen über die tatsächlichen Werte der Spannungsqualitätsparameter sind die erste Voraussetzung für das Bereitstellen der Versorgungsspannung gemäß der Norm. Viele Verteilnetzbetreiber installieren daher Spannungsqualitäts-Messgeräte in ihren Netzen. Das Problem ist, dass Verteilnetze viele Knoten haben und dass die Messgeräte relativ teuer sind. Daher ist eine Optimierung der Anzahl und der Standorte dieser Messgeräte erforderlich, um ein funktionierendes System zu installieren und gleichzeitig die Kosten zu minimieren und die Effekte zu maximieren. Die bisherigen Forschungen haben den Standort und die Anzahl der Messgeräte meistens nur aus dem Blickwinkel der Überwachung von Spannungseinbrüchen oder Oberwellenspannungen optimiert. Es existiert daher immer noch viel Forschungsbedarf für die Optimierung der Überwachung anderer Spannungsqualitätsparameter. Darüber hinaus haben fast alle bisher durchgeführten Forschungsarbeiten die Standorte der Messgeräte nach nur einem Spannungsqualitätsparameter optimiert, während die Überwachungssysteme immer mehrere Parameter gleichzeitig messen, wobei das Überwachungssystem nur dann wirtschaftlich sein kann, wenn die Standorte der Messgeräte nach mehreren Spannungsqualitätsparametern optimiert im Netz angeordnet werden.

Der Fokus dieser Arbeit ist die Herausforderung der optimalen Platzierung von Spannungsqualitätsparameter-Messgeräten in Mittelspannungsverteilnetzen. Der Fokus dieser Forschungsarbeit liegt auf mehreren wichtigen Spannungsqualitätsparametern, die aus der, in EN 50160 definierten Parameterliste ausgewählt sind (Oberwellenspannungen, Spannungsflicker, Spannungsasymmetrie und Spannungseinbrüche). Für die gewählten Parameter wurden neue Modellierungsmethoden angewendet, um längere Zeitreihen (z. B. Woche oder Monat) des Parameterverhaltens in einem großen realen Mittelspannungsverteilnetz zu modellieren. Das gesamte Modell wurde in einem großen realen Mittelspannungsverteilnetz aus Österreich durchgeführt. Es wurden reale Kunden-, Verbrauchs-, Lastprofil- und Netzdaten verwendet. Die Modelle der Spannungsqualitätsparameter wurden durch Messungen validiert. Um die Standorte der Messgeräte zu erhalten wurde die Multivariable Regression (MVR) angewendet, während der R2-Bestimmungskoeffizient das Wahlkriterium war, was die Variabilität darstellte, die vom Regressionsmodell erklärt wurde. Alle Berechnungen wurden mit kommerziellen Softwaretools durchgeführt: Digsillent PowerFactory, Matlab und Microsoft Excel. Die Ergebnisse haben gezeigt, dass nur zwei Messgeräte erforderlich sind, um das analysierte Mittelspannungsnetz zu überwachen.

Diese Dissertation ist die erste Forschungsarbeit, die Standorte von Messgeräten nach mehreren Spannungsqualitätsparametern optimiert und reale Daten zur Entwicklung der Modelle verwendet.

Die Methodik ist relativ unkompliziert und leicht umsetzbar und kann daher auf zahlreiche andere Netzwerke angewendet werden.

iv) TABLE OF CONTENTS

v) LIST OF ABBREVATIONS

AC	Alternating current
AMR/AMI	Automated Meter Reading / Advanced Metering Infrastructure
APCS	Austrian Power Clearing and Settlement
cdf	Cumulative distribution function
CB	Circuit breaker
CEST	Central European Summer Time
CFL	Compact fluorescent lamp
CP	Covering and Packing
DC	Direct current
DG	Distributed generator
DPL	DIgSILENT Programming Language
DSO	Distribution system operator
EN	European Standard
EU	European Union
EV	Electric vehicle
EVMS	Electric Vehicle Management System
FFT	Fast Fourier Transform
GPS	Global positioning system
GT	Graph Theory
HV	High voltage
HVAC	Heating, ventilation and air conditioning
IEC	International Electrotechnical Commission

IPQMS	Integrated Power Quality Monitoring System
LED	Light-emitting diode
LV	Low voltage
MV	Medium voltage
MVR	Multivariate regression
MRA	Monitor Reach Area
PCC	Point of common coupling
PQ	Power quality
PQM	Power quality monitor
PQMS	Power Quality Monitoring System
PV	Photovoltaic
RMS	Root Mean Square
RVC	Rapid voltage change
SCADA	Supervisory Control and Data Acquisition
THD	Total harmonic distortion
UTC	Coordinated Universal Time
VSD	Variable speed drive

vi) LIST OF SYMBOLS

α_i,	Weighting factor
AIC	Akaike information criterion
B	(*p* x 1) vector of regression coefficients in linear regression
b_0	Intercept in linear regression
b_1	Slope in linear regression
b_j	Partial regression coefficients in linear regression
β_{ij}	Weighting factor
BIC	Bayesian information criterion
c	Factor for calculating short-circuits according to the standard IEC 60909-0
C_j	Cost of each variable
c_f	Flicker emission coefficient
c_i	Current unbalance factor
$c_{i50\%}$	50% quantile of current unbalance factor
$c_{i\ upper\ envelope}$	Upper envelope of 50% quantiles of current unbalance factor
$c_{i\ lower\ envelope}$	Lower envelope of 50% quantile of current unbalance factor
c_u	Voltage unbalance
C_p	Statistical indices
γ_{ij}	Weighting factor
ε	Error in linear regression
E	(*n* x 1) vector for random errors in linear regression
h	Harmonic order
$I_{h\_rectifier}(\%)$	Emission of a three-phase rectifier with DC-link inductance and capacitance

I_1	Positive sequence current
I_2	Negative sequence current
k	Numerator in linear regression
$k_{flicker}$	Flicker transfer factor
k_u	Voltage transfer factor
$k_{unbalance}$	Unbalance transfer factor
MAE	Mean absolute error
$MAPE$	Mean absolute percentage error
MSE	Total mean square error
N	Number of nodes
n	Bus number
n_i	Number of observations
Ni	Number of components at bus i
NM_{min}	Minium number of monitors
NM_{max}	Maximum number of monitors
$Ones$	Matrix with all its elements equal to one
P_{lt}	Long term flicker
P_{max}	Maximum power of the customer
p_{motor} $(\%)$	Percentage of motor electricity use by different industry groups
P_{st}	Short term flicker
$P_{st,i}$	Short term flicker of individual flicker source
$\Delta P_{st\,(ji)}$	Short term flicker increment at bus *j* due to impact from bus *i*
$\Delta P_{st\,(ii)}$	Short term flicker increment at bus *i* due to impact from the same bus *i*
p_{VSD} $(\%)$	Percentage of motors with VSDs
r	Ratio of propagation

R^2	Coefficient of determination in linear regression
$rand(P_{st}\ cdf)$	Random number with a probability distribution according to the data in Fig. 5.3.1.
r_h	Harmonic voltage ratio
r_f	Flicker ratio
r_u	Unbalance voltage ratio
r_{xy}	Correlation coefficient
R_p	Statistical indices
R^2_{min}	Minimum variability explained by the model
R^2_{avg}	Weighted average criterion for choosing the PQM location
R^2_{h5}	Coefficient of determination for 5^{th} harmonic
R^2_{h7}	Coefficient of determination for 7^{th} harmonic
R^2_f	Coefficient of determination for flicker
R^2_u	Coefficient of determination for unbalance
S_i	Apparent power
Ssc	Short-circuit power
Ssc_min	Minimum short-circuit capacity
SSE	Residual sum of square error
THD	Total harmonic distortion
THD_{sel}	Total harmonic distortion calculated for a set of selected harmonics (5^{th} and 7^{th})
Δu	Voltage drop after short-circuit
U_h	Magnitude of the harmonic voltage (order h)
$U_{h,m}$	Magnitude of the various m individual harmonic emission levels (order h)
$Uh_{,PQM}$	Magnitude of harmonic voltage (order h) at the node with the location of PQM
U_n	Nominal line-line voltage

$u_{residual}$	Residual voltage after short-circuit
Δu_{SC}	Voltage drop at the node of the short-circuit
U_1	Positive sequence voltage
U_2	Negative sequence voltage
V_{dip}	Dip matrix that contains the residual voltage of all the buses
w_5	Weighting factor for 5th harmonic
w_7	Weighting factor for 7th harmonic
w_h	Weighting factor for harmonics
w_f	Weighting factor for flicker
w_u	Weighting factor for unbalance
x	Predictor variable in linear regression
x_j	The optimisation variable
X	(n x p) matrix corresponding to k number of independent variables ($p = k + 1$) in linear regression
x_k	Predictor variables in linear regression
y	Response variable in linear regression
y_i	Data points in linear regression
$\overline{y}$	Horizontal sample mean line
$\hat{y}_i$	Estimated sloped regression line
Y	(n x 1) vector for observation variables in linear regression
$\hat{Y}$	Estimated observation variables in linear regression
Z	Impedance matrix
Z_1	Positive sequence impedance
Z_2	Negative sequence impedance
φ_1	Phase angle between the fundamental current and the fundamental voltage

$\varphi_{1\ (sine)}$	Phase angle of fundamental voltage or current in the sine referencing convention
$\varphi_{1\ (cosine)}$	Phase angle of fundamental voltage or current in the cosine referencing convention
$\varphi_{h\ (cosine)}$	Phase angle of harmonic voltage or current (order h) in the cosine referencing convention
$\varphi_{h\ (sine)}$	Phase angle of harmonic voltage or current (order h) in the sine referencing convention
$\varphi_{h\ (model)}$	Harmonic current source phase angle serving as input for the chosen software tool
$\varphi_{h\ (measurement)}$	Harmonic current source phase angle parameterised from measurements

vii) LIST OF PUBLICATIONS FROM THE PHD THESIS

[1] A. Bosovic, H. Renner, A. Abart, E. Traxler, J. Meyer, M. Domagk, M. Music, "Deterministic aggregated harmonic source models for harmonic analysis of large medium voltage distribution networks", IET Generation, Transmission & Distribution, Volume 13, Issue 19, 08 October 2019, p. 4421 – 4430.

[2] A. Bosovic, H. Renner, A. Abart, E. Traxler, J. Meyer, M. Domagk, M. Music, "Modelling the Propagation of Harmonic Voltages in Large Medium Voltage Distribution Networks", 25th International Conference on Electricity Distribution (CIRED 2019), Madrid, Spain, 3-6 June 2019, Paper n° 416

[3] A. Bosovic, H. Renner, A. Abart, E. Traxler, J. Meyer, M. Domagk, M. Music, "Validation of Aggregated Harmonic Current Source Models Based on Different Customer Type Configurations", 2016 Electric Power Quality and Supply Reliability (PQ), August 29-31, 2016, Tallinn, Estonia.

[4] A. Bosovic, H. Renner, A. Abart, E. Traxler, M. Music, "Modelling of flicker in large real medium voltage distribution networks", 26th International Conference on Electricity Distribution (CIRD 2021), Geneva, Switzerland, 21 – 24 June 2021, Paper n° 290.

1 INTRODUCTION

1.1 Motivation

With the process of de-regulation of electricity sector, electricity is being treated as goods, and as any other goods it has to satisfy quality standards. Power quality is regulated in most of the EU countries and the DSOs are obliged to supply the electricity according to voltage quality European norm EN 50160. The information about actual levels of power quality is the first prerequisite for supplying electricity according to the norm. Many DSOs are therefore installing power quality monitoring systems in their networks. The problems are that distribution networks have many nodes and the voltage quality monitoring devices are rather expensive. Therefore, the optimisation of number and locations of these measurement devices is needed in order to install the system, while minimising cost and maximising observability. Research done so far has mostly optimised the location and number of voltage quality monitoring devices only from the aspect of monitoring of one PQ parameter, mostly voltage dips. These algorithms are therefore not a complete solution of the problem, since voltage quality monitors need to be placed while taking into account multiple PQ parameters that they measure. There is therefore much space for research in:

1) Optimisation from the point of monitoring of several PQ parameters individually and not just voltage dips.
2) Optimisation taking simultaneously into account several PQ parameters.

This PhD thesis tackles these two presented challenges.

1.2 Outline of the Thesis

After this first introduction chapter, which gives a motivation for this research, a short outline of the rest of the thesis is given below.

Chapter 2 gives a theoretical background of the necessary topics of this thesis.

Chapter 3 provides a literature review of the state of the art of voltage quality monitoring device placement algorithms, as well as a short outlook on power quality monitoring in the future smart distribution grids.

Chapter 4 gives a research hypothesis, scope and focus of this research.

Chapter 5 presents the methodology of this research, divided in subchapters corresponding to the parts of the calculation (chosen network and software tools, modelling of harmonics, flicker, unbalance, approach to voltage dips, MVR).

Chapter 6 presents the results of the calculation, again with subchapters corresponding to the parts of the analysis (harmonics, flicker, unbalance, voltage dips, MVR), with addition of the sensitivity analysis and discussion of the results.

Chapter 7 brings out the conclusions, answers to research questions and the contributions of this PhD thesis.

Chapter 8 gives suggestions for future work.

2 THEORETICAL BACKGROUND

2.1 Power Quality

The definition of power quality, as stated in the standard IEC 61000-4-30, is:

"*The characteristics of the electricity at a given point on an electrical system, evaluated against a set of reference technical parameters*" [1, p. 10]

Within power quality, limits for voltage quality in public electricity networks are defined in international standards, while the limits for current quality in public electricity networks are not specified. European norm EN 50160 [2], widely used in Europe, defines the values of the reference technical parameters used for evaluating voltage quality in public AC electricity networks under normal operating conditions. Voltage quality parameters defined in EN 50160 [2] are:

- Continuous phenomena
    - Power frequency
    - Supply voltage variations
    - Single rapid voltage change
    - Flicker severity
    - Supply voltage unbalance
    - Harmonic voltage
    - Interharmonic voltages
    - Mains signaling voltages
- Voltage events:
    - Interruptions of the supply voltage
    - Supply voltage dips
    - Supply voltage swells
    - Transient overvoltages

This chapter gives in brief a theoretical background for modelling the voltage quality parameters that are in the focus of this thesis. The focus of the thesis is presented in the subchapter 4.2.

2.1.1 Harmonics

This subchapter 2.1.1 was previously published by the author of this thesis in [3].

Harmonic voltages are PQ parameter defined in the EN 50160 [2]. Harmonics in electricity networks are caused by non-linear loads that inject harmonic currents in the network, which consequently cause harmonic voltage drops on the network impedances. The types of non-linear loads connected to electricity distribution networks are different for different customer categories. Dominant non-linear loads of residential customers are: consumer electronics, modern lighting devices such as CFLs, LEDs, as well as other appliances. The most important non-linear loads of offices are: computers, lighting such as CFLs and LEDs, and HVAC systems. For industry the dominant non-linear loads can vary depending on the type of industry, and they can include: VSDs, industrial electronics, arc furnaces etc. Other customer categories that can be sources of harmonics in electricity distribution networks include PVs, EVs, public lighting, mobile phone base stations etc. [3]. [4]. [5].

For harmonic voltage studies in AC electricity distribution networks, there are two types of harmonic sources: i) background harmonics from higher voltage levels, coming from harmonic emission in other connected networks and ii) harmonic emission of loads connected to the considered network. Background harmonics are usually modelled as background harmonic voltage source, while harmonic emission of loads is usually modelled as harmonic current source [4]- [5]. In large MV distribution networks, modelling of harmonic sources is especially challenging due to the presence of a large number of different harmonic sources in the network having an influence on harmonic voltage distortion. For MV network studies, where whole LV networks are represented as individual loads, an aggregation of the harmonic current emission of the downstream LV networks needs to be done. For analysing harmonic load flow for longer time series (day, week, etc.), a trend of harmonic emission in time is needed. In order to prove the validity of the model, the challenge is always to verify the results of the model with the measurements in the network [3].

2.1.2 Flicker

This subchapter 2.1.2 was previously published by the author of this thesis in [6].

Flicker is the subjective impression of luminescence variations as a result of voltage fluctuations. The origin of voltage fluctuations is generally in customer's installations with fluctuating load [7]. Fluctuating loads draw fluctuating currents from the network, which consequently cause voltage fluctuations over network impedances, hence causing flicker. Typical flicker producing loads at HV level are: electric arc furnaces and switching of reactive power compensation units, at MV level: industrial installations with large induction motors and automatic welding machines, and at LV level: starting of motors, fluctuating load torque of motors, electro heat devices controlled by thermostat [7]. Flicker is one of the voltage quality parameters, with measurement techniques defined in IEC 61000-4-30 [1] and IEC 61000-4-15 [8], and limits for public distribution networks in Europe defined in EN 50160 [2], [6].

In electricity distribution networks, voltage flicker can be generally calculated by taking into account: i) background flicker emission from higher voltage levels, usually represented as background voltage flicker, ii) flicker emission of installations in the analysed network, usually represented as fluctuating current emission. For calculating emission of loads, knowing the values of their flicker emission coefficients is essential. Flicker emission coefficient represents a characteristic emission coefficient, which is used together with statistical distribution of emission, usually corresponding to the 99% quantile P_{st} value. The main challenge in modelling flicker in large real MV distribution networks is the number of different flicker sources in such networks, for which the flicker emission coefficients are mostly not yet available in the published literature [6].

2.1.3 Unbalance

Unbalance is a condition in a three-phase system in which the RMS values of the line voltages (fundamental component), and/or the phase angles between consecutive line voltages, are not all equal [2]. It is expressed as a ratio of negative sequence component divided by positive sequence component [2]. Main cause of unbalance voltages are unbalanced loads. Unbalanced loads draw unbalance currents, which when conducted over network impedances cause unbalance voltages. Typical larger unbalanced loads at HV and MV level are different types of furnaces, railways and welding machines, while single-phase connected customers are typical unbalanced load at LV level. Unbalance is one of the voltage quality parameters, with measurement techniques defined in IEC 61000-4-30 [1], and limits for public distribution networks in Europe defined in EN 50160 [2]. Unbalance due to unbalanced line impedances are out of this thesis' scope.

IN MV electricity distribution networks, voltage unbalance can generally be modelled by taking into account the following: i) background voltage unbalance coming from HV network, ii) current unbalance, coming from all the connected LV networks. For modelling of current unbalance at LV level, unbalance factors of all the different connected customers need to be known. Unbalance factor is essentially the negative sequence of the load current divided by positive sequence of the load current. Major challenge in modelling unbalance in large real MV distribution networks is that unbalance factors for many different customer categories must be used, but there are no results in the published literature on unbalance factors for majority of customer categories.

2.1.4 Voltage Dips

Voltage dip (or sag) is a temporary reduction of the RMS voltage at a point in the network below a specified start threshold [2]. Typical causes of voltage dips are faults occurring in the public networks or in network users' installations [2]. During the fault, high fault currents cause voltage drops over the network impedance and hence cause voltage dips in the networks. Residual voltages are lowest at the source of the fault, and are higher further upstream from the fault location according to the values of three-phase short circuit power of the network. Voltage dips is one of the voltage quality parameters, with measurement techniques defined in IEC 61000-4-30 [1], and classification tables for public distribution networks in Europe defined in EN 50160 [2]. Since voltage dips are by their nature very unpredictable and variable, due to unpredictability and variability of the faults, from node to node and from time to time, there are no limits for voltage dips in EN 50160, and only classification statistics are kept. According to the EN 50160, the voltage dip start threshold is 90 % of the nominal voltage U_n. [2]

Voltage dips are usually modelled by running short-circuit calculations, since short-circuits are the most common causes of voltage dips. After the calculation, residual voltages during the short-circuit are analysed, which represent the depth of the voltage dip in different nodes of the network. Voltage dips can also be modelled using time-domain simulation of the complete event, but for this purpose dynamic behaviour parameters of the grid components need to be taken into account. The approach using short-circuit calculations has been used in this PhD thesis, since it is adequate for the purpose of calculating transfer factors for flicker and unbalance propagation.

2.2 Multivariable Regression (MVR)

Simple linear regression is a statistical method that allows us to summarize and study relationships between two continuous (quantitative) variables [9]:

- One variable, denoted x, is regarded as the predictor, explanatory, or independent variable.
- The other variable, denoted y, is regarded as the response, outcome, or dependent variable.

Simple linear regression model is shown in formula 2.6.1. and also shown graphically in Fig. 2.6.1.

$$y = b_0 + b_1 \cdot x + e \quad (2.6.1.)$$

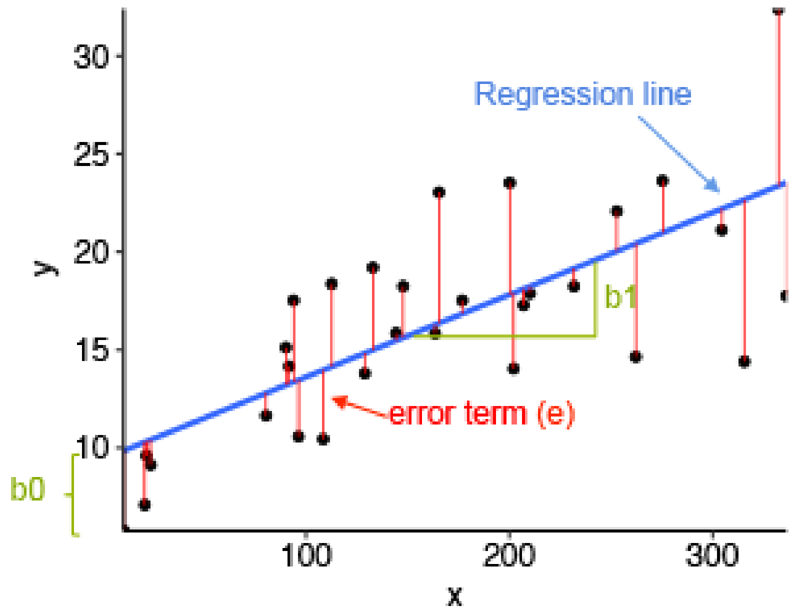

Fig. 2.6.1. *Simple linear regression example*

where b_0 is an intercept, b_1 is a slope and ε is an error.

A simple linear regression is when there is only one independent variable, while multiple regression or sometime multivariable regression is when there are more than one independent variable [10].

A set of partial regression coefficients, b_j such that the dependent variable, y can be approximated by a linear combination of the 'k' independent variables, x is found by multiple regression. A predicted value, denoted by y dependent variable is given by the following equation [10]:

$$y = b_0 + b_1 x_1 + b_2 x_2 + \cdots + b_k x_k + \varepsilon \qquad (2.6.2.)$$

where b_j (j = 0, 1, 2, . . . , k) are unknown parameters of regression coefficients (B) and ε is a random error. Equation (2.6.2.), for 'n' number of observations, can be written in matrix form as [10],

$$Y = XB + \varepsilon \qquad (2.6.3.)$$

in which,

$$Y = \begin{bmatrix} Y_1 \\ Y_2 \\ \cdot \\ Y_n \end{bmatrix}, \quad X = \begin{bmatrix} 1 & x_{11} & x_{12} & \cdot & x_{1k} \\ 1 & x_{21} & x_{22} & \cdot & x_{2k} \\ \cdot & \cdot & \cdot & \cdot & \cdot \\ 1 & x_{n1} & x_{n2} & \cdot & x_{nk} \end{bmatrix}, \quad B = \begin{bmatrix} b_0 \\ b_1 \\ \cdot \\ b_k \end{bmatrix}, \quad E = \begin{bmatrix} \varepsilon_1 \\ \varepsilon_2 \\ \cdot \\ \varepsilon_n \end{bmatrix} \qquad (2.6.4.)$$

where Y is a (n x 1) vector for observation, X is a (n x p) matrix corresponding to k number of independent variable ($p = k + 1$), B is a (p x 1) vector of regression coefficients, and E is a (n x 1) vector for random errors [10].

The best estimation for B is the one which minimizes the sum of the squared errors. Consider the following equation to minimize the vector of least squares estimate [10]

$$L = \sum_{i=1}^{n} \varepsilon_i^2 = E'E = (Y - XB)'(Y - XB) \quad (2.6.5.)$$

expanding (2.6.5.) we get,

$$L = Y'Y - B'X'Y - Y'XB + B'X'XB = Y'Y - 2B'X'Y + B'X'XB \quad (2.6.6.)$$

Now differentiate (2.6.6.) with respect to B and setting to zero, the minimum square estimate has to obey [10]

$$\frac{\partial L}{\partial B} = -2X'Y + 2X'XB = 0 \quad (2.6.7.)$$

where $X'XB=X'Y$ is a function of minimum square normal to the solution that gives the value of minimum square estimate, B which is written as, [10]

$$B = (X'X)^{-1}X'Y \quad (2.6.8.)$$

The estimated regression model is now, [10]

$$\widehat{Y_i} = b_0 + \sum_{j=1}^{k} b_j\, x_{ij} \quad \text{i=1, 2, …, n} \quad (2.6.9.)$$

The difference between the observed (Y_i) and estimated ($\widehat{Y_i}$) variables is given in the following equation representing error. [10]

$$E = Y - \hat{Y} \quad (2.6.10.)$$

In this research, R^2 coefficient of determination is used as the criteria for choosing PQ monitor locations, and therefore this coefficient is introduced below.

Now an example in which the plot illustrates a fairly convincing relationship between y and x is examined, shown in Fig. 2.6.2. The relatively steep slope of the estimated regression line suggests that as the predictor x increases, there is a fairly substantial decrease in the response y [11].

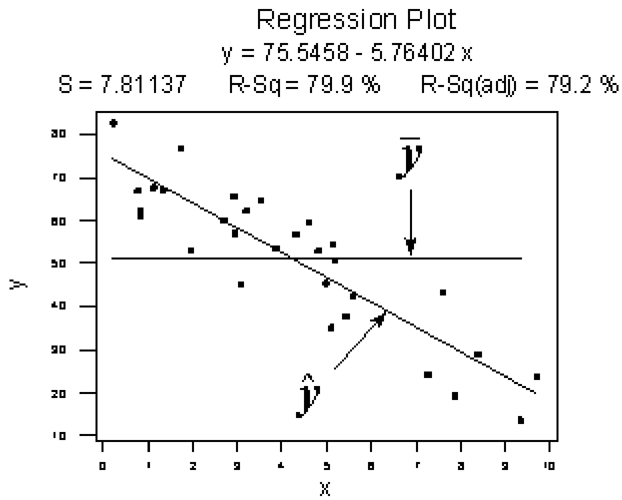

Fig. 2.6.2. *Simple linear regression example for introducing r^2*

$$SSR = \sum_{i=1}^{n} (\hat{y}_i - \overline{y})^2 = 6679.3 \quad (2.6.11.)$$

$$SSE = \sum_{i=1}^{n} (y_i - \hat{y}_i)^2 = 1708.5 \quad (2.6.12.)$$

$$SSTO = \sum_{i=1}^{n} (y_i - \overline{y})^2 = 8487.8 \quad (2.6.13.)$$

The calculations (2.6.11. – 2.6.13.) given below the Fig 2.6.2. show contrasting "sums of squares" values [11]:

- SSR is the "regression sum of squares" and represents how far the estimated sloped regression line, $\hat{y}_i$, is from the horizontal "no relationship line", the sample mean or $\overline{y}$.
- SSE is the "error sum of squares" and represents how much the data points, y_i, vary around the estimated regression line, $\hat{y}_i$,.
- SSTO is the "total sum of squares" and represents how much the data points, y_i, vary around their mean, $\overline{y}$.

The regression sum of squares divided by the total sum of squares is the "coefficient of determination" or "r-squared value", denoted R^2. Alternatively the quantity also equals one minus the ratio of the error sum of squares to the total sum of squares, since SSTO = SSR + SSE [11]:

$$r^2 = \frac{SSR}{SSTO} = 1 - \frac{SSE}{SSTO} \quad (2.6.14.)$$

Here are some basic characteristics of the R^2 [11]:

- Since R^2 is a proportion, it is a number between 0 and 1.
- If $R^2 = 1$, all of the data points fall perfectly on the regression line. The predictor x accounts for *all* of the variation in y!
- If $R^2 = 0$, the estimated regression line is perfectly horizontal. The predictor x accounts for *none* of the variation in y!

The coefficient of determination R^2 is therefore understood and interpreted as the measure of variability explained by the regression model. In this research, it is used to measure relationships between time series of a PQ parameter in different nodes in the network. It establishes a measure of how much variability in one node is explained by the regression model by variability in the other node. Nodes with higher R^2 have more similar behavior, while the nodes with lower R^2 have less similar behavior. The method is applied to different PQ parameters individually.

3 LITERATURE REVIEW

3.1 State of the Art of Modelling Harmonics in Large Real Medium Voltage Distribution Networks

This subchapter 3.1 was previously published by the author of this thesis in [3].

Until now, only a few research papers have tried to verify the results of harmonic models with real measurements in the network. In paper [12], the results of simulations were verified with field measurements, on a relatively small MV feeder and for one moment in time, for each one of several system configurations. Works of [13] and [14] developed load models for real industrial networks and verified them using PQ measurements for one moment in time. Reference [15] verified the results of a probabilistic approach of modelling aggregate harmonic load models with measurements, on an example of a large real 137-bus MV network. In [15] it was shown that the range of results of the measurements for one day fit with the range of results of the probabilistic model (0,5 % - 1,5% value of THD_V), that was influenced by the input parameter uncertainties of the model. It can be summarised that the challenge of achieving the exact match between harmonic load flow results and measurements in large MV distribution networks still needs to be achieved, especially when analysing longer time periods (day, week etc.) [3].

For harmonic load flow studies in MV networks, aggregate harmonic current emission load models need to be developed for LV networks. Therefore, several papers have presented models for an aggregated representation of harmonic current emission in distribution networks. However, as also stated in the literature review in [16], the problem is that the majority of already published works are focused only on specific customer categories or they are based on extensive measurements. In paper [17] a probabilistic approach for developing time-varying harmonic current emission models of the residential customers is presented. In [18], a stochastic model of harmonic emission of aggregate residential customers is developed, using a measurement-based approach. Paper [19] proposed a bottom-up probabilistic harmonic emission technique for residential customers and feeders. Paper [20] proposes a prediction tool to identify both the stochastic and the time varying behavior of harmonics on the secondary of a distribution transformer feeding an institutional building. In [21] a deterministic component-based technique for development of aggregate load models of a residential sector, that can be used for harmonic load flow and that are also applicable to other sectors, is proposed. Paper [22] presents a piecewise probabilistic harmonic model of aggregate residential loads. In [22] results of the model are verified on a fictional MV residential distribution grid, but only with comparison to other simulation models and without the comparison with the measurements. Only research [16] presents a comprehensive methodology for developing aggregate harmonic load models for different customer categories, using a stochastic (probabilistic) approach and field measurements. It can be summarised that there is still a need in the literature for a simple, especially deterministic, methodology for aggregate harmonic current source modelling for all major customer categories, that can easily be applied for MV network harmonic studies [3].

For the harmonic source modelling, there are two commonly used methods: i) modelling according to the IEC 61000-3-6 summation law and ii) modelling using complex phasors. There are no papers known to the authors, that implemented these two methods of harmonic source modelling on an example of a large real MV distribution network, compared the results of simulations, and gave recommendations about which method is more suitable for large real MV distribution networks [3].

3.2 State of the Art of Modelling Flicker in Large Real Medium Voltage Distribution Networks

This subchapter 3.2 was previously published by the author of this thesis in [6].

Until now, data on flicker emission coefficients has been published only for several distinct categories of installations. Reference [7] reports flicker emission coefficient of uncompensated arc furnaces in the range 48 - 85, with a mean value of 60. Reference [23] reports values in the range 40 - 80 for the same customer category. Paper [24] reports flicker emission coefficient of PV plants to be in the range 1.31 - 5.09 for network impedance angles from 30° - 85°. In work [25] flicker emission coefficient in the range 3.1 – 4.2 is reported for wind turbines for different average wind speeds and for different network impedance angle in the range of 30° - 85°. Work [26] reports flicker emission coefficients of 6 and 13 for switching operation of different wind power plant technologies. Paper [27] reports the maximum flicker emission coefficient of 8 for tidal wave power plant. These works report flicker emission coefficient for calculating Pst99% - short term flicker severity with a 99% probability of not being exceeded over the measurement period. Work [28] modelled flicker in large real MV distribution network for the purpose of optimal PQ monitor placement, but using fictitious currents and without using real measurements to develop a model [6].

Generally, according to the best knowledge of the authors, there is a lack of published literature on modelling of flicker in large real distribution networks. When developing such a model, it is crucial to validate the model with the power quality (PQ) measurements [6].

3.3 State of the Art of Modelling Unbalance in Large Real Medium Voltage Distribution Networks

Knowing unbalance factors of different customer categories is essential for modelling unbalance in large real MV distribution networks. For some of the customer categories, there are published results of the measurement or different unbalance load models. Paper [29] presents a probabilistic model of household loads for unbalance studies, developed and verified using measurements. In work [30] load model of electric vehicles chargers for load flow and unbalance studies was presented.

Paper [31] analysed the propagation of voltage unbalance in radial distribution networks, and a radial example of MV test distribution network was used for the analysis. Work [28] modelled unbalance in real large MV distribution network for a purpose of optimal PQ monitor placement, but using fictitious currents and without using real measurement data to develop a model. According to the knowledge of the author of this thesis, there is no published research that developed a model for unbalance study on a large real MV distribution network, based on real measurements to develop a model, and therefore this is a research gap.

3.4 State of the Art of Modelling Voltage Dips in Electricity Networks

Paper [32] analysed a case study where voltage sags indices are estimated using Monte Carlo approach combined with short-circuit calculation program and ATP (Alternative Transient Program). The correlation between both programs is evaluated using voltage sag magnitude and frequency. The results indicate that similar voltage sag indices are obtained using time-domain simulation and short-circuit calculation. Therefore, based on the high correlation between the results, short-circuit calculation programs are preferable over the time-domain simulation tools as the modelling for time-domain simulation rarely covers the whole network, it is more complex and time consuming [32]. In paper [33], two methods to calculate voltage sags are validated against actual measurements. One of the methods is an electromagnetic transient program resulting in voltage waveform in relation to time. The other is a short-circuit calculation program resulting directly in sag magnitude during the fault. The simulations agreed well with the measurements for the study case. However, the choice of the right values for the fault characteristics is still a great challenge when running simulations. Depending on the kind of study, the choice of an electromagnetic transient program or a short-circuit calculation program is made. The short-circuit program is recommended for stochastic calculation of the system performance, because of faster computation algorithm and simpler equipment modeling. In contrast to that, for the detailed study of individual events, the ATP is advisable [33]. To conclude, for this PhD thesis, short-circuit method of calculating residual voltages following voltage dips was used as a simpler and more adequate method, needed for calculating transfer factors for flicker and unbalance propagation.

3.5 State of the Art of Power Quality Monitoring Placement Algorithms

Optimal placement of PQ monitors has been an active research area so far. However, majority of papers presented algorithms for PQ monitor placement but only from the aspect of one the following PQ parameters: voltage dips or harmonic voltages. Detailed review of main methods for PQ monitor placement to monitor voltage dips and harmonic voltages is presented below, as well as an only work to include several PQ parameters at the same time. At the end, research gaps in this field are recognised.

3.5.1 Methods for Optimal Placement of Voltage Dips Monitors

Monitor Reach Area (MRA) Method

"In [35] a method based on the Monitor Reach Area (MRA) concept is presented, which is based the area of the network that can be observed from a given PQ monitor location. If a fault is inside the MRA the event will trigger the sag meter, while for the faults outside the MRA the event will not trigger the sag meter [36]. To establish and to formulate the optimisation problem that is solved using the branch and bound search, the MRAs of all possible locations are determined [37]- [38]. The dip voltage of any given bus per unit can be obtained by knowing the bus impedance matrix Z:

$$V_{dip} = Ones - Z * Inv(Diag(Z)) \quad (3.5.1.)$$

where V_{dip} is the dip matrix that contains the residual voltage of all the buses, *Diag.(Z)* is the diagonal matrix of *Z*, and *Ones* is a matrix with all its elements equal to one.

According to (3.5.1.) and to the definition of MRA, *MRAp* can be obtained as:

$$MRA_p = MRA_{ij} \begin{Bmatrix} 1 \rightarrow if v_{ij} \leq p \\ 0 \rightarrow if v_{ij} \geq p \end{Bmatrix} \quad (3.5.2.)$$

where all the MRAs use a binary matrix in which "1" in (i , j) indicates that node j belongs to the MRA of a meter located at bus i with a voltage threshold p. In addition in [35], to find the optimal placement of PQMs in transmission systems, the concept of monitor observability is used. Because its formulation is based on a limited number of fault positions and is applied to a single type of fault, the proposed approach cannot assure complete observability. Moreover, it is not suitable for radial distribution networks [34], [39].

There were several research works that improved the MRA method. Work [39] introduces an improved optimal monitoring algorithm that finds the optimal locations of PQ meters using a genetic algorithm approach. Moreover, [40] presents a new algorithm for the optimal placement of PQ monitors based on genetic algorithm and combined with fuzzy logic. Comparing this technique with the original MRA, the fuzzy boundary concept allows better arrangement of PQ monitors and improves the observation index, as presented in [40]. In [41], an approach obtained from the solution to analytical expressions was presented for the optimal location of voltage sag monitors. Complete observability of the power system for any type of fault (balanced or unbalanced) can be ensured. Another algorithm was presented in [42] based on the concept of the MRA and the sag severity index for the placement of PQMs. To solve the optimisation problem, this paper used GA. Moreover, the authors developed an algorithm to solve the optimal PQM placement in both transmission and distribution systems, based on particle swarm optimisation (PSO)[43]. In [44], a technique was presented based on the MRA and the fault location observability analysis (FLOA). Two issues were solved: determining the monitor placement sequence of optimal monitoring programmers and of evaluating the effectiveness of sub-optimal monitoring programs [44]. In [45], the MRA was used to determine the optimisation problem, which was solved using the PSO algorithm [34].

Covering and Packing (CP) Method

In [46] the Covering and Packing (CP) method is presented to determine the optimum position and number of PQMs. The approach is to minimize the cost of PQ monitors when formulated as a CP problem using the ILP technique [47]. The objective function is defined as [34]:

$$f(x) = C_1x_1 + C_2x_2 + \cdots + C_nx_n \quad (3.5.3.)$$

$$f(x) = \sum_{j=1}^{n} C_jx_j \quad (3.5.4.)$$

where x is the optimisation variable, C is the cost of each variable, and n is the bus number.

The observability of the state variables (i.e., voltages and currents) is ensured by using the constraints of this objective function. The observability of a system is dependent on its state equations. These equations are written based on Kirchof's voltage and the current law. The use of Kirchhoff's current law and Ohm's law to obtain the whole picture of the system's connectivity to evaluate the observability of monitors in the system is one of the limitations of the CP method. Moreover, based on steady state information rather than on actual voltage sag information the constraints of the optimisation problem formulation in the CP method are defined. In [48], a new algorithm based on the CP method was presented . The method in [46] was only tested on a system with one voltage level. The method from [48] improved the CP method for multi-voltage level power systems [34].

Graph Theory (GT) Method

In [49] a new algorithm to monitor the voltage sag in a power system based on the Graph Theory (GT) is presented. A simple graph represented the power system network and then it is converted into the corresponding incidence matrix to obtain a network matrix. Hence, the methodology is suitable for showing the relationship between the real nodes in power networks and the elements [50]. Moreover, the concepts of rooted tree [51], up/down area [52], [53], [54], coverage matrix [52], and weighting factors [55] are used to optimise the number and locations of PQ monitors. The optimisation routine for finding the optimal number and location of the PQ monitors can be formulated. Equations 3.5.5. and 3.5.6. give the objective function and its constraints [34]:

$$\min F(x) = min\left[\sum_{i=1}^{n}\left\{\alpha_i \sum_{j=1}^{N_i}\left(\beta_{ij}\gamma_{ij}x_{ij}\right)\right\}\right] \quad (3.5.5.)$$

$$\text{subject to } NM_{min} \leq \sum_{i=1}^{n} N_i - \sum_{i=1}^{n}\sum_{j=1}^{m} x_{ij} < NM_{max} + 1 \quad (3.5.6.)$$

where α_i, β_{ij}, γ_{ij} are the weighting factors, i is the bus number, j is the component number, n is the total number of buses, N_i is the number of components at bus i, min NM_{min} and NM_{max} are the minimum and maximum numbers of monitors, respectively, and x_{ij} is "0" (if c_{ij} is monitored) or "1" (if component c_{ij} is not monitored). The results show that the method is suitable only for radial power networks, and with the number of buses in the network the number of PQMs increases [34].

Multivariable Regression (MVR) Method

In [56], a new method based on the MVR model was presented. For the placement of PQ monitors, Cp and Rp statistical indices were used [57]. First, all data are collected on single phase to ground (LG), double phase to ground (LLG), and triple phase to ground (LLL) faults in each bus. Then, the correlation coefficient (CC) is calculated, and the CC shows the relationship among buses during system disturbances. Next, the two buses with the highest CC values are identified, and these buses are considered as the more sensitive buses in the system. The identified bus voltages are then considered as independent variables to estimate the other bus voltages, in the developed MVR model [34], [58].

$$B = (X'X)^{-1}X'Y \quad (3.5.7.)$$

$$\widehat{Y_i} = b_0 + \sum_{j=1}^{k} b_j\, x_{ij} \quad \text{i=1, 2, …, n} \quad (3.5.8.)$$

$$E = Y - \hat{Y} \quad (3.5.9.)$$

where B, X, Y, E, $\hat{Y}$ are the regression coefficient, independent variable, dependent variable, error, and the estimated voltages, respectively.

Finally, two or three buses are selected, which have maximum and minimum frequencies of the CC. Afterwards, using the sum of square error of the estimator and the mean square error, the *Cp* and *Rp* statistical indices are calculated. The optimal number and locations of PQMs are then determined based on the suitable value of the *Rp* and on the lowest value of the *Cp* [59], [60]. The *Cp* statistic and the *Rp* are given by [34]:

$$C_p = \frac{SSE(p)}{MSE(p)} - n + 2p \quad (3.5.10.)$$

$$R_p = 1 - \frac{SSE(p)}{SSTO(p)} \quad (3.5.11.)$$

where *SSE* is the residual sum of square error, *MSE* is the total mean square error, *SSTO* is the total sum of square, *n* is the number of observations, and *p* is the number of variables. The IEEE 6, IEEE 9, and IEEE 30 bus test systems are used as the transmission network, and the 69 bus test system is used as the radial distribution network, are used to validate the proposed placement of the PQM method [34].

3.5.2 Methods for Harmonic Monitor Placement

K-means clustering method

The study [61] presents a new method for placement of power quality measurement instruments. The disturbances that are taken into consideration are power harmonics and capacitor switching transients. The first step of the proposed method is to utilise harmonic voltages and wavelet coefficients as PQ features. Then, the authors propose an enhanced genetic algorithm for solving the modified K-means clustering to obtain locations of PQ measurement instruments. This work finds clusters, based on K-means clustering algorithm, by minimising the distance (error) of the groups towards the centre of the cluster. An 18-bus system was used to test the simulation results [61].

Evolutionary Algorithms approach

In the paper [62], a methodology based on Evolutionary Algorithms (EAs) is described, that defines the configuration required for a monitoring system, aimed to monitor in a power network voltage and current state variables. Apart from the sites where the meters should be installed, the methodology defines also how the connection of their transducers (PTs and CTs) should be performed. Three different rules based on Kirchhoff's laws are used to verify the monitoring system's observability. To solve the optimisation problem, a branch-and-bound algorithm and a modified Genetic Algorithm (GA) are used. To reduce the cost of the whole monitoring system is the objective. Why the intelligent searching methods are required for solving the optimisation problem is also shown. To assess the methodology's performance, three different networks were used: IEEE 14-bus system, IEEE 30-bus system and a real power distribution feeder. [62]

Genetic Algorithm-Based approach

In the paper [63], authors propose a method, based on genetic algorithm (GA), to find optimal locations of monitors for static estimation of harmonic sources in a power system. In this work it has been observed, based on the case studies undertaken in this work, that the GA-based optimal monitor location strategy always yields the same solution as obtained from the complete enumeration (CE) technique [63].

Minimum Condition Number of the Measurement Matrix approach

The paper [64] focuses on a new technique for optimal measurement placement for power system harmonic state estimation (HSE). The solution provides the optimal number of measurements and the best positions to place them, in order to identify the locations and magnitudes of harmonic sources. The minimum condition number of the measurement matrix is used as the criteria in conjunction with sequential elimination to solve this problem. Two different test systems are provided to validate the measurement placement algorithm. A three-phase asymmetric power system has been tested using the New Zealand test system, while the IEEE 14-bus test system has been used for testing a balanced power system.

3.5.3 Methods for Multiple PQ Parameter Monitor Placement

According to the knowledge of the author, the only research that developed a method for optimal PQ monitor placement, taking into consideration several PQ parameters, is the work [28]. In [28], optimal PQ monitor placement method for harmonic voltages is presented, while the authors developed an analogous method also for flicker and voltage dips. The authors of [28] used fictitious currents to model time-course data of different PQ parameters. Also, the method is based on correlation and regression coefficients for choosing the PQ monitor locations. The correlation coefficient is defined as:

$$r_{xy} = \frac{\sum_{i=1}^{n}(x_i - \bar{x})(y_i - \bar{y})}{\sqrt{\sum_{i=1}^{n}(x_i - \bar{x})^2 \sum_{i=1}^{n}(y_i - \bar{y})^2}} \quad (3.5.12.)$$

while the regression coefficient b_1 is taken from linear regression model:

$$y = b_0 + b_1 \cdot x + e \quad (2.6.1.)$$

In research [28] $r_{xy}>0{,}8$ has been taken as a measure of good correlation and $0{,}8<b_1<1{,}2$ has been taken as a measure of good coherence. The correlation and regression has been calculated for all the combination of busses in the network, and if both criteria are met (using logical AND operation) the value in the MRA matrix is set to 1, otherwise the value is set to 0. After graphical post processing, clusters of busses with similar behavior are obtained, which serve as a basis for choosing PQM locations.

3.5.4 Recognised Research Gaps

After the literature review, it has been recognised that there is a lack of published literature for PQ monitor placement algorithms except for voltage dips and harmonics. Most importantly, except the work of authors [28], there are no works that take into account several PQ parameters simultaneously for choosing PQ monitor locations. This is an essential lack of the published methods, since PQ instruments monitor a large number of PQ parameters at the same time and it is absolutely uneconomical to install several instrument configurations for different PQ parameters. Chosen PQ monitor locations need to be optimal for several PQ parameters simultaneously. Also, for modelling the PQ parameter time series, that serve as an input for PQ monitor placement algorithm, real data (customer data, energy usage, load profiles, PQ measurements etc.) and not fictitious data need to be used to obtain realistic results. These are some of the challenges tackled by this PhD thesis.

3.6 Overview of Measurement Devices and Systems for Power Quality Monitoring in Smart Distribution Grids

This subchapter 3.6 was previously published by the author of this thesis in [67].

3.6.1 State of PQ Measurement in EU Countries

In EU countries the implementation of power quality norm EN 50160 is being enforced by the regulators. The information about the state of power quality in distribution networks, gained by power quality measurements, is the first precondition for management and correction of power quality in the network. Many DSOs are therefore installing power quality monitoring systems based on fixed power quality monitors. Fixed power quality monitors are however relatively expensive and it is not feasible to install them in all the points interesting from the point of power quality. Many researchers are investigating the possibilities of utilizing power quality data from other measurement devices being installed in distribution networks [65], [66], [67], [68]. The report [68] gives an overview of the PQ parameters monitored by smart meters in different countries across the EU.

3.6.2 Integrated Power Quality Monitoring System

The idea and the architecture of the IPQMS – Integrated Power Quality Monitoring System is originally presented in [65]. This system integrates power quality data from all the devices and systems available in the smart distribution grid [65], [66], [67]:

- PQMS – Power Quality Monitoring System
- AMR/AMI – Automated Meter Reading / Advanced Metering Infrastructure
- SCADA - Supervisory Control and Data Acquisition
- EVMS - Electric Vehicle Management System
- Other systems and devices

The main idea is to utilize all the devices and systems that can be used for power quality monitoring as sources of data for the IPQMS. Thus, the measurements from a relatively smaller number of power quality monitors are supplemented. The principal architecture of the IPQMS in the context of the smart distribution grid is presented in Fig. 3.2.1. From Fig. 3.2.1. it can be noticed that the integration of data is performed at the system level via communication between the individual systems (PQMS, AMR/AMI, SCADA, EVMS, etc.) and the IPQMS. This means that the IPQMS utilizes the existing architecture of the PQMS, AMR/AMI, SCADA, EVMS, etc. (data concentrators, communication infrastructure, servers, software etc.) for the collection of power quality data. In order for the comparison of data from different systems to be possible, all the devices need to be synchronized in real time. The process bus in Fig. 3.2.1. represents the future anticipated implementation of the IEC 61850 standard for the communication at the substation level between the devices designed for different purposes [65], [66], [67].

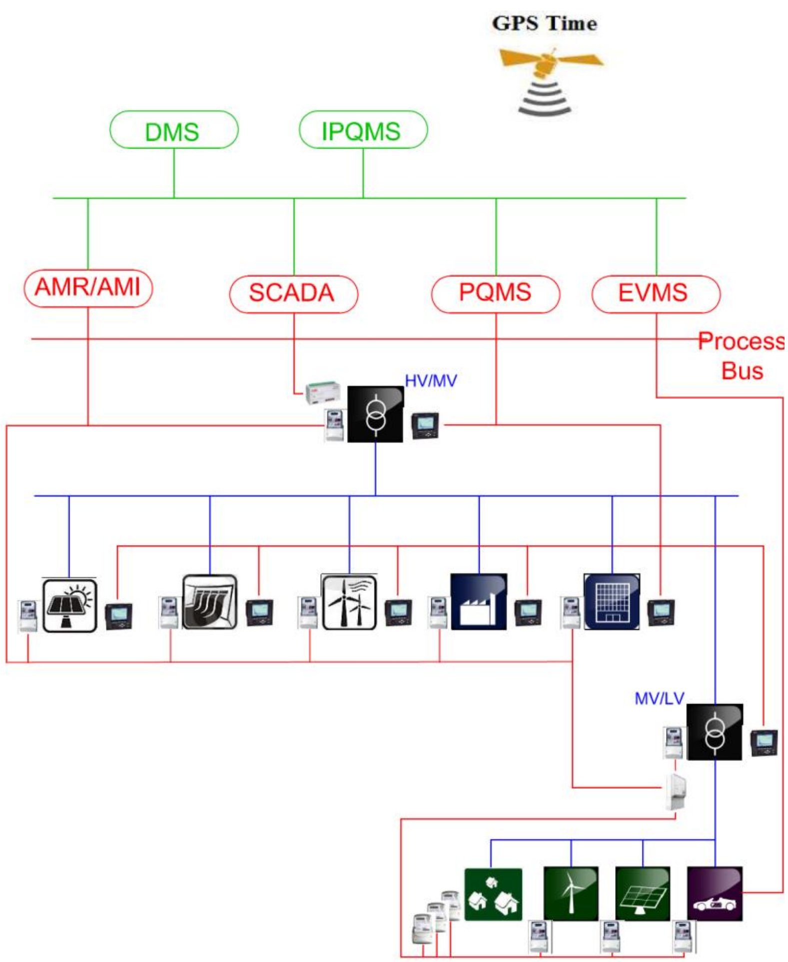

Fig. 3.2.1. *Principal architecture of the IPQMS system in smart distribution grid*

The main source of data for the IPQMS is the PQMS, i.e. power quality monitors on which the PQMS is based on. According to the IEC 61000-4-30 standard, class A instruments should be used in cases of judicial matters or when the power quality is assessed according to power quality standards. The installation of power quality monitors of class A is thus recommended in the following nodes in the distribution grids: nodes in which the electricity transfer from the transmission grid and the neighboring distribution systems is made, nodes of connection of distributed generators, bigger consumers which have a significant effect on power quality and consumers sensitive to power quality disturbances etc. The installation of class S power quality monitors is recommended for other nodes in the distribution network. The number and the locations of installation of power quality monitors should to be selected by optimisation algorithms [65], [66], [67].

Monitoring of power quality by smart meters is of great significance to the IPQMS. The main reason for this is the planned installation of smart meters in all the nodes of customer's/producer's connection as well as in the nodes of electricity transfer between different systems. This enables the monitoring of power quality in all the nodes in the grid in which compliance to power quality standards is necessary. State-of-the-art smart meters, depending on the producer and the model, can monitor following power quality parameters: voltage variation, frequency, voltage interruptions, voltage undervoltages/overvoltages, voltage and current harmonics and THD. With every new generation, smart meters are getting closer to the demands of IEC 61000-4-30 standard. Smart meters are however not primarily designed for power quality monitoring. It should not be expected that they can provide the functionalities and accuracy of power quality monitors. There is surely no need for the smart meters to ever become class A devices, since this would increase the price of these devices significantly. Nevertheless, they can be utilized as very useful indicators of possible power quality disturbances in the grid [65], [66], [67].

By integrating power quality data from different devices, the propagation of specific disturbances from the source of the disturbance throughout the distribution grid can be monitored. After one of the devices in the IPQMS registers a power quality disturbance, the IPQMS gives an instruction for the collection of data about that disturbance from all the devices in the affected area. The disturbance can be in the form of an event (voltage interruption, sag, swell, and transient) or in the form of noncompliance of one of the continuous power quality parameters according to the standard (frequency, voltage variation, flicker, RVC, unbalance, harmonics, interharmonics, signaling voltage, etc.) [65], [66], [67].

3.6.3 Overview of Parameters Measured by Different Measurement Devices in Smart Distribution Grids

Dedicated power quality monitors can register all the power quality parameters specified in power quality standards. Measurement methods, aggregation intervals and measurement uncertainty are all defined in IEC 61000-4-30 standard. Measurements from these instruments can be therefore treated as reference [65], [66], [67].

Smart meters, SCADA and PMUs can register only some of the power quality parameters. They are not primarily designed for power quality monitoring and therefore they do not comply with the requirements of IEC 61000-4-30 standard. They can however serve as good indicators of possible power quality problems [65], [66], [67].

Table 3.2.1. *List of parameters measured by different measurement devices* [68], [69], [70], [71], [72], [73]

Parameter	Power quality monitors	Smart meters	SCADA	PMU
Parameters defined in EN 50160				
Supply voltage variations	✓	*	✓	✓
Interruptions of the voltage supply	✓	✓	✓	✓
Power frequency	✓	*	✓	✓
Harmonic voltage	✓	*	X	✓
Supply voltage unbalance	✓	*	X	***
Supply voltage dips/swells	✓	**	X	***
Voltage flicker	✓	X	X	***
Mains signaling voltages	✓	X	X	***
Transient overvoltages	*	X	X	✓
Rapid voltage changes (RVC)	*	X	X	***
Interharmonic voltage	*	X	X	***
Measurement of other parameters				
Current variation	✓	*	✓	✓
Current harmonics	✓	*	X	✓
Current unbalance	✓	*	X	***
Power factor	✓	✓	✓	✓
Power	✓	✓	✓	✓
Energy	✓	✓	X	***
Interruption waveforms	✓	X	✓	✓

* Some devices can measure this parameter, depending on the producer and the model

** Some smart meters can register voltage dips/swells, but of minimum duration of 200 ms or similar - for this reason it is correct to note that smart meters can measure undervoltages/overvoltages rather than dips/swells.

*** PMUs do not register this parameter directly, but it can be derived from voltage and current waveforms with additional post-processing

4 RESEARCH HYPOTHESIS, SCOPE, FOCUS AND RESEARCH QUESTIONS

4.1 Research Hypothesis

The research hypothesis is that it is possible to develop an algorithm that would calculate optimal placement of voltage quality monitoring devices in MV distribution networks, taking into account several of the most important PQ parameters simultaneously, and by using real network models and measurements to develop the models.

4.2 Scope and Focus of Research

The scope of this PhD thesis is the problem of optimal placement of voltage quality monitoring devices in MV distribution networks.

Six possible purposes of PQ monitoring have been recognized by CIGRE/CIRED JWG C4.112 [74]:

1) Compliance verification
2) Performance analysis
3) Site characterisation
4) Troubleshooting
5) Advanced application and studies
6) Active PQ management.

Optimal placement of PQ monitors in this PhD thesis is going to be analysed from the *performance analysis* purpose aspect.

The focus of this research is on the key PQ parameters chosen from the list of parameters defined in the EN 50160:

- Harmonic voltage
- Voltage flicker
- Supply voltage unbalance
- Supply voltage dips/swells

The following parameters are already being monitored by other devices in distribution networks (smart meters and SCADA):

- Supply voltage variations
- Interruptions of the voltage supply

The following parameters are not in the focus of this thesis, either because the limits for these parameters are not clearly defined in EN 50160 or because they are of low importance:

- Interharmonic voltage (limits not clearly defined)
- Transients overvoltages (limits not clearly defined)
- Rapid voltage changes (limits not clearly defined)
- Mains signaling voltage (low importance)
- Power frequency (system parameter, no need to monitor it in distribution networks)

Power quality disturbances are modelled on a real MV distribution network model, using commercial software tools.

The results of the model are verified (where possible) with real PQ measurement results from the voltage quality monitoring devices installed in the network of an Austrian DSO.

Another point which was not in the focus of the thesis was the robustness of the result against topology changes of the grid.

4.3 Research Questions

This PhD thesis will try to answer the following research questions:

1. Is it possible to develop a model for the harmonic load flow in a large real MV distribution network, and to verify the model with the measurements for a longer time period (e.g. one week)?
2. Which method is more suitable for the harmonic studies in large real MV networks:
    a. Modelling according to the IEC 61000-3-6 summation law or
    b. Modelling using complex phasors
3. Is it possible to model flicker in a large real MV distribution network, and to verify the model with the measurements for a longer time period (e.g. one month)?
4. Is it possible to model unbalance in a large real MV distribution network, and to verify the model with the measurements for a longer time period (e.g. one month)?
5. What is the best way to consider voltage dips in the optimal PQ monitor placement algorithm if the MV network has no or low number of circuit breakers in the MV feeders, except the circuit breakers in the feeding HV/MV transformer substation?
6. Which optimisation algorithm or statistical technique is the most appropriate for the problem of optimal placement of voltage quality monitoring devices in distribution networks?

7. Is it possible to develop a model for voltage quality monitoring devices optimal placement that is verified with PQ measurements?
8. Is it possible to optimise the number and location of voltage quality monitoring devices for different most important PQ parameters individually?
9. Is it possible to optimise the number and location of voltage quality monitoring devices for several most important PQ parameters simultaneously?
10. How to develop an optimisation algorithm that is robust enough to take into account:
    - Possible connection of new customers/producers on the network
    - Possible communication failure with some of the voltage quality monitoring devices
    - Existing devices that can measure some of the power quality parameters
    - Accuracy of measurement of voltage quality monitoring devices
    - Different configuration of distribution network as a result of reconfiguration after voltage interruption

5 METHODOLOGY

5.1 Methodology structure

General structure of the methodology used in this PhD research is given in Fig. 5.1.1. All the PQ parameters that are in the focus of this research (subchapter 4.2) are taken into consideration in the presented methodology. Harmonics, flicker and unbalance are modelled, while the voltage dips are taken into consideration via a simple methodology. Results of the models for harmonics, flicker and unbalance serve as an input data for MVR algorithm. Afterwards, the optimal placement of PQ monitors is calculated using choice criteria. Structure of the subchapters in this PhD thesis follows this general structure of the methodology.

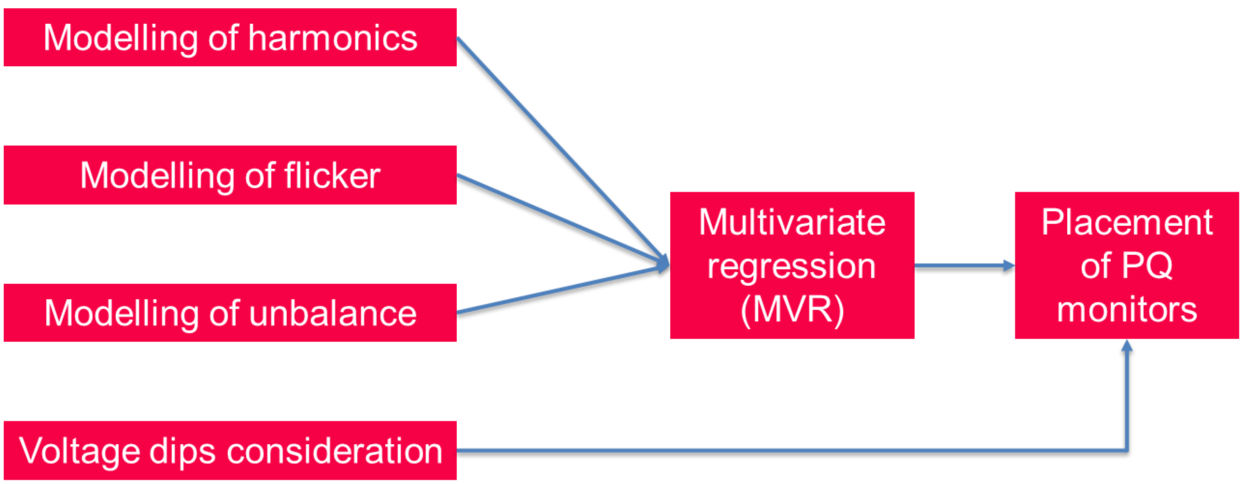

Fig. 5.1.1. *General structure of the methodology used in this research*

5.2 Application to a Real Network

5.2.1 Chosen MV Network

This subchapter 5.2.1 was previously published by the author of this thesis in [3].

In this research, a real MV network of a DSO in Upper Austria, was analysed. This MV network is supplied from one 110/30 kV transformer substation with two 110/30 kV transformers for two 110 kV lines, with one switched on in normal operation. The analysed MV network has a nominal voltage of 29.2 kV. In the analysed year, this MV network supplied a total of 153 individual 30/0.4 kV distribution transformer substations and 12,347 customers by seven feeders [3], [4], [5].

The chosen network is an example of a medium-sized MV distribution rural network, whose largest portion of load belongs to residential customers and not the industry. Table 5.2.1. presents the customer structure in the analysed network, according to the Austrian balance group coordinator (APCS) customer categories.

Table 5.2.1. *Yearly customer consumption structure in the analysed network, according to the Austrian balance group coordinator (APCS) customer categories*

Customer category	Percentage of total load
H0 Household	35.60%
Not assigned (industry)	21.01%
G0-G6 Enterprises	14.94%
TPP own consumption	11.66%
L0-L2 Agriculture	9.54%
ULA-ULF Switched supply (heaters, boilers etc.)	4.59%
B1 Public lighting	0.30%
E1 Photovoltaic	-2.25%
E0 Power plant	-0.08%

Fig. 5.2.1 presents the structure of this network by geographical diagram with feeder coloring. Table 5.2.2. gives the length of overhead and cable lines, as well as the number and installed power of 30/0.4 kV distribution transformer substations, for all the feeders in the network [3], [4], [5].

Table 5.2.2. *Network data by MV feeders*

Feeder no.	Overhead lines (km)	Cables (km)	Number of 30/0.4 kV transformer substations	Installed power of transformers (MW)
Feeder 1	52.8	14.7	42	11.7
Feeder 2	37.3	3.1	35	7.5
Feeder 3	13.1	3.1	19	5.0
Feeder 4	26.2	9.8	34	9.6
Feeder 5	22.8	3.1	21	10.0
Feeder 6	0	0	Thermal power plant own consumption	
Feeder 7	0	0	Reserve	

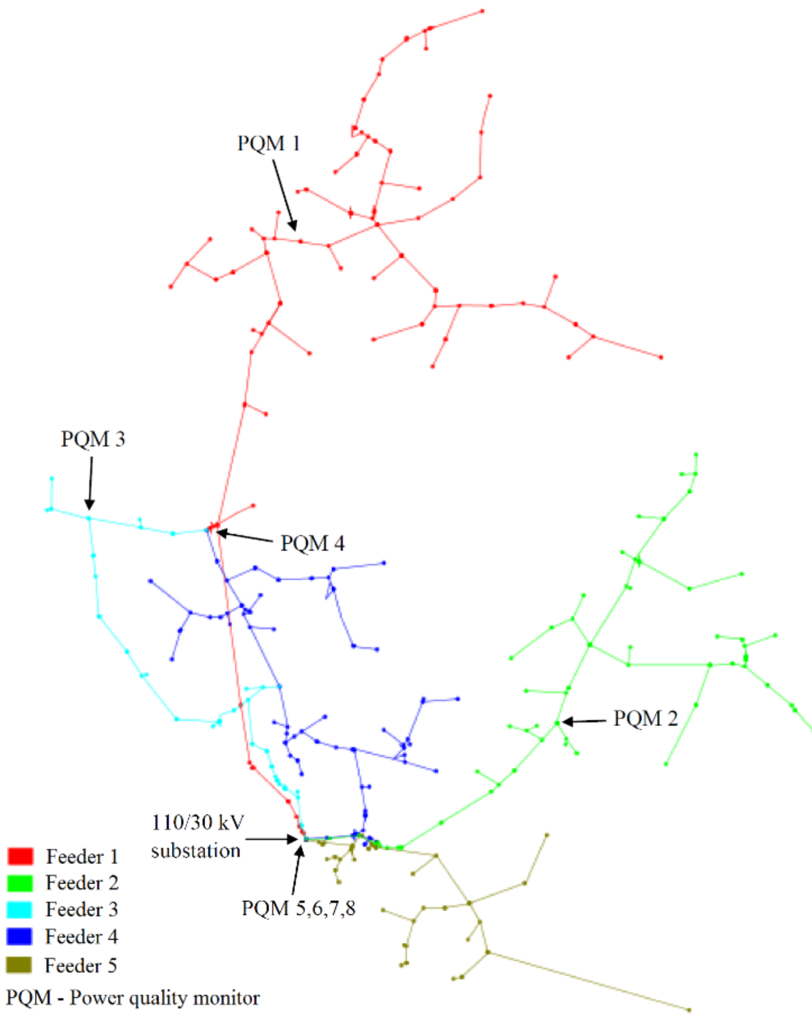

Fig. 5.2.1. *Geographical diagram of analysed MV network with feeder colouring and locations of PQMs*

In order to present the results more clearly, in this PhD thesis, a modified geographical diagram of analysed MV network has been used further in the text. The goal was to show the feeders clearly, without the intersecting of some of the feeder sections. The modified geographical diagram is shown in Fig. 5.2.2.

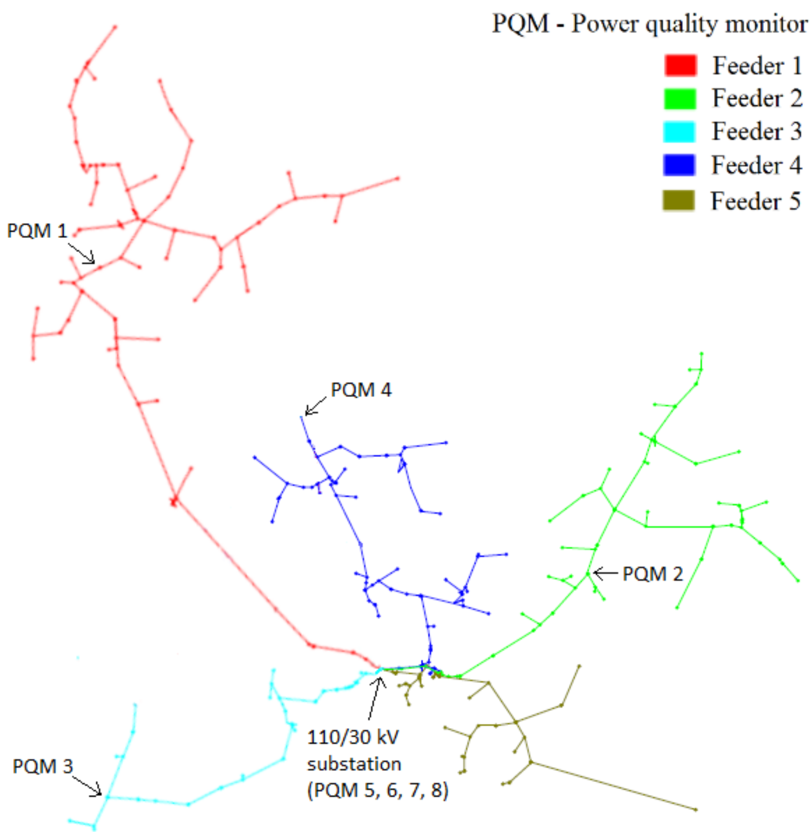

Fig. 5.2.2. *Modified geographical diagram of analysed MV network with feeder colouring and locations of PQMs*

Network model included external HV grid element, HV/MV transformers, all the MV lines and MV busbars, all the MV/LV transformers, all the LV busbars of MV/LV transformers, and customers modelled as groups at the LV busbars of the MV/LV transformers.

Typical weeks and months were chosen for the models of harmonics, flicker and unbalance. The selection took into account the level of the PQ parameter and factors, that might influence the individual parameters leading to non representative results. For harmonic modelling, first week of June was chosen for the analysis. For modelling of flicker a month of January was chosen, while for modelling of unbalance a month of February was chosen. Base year for all the analysis was 2014.

5.2.2 Data Needed to Develop the Models

In order to develop the models, the following data is needed from a local DSO:

- Network model in a chosen software tool

- Yearly customer consumption data
- Information on customer category and transformer station area that the customers belong to
- Yearly load profiles of (preferably the largest) customers measured by smart meters (if available)
- Characteristic synthetic load profiles applicable for that area (e.g. APCS - Austrian Power Clearing and Settlement GmbH synthetic load profiles)
- SCADA measurements for the analysed network
- PQ measurement at HV busbars of the feeding HV/MV transformer substation for the analysed period (essential for modelling the background harmonics, flicker and unbalance)
- Background voltage phase angle measurements at the feeding HV/MV substation of the analysed network (only if modelling of harmonics using complex phasors is performed)
- Optional PQ measurement data for the analysed MV network (from PQ monitoring system or from portable PQ monitors) for verification of the model

Additional data needed to develop the models, that can be used from measurements in other similar networks or from the literature:

1. Harmonic current emission of characteristic customer categories (residential, small commercial, industry, agriculture etc.)
2. Phase angles of the fundamental and the harmonic currents injected by characteristic customer categories (only if modelling of harmonics using complex phasors is performed)
3. Flicker emission coefficients for the major customer categories and the largest industrial customers (estimated or measured)
4. Unbalance factors for the major customer categories

5.2.3 Characteristics of the Used PQ Monitoring System

This subchapter 5.2.3 was previously published by the author of this thesis in [3].

The PQ monitoring system, installed in the investigated MV network, is based on PQ monitoring instruments, which measure all the voltage quality parameters defined in the EN 50160 [2]. The instruments comply with class A according to the IEC 61000-4-30 [1]. They measure harmonics up to the order of the 50^{th} harmonic, based on the method defined in the IEC 61000-4-7 [75, 18]. The instruments are installed at primary 110/30 kV and some 30/0.4 kV transformer substations. All instruments are equipped with time synchronisation by GPS receiver, and the data is archived in a PQ database [3], [4], [5].

The analysed MV network has six PQ monitors installed at the 30 kV voltage level and two PQ monitors at the 110 kV voltage level. The list of all the PQ monitors with the voltage levels they measure is given in Table 5.2.3., while the geographical locations of the PQ monitors are given in Fig. 5.2.2. in section 5.2.1. From Fig. 5.2.2. it can be seen that the PQ monitors are installed in the primary 110/30 kV substation as well as in four out of five 30 kV feeders [3], [4], [5].

Table 5.2.3. *List of PQMs in analysed MV distribution network*

No.	Location	Voltage level
PQM 1	Feeder 1	30 kV
PQM 2	Feeder 2	30 kV
PQM 3	Feeder 3	30 kV
PQM 4	Feeder 4	30 kV
PQM 5	110/30 kV substation – Transformer 1	30 kV
PQM 6	110/30 kV substation – Transformer 2	30 kV
PQM 7	110/30 kV substation – 110 kV line 1	110 kV
PQM 8	110/30 kV substation – 110 kV line 2	110 kV

The measurement results were used to develop the models for harmonics, flicker and unbalance. Also, the PQ monitoring system was used to compare and validate the results of the model with the measurements at 30 kV nodes [3].

5.2.4 Chosen Software Tools

This PhD research has been performed using three software tools:

1. DIgSILENT PowerFactory
2. MATLAB
3. Microsoft Excel

DIgSILENT PowerFactory

DIgSILENT PowerFactory is one of the leading software programs for modelling, analysis and simulation of electricity networks. It has been used in this PhD research to:

1. Model the analysed MV network
2. Perform calculations of harmonic load flow for one whole week with 15-minute intervals, using DPL scripts
3. Perform three-phase short circuit calculations for all the nodes in the network

MATLAB

MATLAB is a programming and numeric computing platform used to analyze data, develop algorithms, and create models. In this PhD research it has been used to:

1. Develop and run the MVR algorithm for optimal PQ placement
2. Develop and run the algorithm for calculation of flicker emission and propagation
3. Develop and run the algorithm for calculation of unbalance emission and propagation
4. Run the fft calculation to extract harmonic phase angles from waveform measurements
5. Processing of input measurement data
6. Visualisation of the results
7. Various smaller mathematical calculations needed for this PhD thesis

Microsoft Excel

Microsoft Excel is the leading spreadsheet software program, a powerful data visualisation and analysis tool. It has been used in this PhD research to:

1. Calculate synthetic yearly load profile of the analysed network
2. Calculate synthetic monthly and weekly load profiles for all the LV customer groups in every secondary transformer station area
3. Prepare input matrices for DPL code of DIgSILENT PowerFactory
4. Prepare data for MATLAB flicker and unbalance models
5. Visualisation of the results
6. Various smaller mathematical calculations needed for this PhD thesis

5.3 Modelling of Harmonics

5.3.1 This subchapter 5.3 was previously published by the author of this thesis in [3].Overview of the Modelling Methodology

The list of major steps of the proposed deterministic methodology for harmonic analysis of large real MV distribution networks is given below, while the individual steps of the methodology are presented in the following subchapters.

1. Prepare a distribution network harmonic model, by updating the distribution network load flow model with frequency dependencies of network component impedances.
2. Obtain measurement results of the background harmonic voltage distortion from HV network for a representative time interval.
3. Develop aggregate harmonic current source models for LV customers:
    a. Calculate synthetic load profiles of aggregated LV customer groups in every MV/LV transformer substation, using data on customer structure and consumption, as well as real measurements (SCADA, AMI etc.) if available

   b. Obtain percentile values of the harmonic current emission of major customer categories, using measurements or the available literature.
   c. Calculate harmonic current emission of all the aggregated customer groups in every MV/LV transformer substation, by multiplying the synthetic load profiles with the percentile harmonic current emission.
4. Build a harmonic load flow model in the chosen software tool, using all the previously mentioned data.
5. Program a code in the chosen software tool for automated harmonic load flow calculations for longer time periods. Prepare all the input data matrices needed for the calculation of longer time periods.
6. Run the program and export the results.

In Fig. 5.3.1. the steps of the methodology are shown graphically, with the numeration of the steps corresponding between the figure and the list above [3].

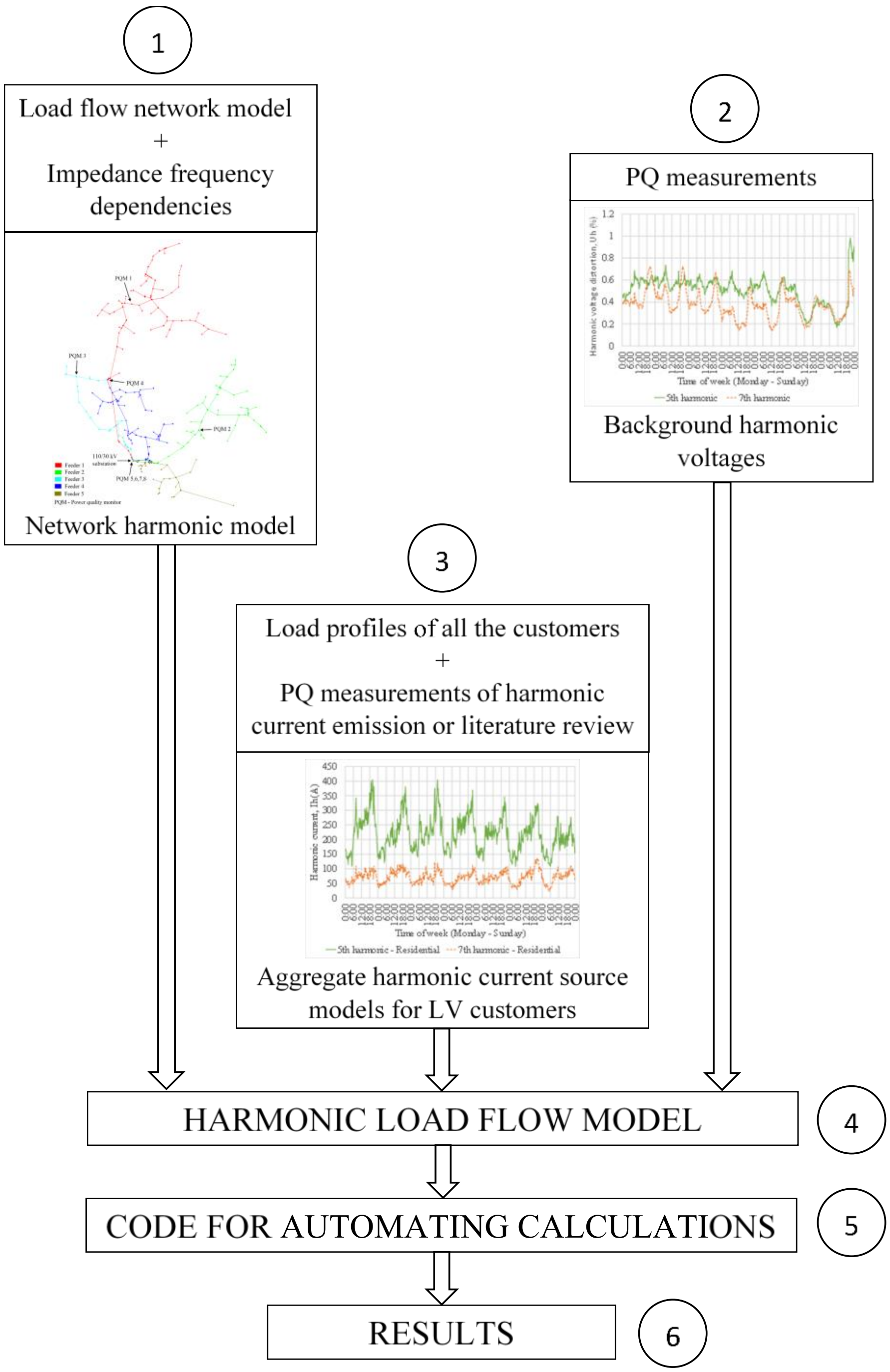

Fig. 5.3.1. *Deterministic methodology for harmonic analysis in large real MV distribution networks*

5.3.2 Network Model for Harmonic Analysis

Network model for the harmonic analysis was developed based on the load flow model, provided by the DSO. All the network impedances needed to be also defined with frequency dependencies of their R and L due to skin and proximity effect for different harmonic orders. The frequency dependencies of the impedances of all the specific network components (transformers, cables and overhead lines), installed in this network, were not known. Therefore, the frequency dependencies of impedances for typical network components in distribution networks were used and modelled. The frequency dependencies of resistances and inductances of transmission 110/30 kV and distribution 30/0.4 kV transformers were modelled based on the characteristics of 108/10.5 kV, 40 MVA and 20/0.4 kV, 250 kVA transformers respectively. These characteristics were available in the chosen software tool and are derived from [76]. Cables and lines are modelled with their Pi-equivalent, taking into account capacitances. The frequency dependencies of resistances and inductances of cables were modelled based on the characteristics of 95 mm^2 and 240 mm^2 cables from [77]. Frequency dependencies of resistances of overhead lines were modelled based on characteristics of 50 mm^2 line from [77], while the frequency dependencies of inductances were taken from [76], available in the chosen software tool [3], [4].

Results of the harmonic load flow in a real distribution network depend on the transformer vector groups, due to the phase angle shift of harmonic voltages and currents. Therefore, it is important to have correct transformer vector groups in the model, and in this network model the 110/30 kV transformer is Yy6 and the 30/0.4 kV transformers are Dy5, Dyn5, Yz5 or Yzn5 vector groups [3].

5.3.3 Harmonic Source Modelling Method

Background harmonics, originating from other grids, were modelled as harmonic voltage sources in the external grid element. The harmonic current emission of LV loads was modelled using harmonic current source objects. Aggregate harmonic source models, for different customer categories in every transformer station 30/0.4 kV, were modelled as harmonic current source objects. These harmonic current sources were modelled without the harmonic impedance of LV loads. Thermal loads (hot water tanks and night storage heating) were modelled as resistive impedances. Since the resonances are not expected to happen at the analysed harmonic frequencies (5^{th} and 7^{th}), the resonances were not an issue considered in this model [3], [78].

In this research a balanced harmonic load flow model was developed, and for this purpose all the loads, DGs production, as well as all the harmonic sources were modelled as balanced. This research focuses on the analysis of the 5^{th} and 7^{th} harmonics [3], [4], [5].

The effect of changeable harmonic current emission due to variations in voltage distortion was not considered in the models in this research. Harmonic current emission of aggregate harmonic sources was measured with a certain level of background harmonic voltage distortion present in the network at that time, and it was taken as such in the models in this research [3].

This research used two methods for modelling harmonic sources [3], [79]:

1. Modelling of harmonic sources according to the IEC 61000-3-6 summation law
2. Modelling of harmonic sources using complex phasors

In the first method (IEC 61000-3-6 method), the harmonic sources were defined according to the IEC 61000-3-6. The basic characteristic of this method is that only harmonic magnitudes are modelled and the summation of harmonic voltages due to different phase angles of different harmonic sources is done according to the IEC 61000-3-6 general summation law [80], with the equation given below [3], [4], [5]:

$$U_h = \sqrt[\alpha]{\sum_{m=0}^{N} U_{h,m}^{\alpha}} \quad (5.3.1.)$$

where:

α - exponent as given in Table 5.3.1. [80].

Table 5.3.1. *Summation exponents for harmonics according to harmonic order, taken from the IEC 61000-3-6* [80]

Harmonic order	α exponent value
h < 5	1
5 ≤ h ≤ 10	1.4
h > 10	2

In the second method (complex phasor method) both harmonic magnitudes and phase angles of all the harmonic sources were modelled. The summation of harmonic voltages due to the impact of different harmonic sources is done in the complex plane, since both magnitude and phase angle values are provided [3].

5.3.4 Analysed Harmonic Orders

In this research the 5^{th} and 7^{th} harmonic orders were analysed, as the dominant harmonic orders with highest harmonic voltages in the analysed MV network. For these harmonic orders, the measurement error of voltage measurement transformers was analysed, and according to the findings of [81] it was concluded that the measurements of analysed harmonic voltages are reliable. The average values of the three phases measured by the PQ monitors are calculated, since a balanced network model is used in this research [3].

Higher harmonic orders were not modelled because of lack of available data to model the LV loads. The method for higher harmonics is basically the same as for the 5^{th} and 7^{th} harmonic. However, uncertainties increase with increasing frequency. Also, the accuracy of measurement transformers is an issue, since they have their first resonance points in the region above the 10^{th} harmonic [3], [81].

In Fig. 5.3.2. the voltage THD graph for the chosen week shows the comparison of voltage THD calculated for all the harmonics until 50^{th} and THD_{sel} calculated for a set of selected harmonics (5^{th} and 7^{th}). Average values for the chosen week are THD = 0.81% and THD_{sel} = 0.64%. We can conclude that the chosen harmonics constitute the predominant share in THD and therefore it is a reasonable approach to focus the analysis on these harmonics [3], [4].

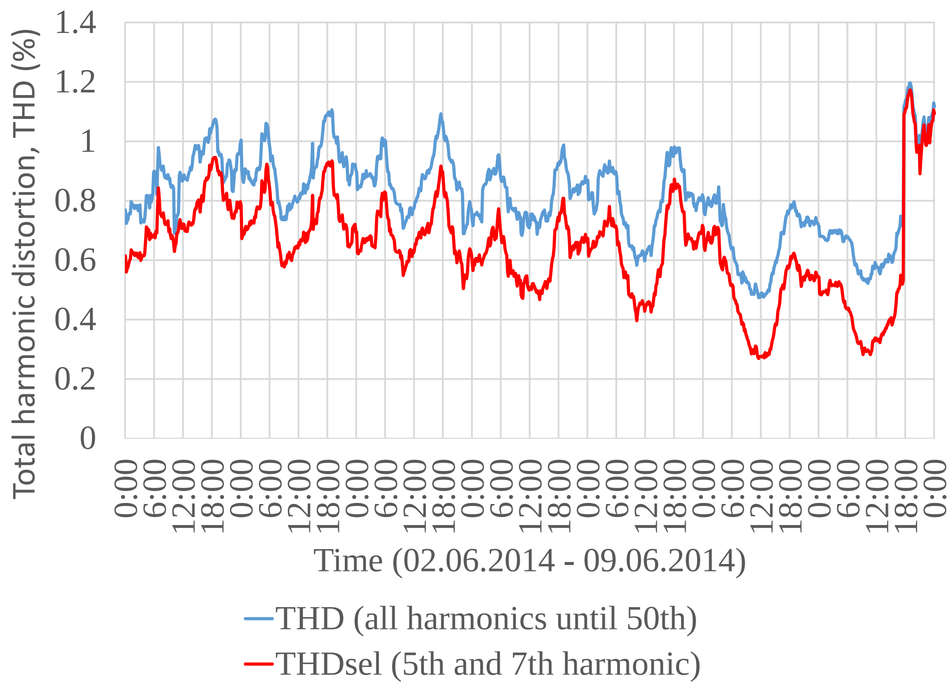

Fig. 5.3.2. *Background total harmonic voltage distortion (THD for all harmonics until 50^{th} and THD_{sel} calculated for only 5^{th} and 7^{th} harmonic)*

5.3.5 Model of Background Harmonic Voltage Distortion

Background harmonic voltage distortion from 110 kV network was parameterised in this research using an existing PQ monitoring system, installed in the analysed MV network [3].

Background harmonic voltage magnitudes were parameterised using harmonic voltage measurement results from PQM 7 and PQM 8, which are installed at 110 kV lines supplying the 110/30 kV substation [4]- [5]. The network was supplied from one of the 110 kV lines, which supplies the network during a normal operating state, for the large majority of the analysed week until 20:00h on Sunday. The weekly trends of the two background harmonic voltage magnitudes used (5^{th} and 7^{th}) are shown in Fig. 5.3.3. [3].

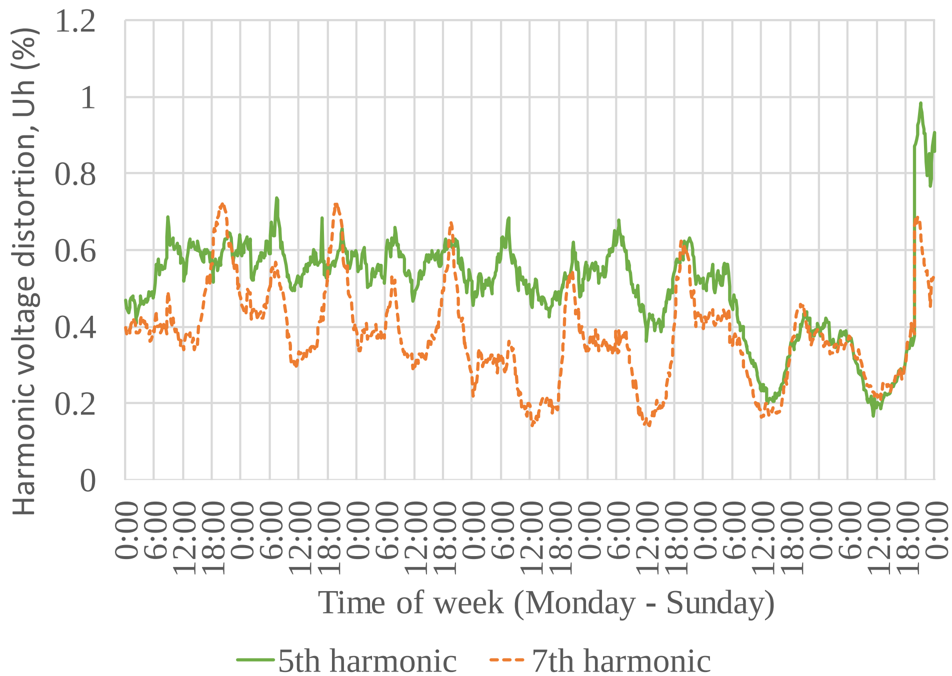

Fig. 5.3.3. *5^{th} and 7^{th} harmonic background voltage distortion magnitudes*

Background harmonic voltage phase angles were in this research parameterised with additional measurements, since the existing PQ monitoring system does not measure harmonic phase angles. A mobile power quality recorder of class A according to the IEC 61000-4-30 was used for this purpose [1]. Measurements of voltage waveforms were recorded at the 110 kV line which supplies this network in a normal operation state. These voltage waveforms were later processed with fast Fourier transform in MATLAB to extract the harmonic voltage phase angles. The measurements were made around 2,5 years after the week analysed in this research. However, it is logical to assume that the structure of the main harmonic sources in the network presumably stayed the same during this period, and therefore the values of background harmonic voltage phase angles should have retained a similar value range. The polar scatter plots of the 5^{th} and 7^{th} harmonic voltage magnitudes and phase angles are shown in Fig. 5.3.4. [3], [5].

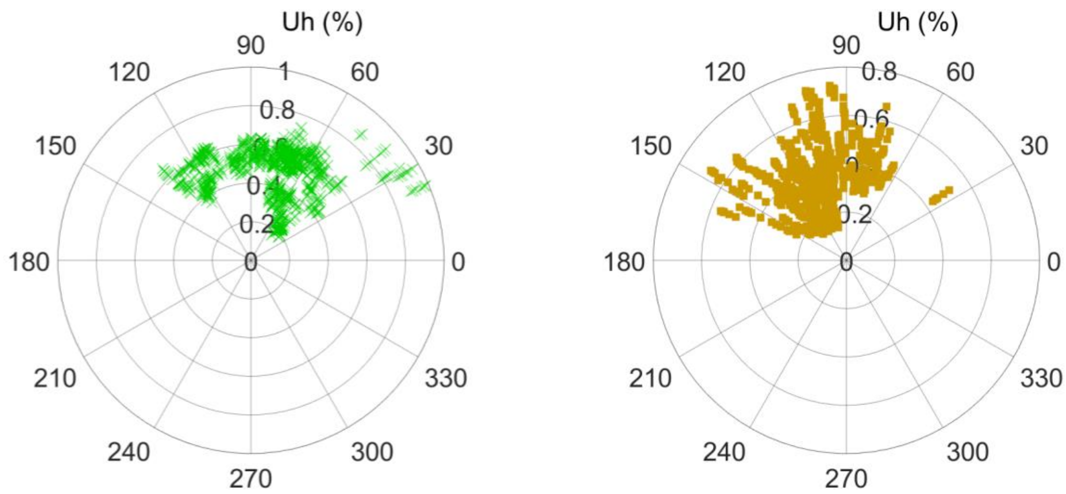

a b

Fig. 5.3.4. *Polar scatter plots of harmonic background voltage distortion*
(a) *5th harmonic,* ***(b)*** *7th harmonic*

5.3.6 Aggregate Harmonic Current Source Models for LV Customers

5.3.6.1 Synthetic Load Profiles

The structure of the customers in the network can be observed from Table 5.3.2. Table 5.3.2. gives the shares of energy consumption/production of different customer categories in the total amount of energy in the network, for the analysed first week of June. From Table 5.3.2., it can be seen that the highest consumption is in the household category, then industry, different small commercial customers, agriculture, etc. Table 5.3.2. also shows which harmonic source models assigned to which customer categories in this research. More detailed information on parameterisation of harmonic source models of residential, small commercial, industrial and agricultural customers is given in subsections 5.3.6.2 and 5.3.6.3. All customers from the categories of night storage heating and hot water tanks are modelled without harmonic emission. Also, the harmonic emission of photovoltaics, thermal power plant own consumption, public lighting and mobile phone base stations is neglected, due to their negligible share in total energy consumption in the network [3], [5].

Table 5.3.2. *Customer categories in the network, with their share in weekly energy consumption and assigned aggregate harmonic source models*

Customer category	Customer category code	Percentage of total weekly energy	Aggregate harmonic source model
Household	H0	40.27%	Residential
Industry	Not assigned	28.05%	Industries
Small commercial customers	G0-G6	17.29%	Offices
Agriculture	L0-L2	11.08%	Agriculture
Night storage heating and hot water tanks	ULA-ULF, U1-U2	4.02%	No harmonic emission
Thermal power plant own consumption	Not assigned	1.34%	Neglected
Public lighting, mobile phone base stations	B1, G7	0.96%	Neglected
Photovoltaics	E1	-2.90%	Neglected
Other distributed generation	E0	-0.11%	No harmonic emission
Total		100.00%	

Weekly load profiles were needed as a necessary part of the methodology of the harmonic emission modelling of customers in the chosen software tool. Therefore, based on measured load profiles of larger customers, yearly energy of all other customers and official Austrian balance group coordinator (APCS) synthetic load profiles for different customer categories [82], several synthetic load profiles were calculated for every 30/0.4 kV distribution transformer substation. The number of these several synthetic load profiles in every 30/0.4 kV distribution transformer substation corresponds to a number of aggregate harmonic source models that are present in that LV network [3].

The resulting total synthetic load profile for the whole MV distribution network did not perfectly fit the real measured SCADA load profile, measured at the feeding 110/30 kV transformer substation. The main reason for the discrepancy between the model and the measurements is that the synthetic load profile used cannot encompass all the changes in load that do happen and that were measured by SCADA: The mean absolute error (MAE) between the synthetic and the measured load profile was 1.24 MW. For comparison, the total load in the network, measured by SCADA, was in the range of 3.2 - 7.7 MW for most of the week. The synthetic load profiles were scaled accordingly to fit the total SCADA load profile, reduced also to take into account the losses in the MV network of 3% [3].

5.3.6.2 Models of Residential and Small Commercial Customers

In this research, harmonic current source models of two major customer categories (household and small commercial) were parameterised using measurements of total harmonic current emissions of different LV networks, dominated by characteristic customer configurations (residential or office). For this purpose, four different measurements of the respective LV grids were used [3], [4], [5]:

- Residential area with 336 households in multi-family houses
- Office area with 26 offices
- 1 office building
- 4 office buildings with 1 canteen

The measurements at these four sites were carried out using PQ measurement devices of class A according to the IEC 61000-4-30 [1]. The measurement accuracy of the devices results in measurement errors of less than 10%/5° for the magnitudes/angles of the harmonic currents for the analysed harmonics. Based on the measurements, the average harmonic current values of the three phases were calculated and used, since a balanced harmonic load flow was used in this research [3].

Based on these measurements, the magnitudes of the harmonic currents were used to calculate the percentages of the fundamental current in 10-minute steps for one whole week, which represented the inputs for the model in the chosen software tool. Therefore, the input for the chosen software tool were load profiles and harmonic currents as percentages of the fundamental current, both in 10-minute steps for one whole week.

Multiplying the individual load profiles for different customer groups, representing the fundamental current, with individual relative harmonic current profiles for different customer groups finally results in individual time series of harmonic currents. This step is performed in the software tool automatically for all the aggregated customer groups in every MV/LV transformer substation. Other software tools might ask for different approaches for this step.

Also, since the total harmonic current emissions of the whole LV networks are taken into account, the cancelation due to phase angle difference between different individual LV harmonic current sources in the same LV network is taken into account properly. Therefore, large LV networks (336 households or multiple offices and office buildings) are used as samples to build a model, to take into account harmonic cancellation effects adequately even in a simple model [3], [18].

The weekly trends of the total arithmetic sum of the 5th and 7th harmonic current magnitudes, injected by all residential customers from all the connected LV networks, are shown in Fig. 5.3.5. From Fig. 5.3.5., the characteristic trends and evening peaks of residential customers can be noticed [3].

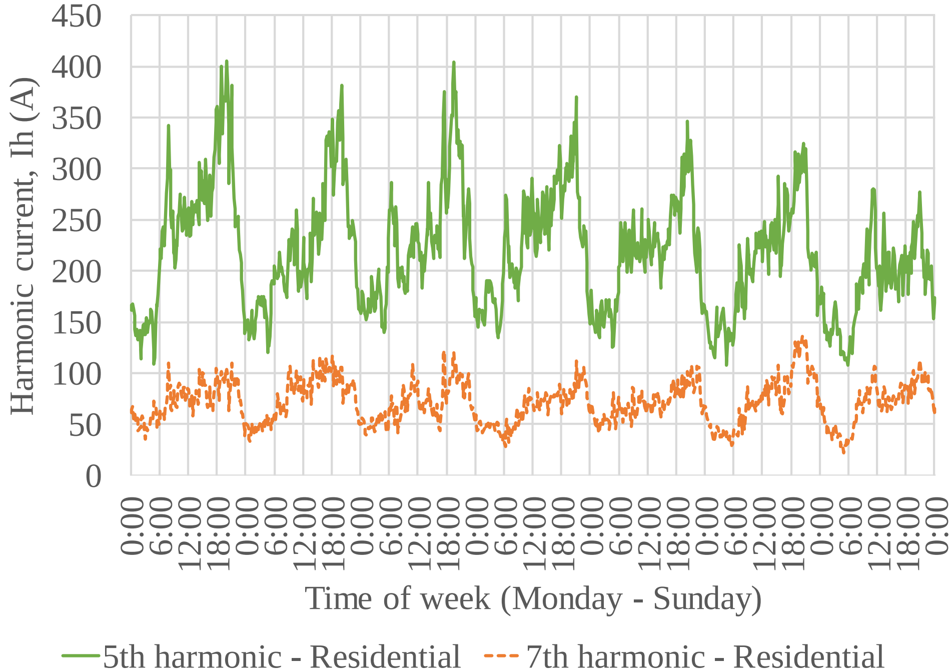

Fig. 5.3.5. *Total arithmetic sum of harmonic current magnitudes injected by all residential customers in the model*

In order to present also the phase angles of the harmonic currents injected by residential customers, polar scatter plots in Fig. 5.3.6. give harmonic current percentage magnitudes and phase angles for the 5th and 7th harmonic. In order to model the realistic phase angle diversity, noticed among different measurements presented in literature [83], a uniform phase angle variation was additionally modelled for different residential customers in the network (5th harmonic: ± 20° with a step of 5°, 7th harmonic: ± 60° with a step of 15°) [3].

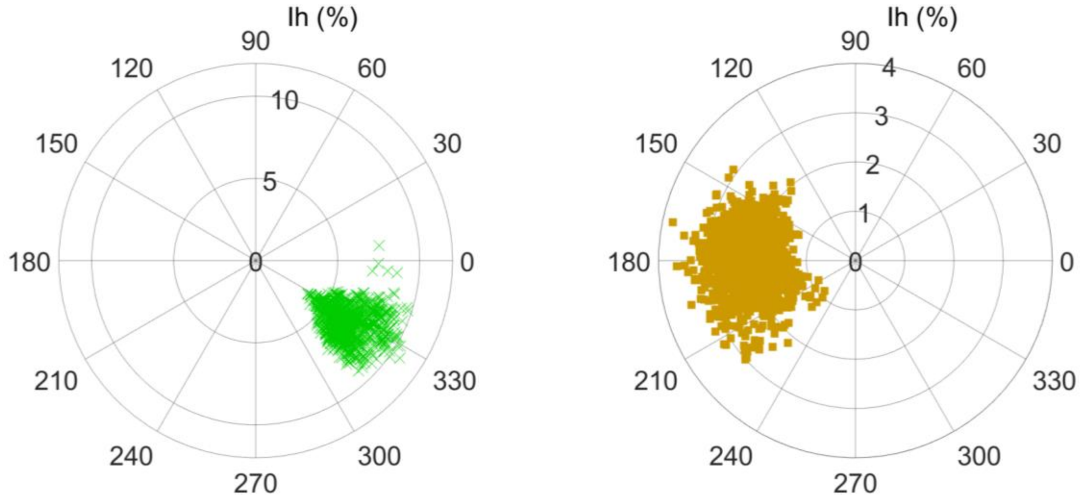

a b

Fig. 5.3.6. *Polar scatter plots of harmonic currents (percentage magnitudes and phase angles) injected by residential customers in the model*
(a) 5th harmonic, **(b)** 7th harmonic

For parameterising the harmonic current emission of different small commercial customers, three distinct measurements of different LV networks with offices were used, to represent the realistic variation in the harmonic current emission of office customers reported in [23]. A uniform distribution of different small commercial customers among all three different aggregate office customer harmonic source models was implemented in this research. [3].

Similar to the previous graph for residential customers, Fig. 5.3.7. presents the weekly trends of the total arithmetic sum of the 5th and 7th harmonic current magnitudes, injected by all small commercial customers from all the connected LV networks. From Fig. 5.3.7., the characteristic trends and morning peaks for small commercial customers can be noticed [3].

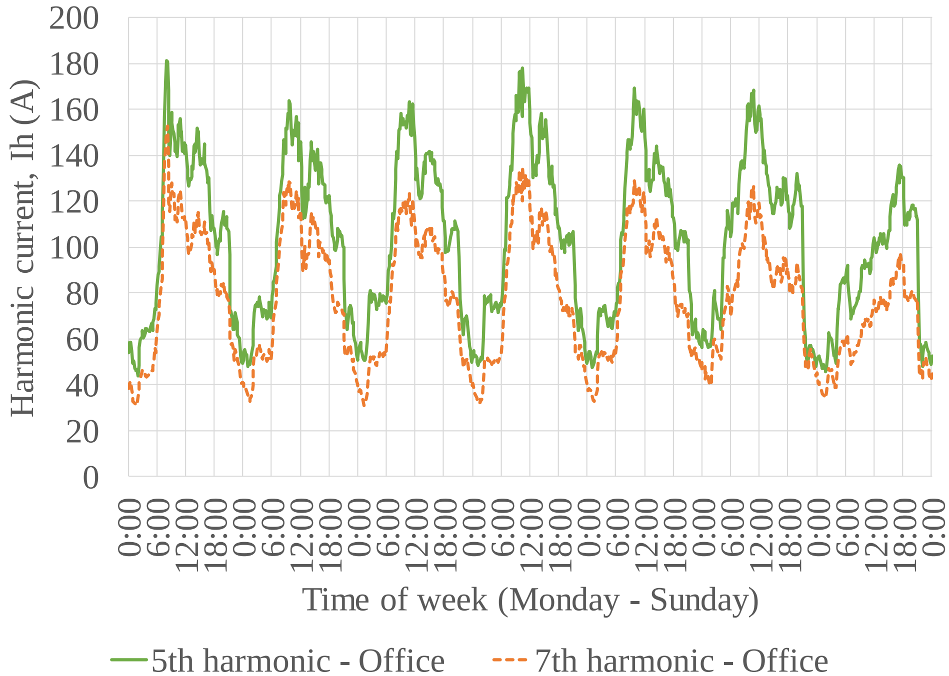

Fig. 5.3.7. *Total arithmetic sum of harmonic current magnitudes injected by all small commercial customers in the model*

Additionally, polar scatter plots in Fig. 5.3.8. give the harmonic current percentage magnitudes and phase angles, for the 5^{th} and 7^{th} harmonic order, for all three aggregate small commercial customer harmonic source models [3].

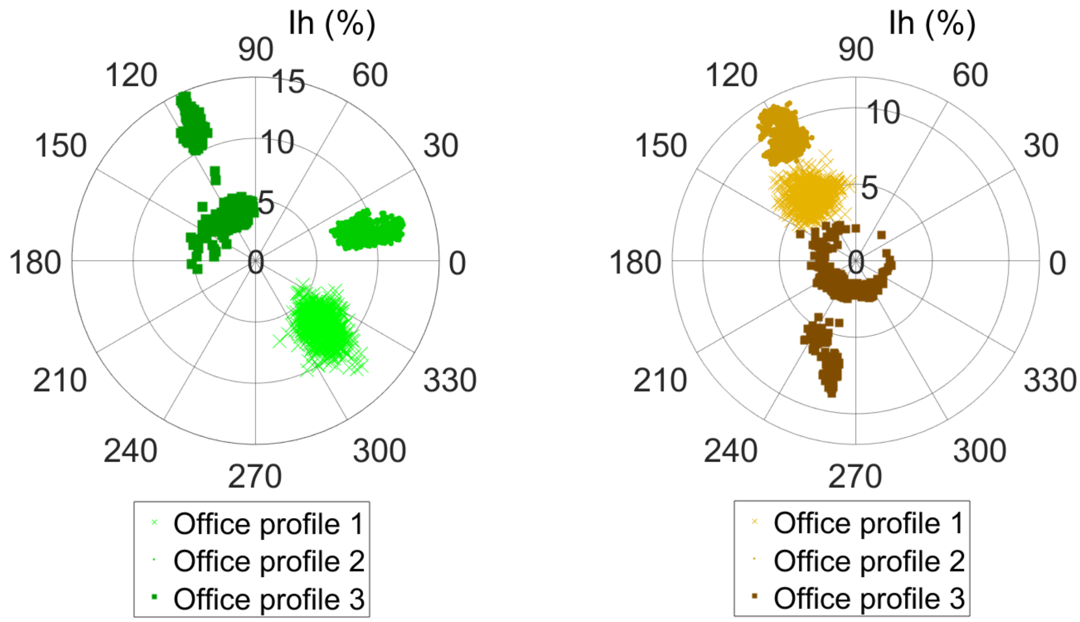

a b

Fig. 5.3.8. *Polar scatter plot of harmonic currents (percentage magnitudes and phase angles) injected by small commercial customers in the model*
(a) 5th harmonic, **(b)** 7th harmonic

5.3.6.3 Models of Industrial and Agricultural Customers

In this research a methodology for parameterising harmonic current source models of industrial customers is developed. Because of the different types of industries that exist, it is not possible to make single or several aggregated measurements of harmonic emission for industry, as was the case for residential and small commercial customers in section 5.3.6.2. Therefore, a methodology for parameterising the harmonic current source models of different individual industries is developed [3].

The methodology is based on the fact that the most common sources of harmonics in industry are VSDs, mostly based on diode rectifiers, that supply motors in industry. According to [84]- [85] a typical case is that large three-phase rectifiers with DC-link inductance and capacitance are connected to points in network with high short-circuit power, which is a case in industry [3].

The formula (5.3.2.) for calculating the harmonic current emission of industry consists of three factors. The first one is a statistical percentage of motor electricity use by different industry groups. The second one is the percentage of motors with VSDs installed. The third one is the emission of a three-phase rectifier with DC-link inductance and capacitance. The formula is [3]:

$$I_h(\%) = p_{motor}(\%) \cdot p_{VSD}(\%) \cdot I_{h\_rectifier}(\%) \quad (5.3.2.)$$

In this research p_{motor} *(%)* is taken from the report of U.S. Department of Energy [86]. The report gives a statistic of motor system energy as a percentage of total electricity, for different standard industrial categories (SIC). Since the types of industrial customers in the analysed network were known, this percentage was taken individually for all the major industrial customers in the network (accounting to total of 75% of industrial energy consumption). Other smaller industries (total of 25% of industrial energy consumption) were parameterised using the average value of motor electricity use for all industries [3].

The variable p_{VSD} *(%)* is taken as estimate, taking into account that according to [87] only 5% of motors were equipped with VSDs in 2004. Also, according to the same report [87], about 3% percent of all motors in applications under 2.2 kW have some form of speed control. This reflects the fact that smaller motors, that form a predominant share of the electric motor market, are less frequently equipped with VSDs than large motors. Therefore, in this research, it was assumed that about 30% of larger motors in industry are equipped with VSDs [3].

The third variable $I_{h\_rectifier}$ *(%)* is taken from [84] and a 6-pulse three-phase rectifier with DC-link inductance and capacitance is taken as a typical case in industry. Even though today, instead of 6-pulse diode rectifiers, the 6-pulse bridge with active front-end or diode bridge with capacitor are more often installed in new applications, still currently the majority of VSDs in the field are with 6-pulse diode rectifiers, because they were installed in the previous period. The harmonic emission of rectifiers depends on the short circuit ratio, that is the ratio between the short-circuit power of the network at the PCC and the installed power of the rectifier. Hence, for all the major industrial customers (accounting to a total of 75% of industrial energy consumption), short-circuit power at their individual PCC was calculated from the network model and combined with the results of [84]. For other smaller industries (a total of 25% of industrial energy consumption) an average short-circuit power in the network was taken. Short circuit powers were slightly reduced to take into account the short-circuit power drop on the connection lines from 30/0.4 kV transformers to the locations of the rectifiers [3].

The phase angles of the harmonic currents for industrial customers are taken directly from [84], and correspond to the phase angles of the harmonic currents of three-phase rectifiers with DC-link inductance and capacitance [3].

Similarly, using the methodology described previously for industrial customers, the harmonic current emission of agricultural customers was also modelled, but with some modifications. The value of p_{motor} *(%)* was also taken from the report [86], which also gives the percentage of motor electricity use for agricultural production. The percentage of motors with VSDs, represented by factor p_{VSD} *(%)*, was taken as 20%. The variable $I_{h\_rectifier}$ *(%)* was also taken from [84], but a three-phase rectifier with DC-link capacitance, but without any DC-link inductance, was taken as a typical case. For agricultural customers a relatively lower short-circuit ratio was assumed, to take into account the drop of short-circuit power in the LV network and on longer connection lines, compared to the higher short-circuit power of industrial customers, mostly connected close to dedicated 30/0.4 kV transformer substations. The phase angles of the harmonic currents for agricultural customers are also taken from [84], and correspond to the phase angles of the harmonic currents of three-phase rectifiers with DC-link capacitance, but without any DC-link inductance [3].

The weekly trends of the total arithmetic sum of the 5th and 7th harmonic current magnitudes, injected by all industrial and agriculture customers in the model, are presented in Fig. 5.3.9. Characteristic trend and higher harmonic current injection can be observed during the workday working hours [3].

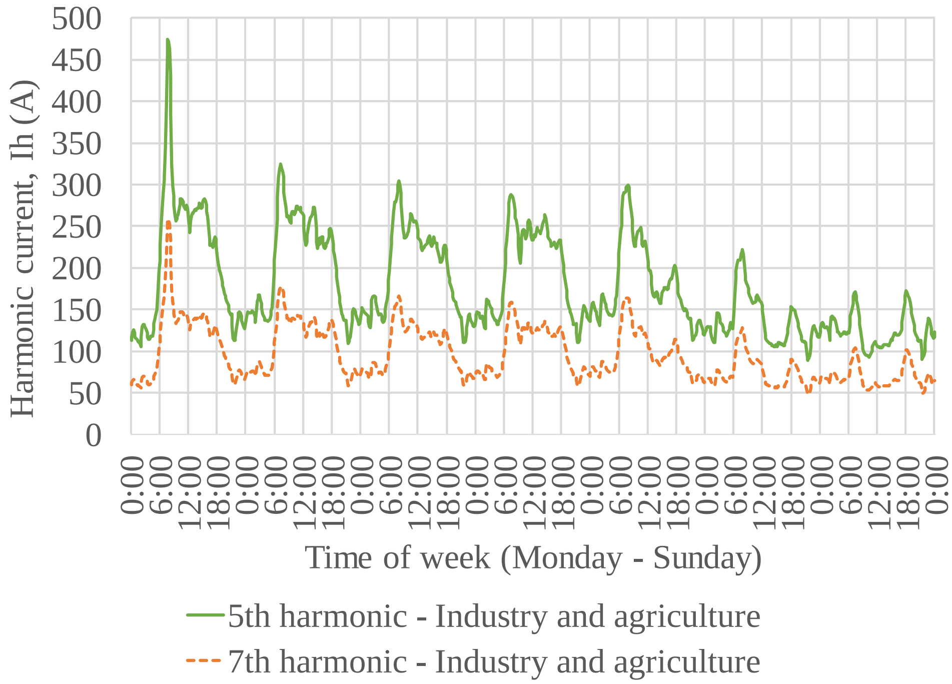

Fig. 5.3.9. *Total arithmetic sum of harmonic current magnitudes injected by all industrial and agriculture customers in the model*

The polar scatter plot in Fig. 5.3.10. gives the harmonic current percentage magnitudes and phase angles for the 5th and 7th harmonic order, for industrial and agricultural customers. The polar scatter plot is not populated with many points, since only constant values of harmonic current magnitudes and phase angles were available for these customer categories, based on [84]. Comparing Fig. 5.3.10. with Fig. 5.3.6. and Fig. 5.3.8., we can see that the harmonic current emission for the 5th and 7th harmonic is in counter-phase between the residential and some office customers on one side (characterised by single phase rectifiers) and industrial customers on the other side (characterised with three-phase rectifiers). This was one of the main conclusions of [3], [85].

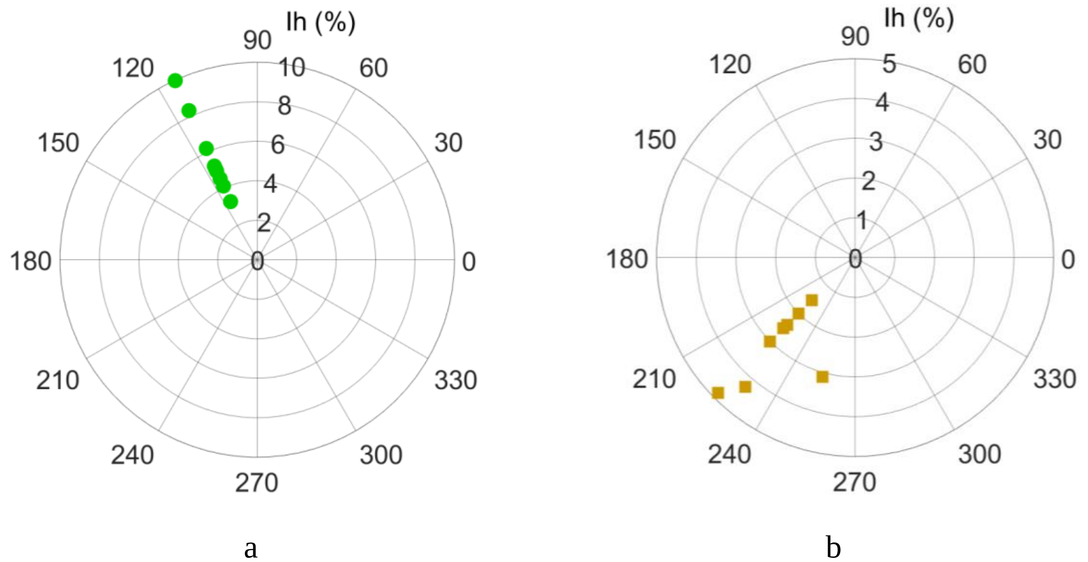

Fig. 5.3.10. *Polar scatter plots of harmonic currents (percentage magnitudes and phase angles) injected by industrial and agricultural customers in the model*
(a) 5th harmonic, **(b)** 7th harmonic

Harmonic current emission of TPP own consumption was not modelled, since the data on distribution transformers and consumers within TPP were not known. However, this does not make a significant impact to the model and is negligible since it constitutes a 1.34% of load in the chosen week and TPP own consumption is zero from this feeder for most of the week [3].

5.3.7 Implementation of the Harmonic Load Flow Model in the Chosen Software Tool

For this research, the DIgSILENT PowerFactory commercial software tool was used to develop harmonic model and perform harmonic load flow. However, the proposed methodology is general and can be applied in other available software tools [3].

Several important implementation issues were encountered while implementing the methodology of this research, and they are discussed along with the recommendations for solving the issues in the paragraphs below. Some of the implementation issues are related to the specific characteristics of the chosen software tool [3].

For this research, various measurements from different sites and time zones were used. Therefore all the measurements needed to be time synchronised to the time zone of the location of the network, and that is CEST, which is +2 h ahead of UTC [3].

Since the chosen software tool calculates harmonic phase angles in the cosine reference convention [88], all the phase angle inputs for the calculation as well as the results were cosine. All the measurements used, that were sine referenced, were recalculated to the cosine referencing convention using the formula (5.3.3) [3].

On the other hand, the values of the phase angles on the polar scatter plot graphs presented in this paper are referenced according to the sine reference convention, which is more common in practice. The final results from the chosen software tool were therefore recalculated to the sine reference convention using the formula (5.3.4). The values of the harmonic phase angles are referenced to the fundamental voltage in all the graphs [3].

$$\varphi_{h\,(cosine)} = \varphi_{h\,(sine)} - \pi/2 - h \cdot (\varphi_{1\,(sine)} - \pi/2) \quad (5.3.3)$$

$$\varphi_{h\,(sine)} = \varphi_{h\,(cosine)} + \pi/2 - h \cdot (\varphi_{1\,(cosine)} + \pi/2) \quad (5.3.4)$$

The chosen software tool uses the phase angles of the harmonic current sources referenced to the fundamental current as input for the model [88]. Because of this characteristic of the chosen software tool, all the harmonic current source phase angles, taken from measurements, were recalculated from referencing to the fundamental voltage (presented in the graphs in this paper) to referencing to fundamental current. This has been done using the following formula, derived directly from [3], [88]:

$$\varphi_{h\,(model)} = \varphi_{h\,(measurement)} - h \cdot \varphi_1 \quad (5.3.5)$$

Since reactive power is not defined in the APCS synthetic load profiles, the power factor was assumed to be cosφ=0.98 for all the customers, except for hot water tanks, night storage heating and all the DGs, which were modelled with cosφ=1. Therefore, the phase angle between the fundamental current and the fundamental voltage in the formula (5.3.5) has a value of $\varphi_1 = -11.48°$ for all the loads with cosφ=0.98. However, it should be explained that the choice of power factor of the loads (cosφ=0.98) does not have an impact on the final results of the harmonic load flow in the model, since the harmonic phase angle difference, which comes from the difference in fundamental angles of voltage and current, is compensated by the formula (5.3.5) [3]..

In this research the harmonic load flow for a whole week was needed, but the toolbox for harmonic analysis in the chosen software tool only enables the harmonic load flow for one moment in time. Therefore, in order to automate the calculation of harmonic load flow for every 10-minute interval in one week, a script in the DPL was developed [89]. In every iteration all the 10-minute loads, the DGs production, as well as the background harmonic voltage source model and harmonic current source models' magnitudes and phase angles were updated. After performing the harmonic load flow for every 10-minute interval, the results for the busses with installed PQ monitors were exported for analysis. Since the interval for calculations was 10-minute, a total of 1,008 harmonic load flow calculations were performed for one chosen week [3], [4].

5.4 Modelling of Flicker

This subchapter 5.4 was previously published by the author of this thesis in [6].

5.4.1 Overview of the Modelling Methodology

The main steps of the methodology for modelling flicker in this research are given below [6]:

1. Model the MV network in a chosen software tool
2. Perform short-circuit calculation for every node individually
3. Export residual voltages in all the nodes resulting from individual short-circuits
4. Based on residual voltages calculate flicker transfer factors
5. Define flicker emission coefficients for every characteristic customer category
6. Calculate flicker from all the individual sources
7. Calculate total flicker values by summing up flicker from individual sources using cubic law

5.4.2 Short-Circuit Calculation

Short-circuit calculation, according to the standard IEC 60909-0 [90], was performed for every MV node in the network in an automated way using DPL scripts. The short-circuits for MV nodes were calculated, since sources of voltage flicker were modelled at the MV and not LV busbars of MV/LV transformer substations. The reason for this was to exclude the influence of MV/LV transformer tap changers, since there are different nominal voltages and different tap positions among transformers in the analysed network. The minimum short-circuit capacity Ssc_min of the superior HV network was used, to represent the switching state with low short-circuit capacity. Factor c=1, valid for MV networks when calculating Ssc_min, was used according to the standard IEC 60909-0 [90]. According to the IEC 60909-0 [90], contribution of DG to short-circuit current can be neglected, since their total power is <5% of Ssc. After every short-circuit calculation for a fault on an individual node, residual voltages for the rest of the nodes in the network were exported [6].

5.4.3 Flicker Transfer Factor

Flicker transfer factor $k_{flicker}$ is equal to voltage transfer factor [91] and describes the transfer of a voltage variation caused in bus “a” (source) towards an arbitrary bus “b” (observer). Based on residual voltages from short-circuit calculations, flicker transfer factors were calculated for all the busses, using the formulas 5.4.1. – 5.4.2. [6]. A short circuit is applied to the source bus “a” and the voltage change in per unit at the observed bus “b” equals:

$$\Delta u_b = 1 - u_{residual,b} \quad (5.4.1.)$$

Consequently the transfer factor results in

$$k_{flicker,ab} = \frac{\Delta u_b}{\Delta u_a} \quad (5.4.2.)$$

with Δu_a being 1 p.u. (short circuit with fault impedance being zero).

5.4.4 Flicker Emission Coefficients

Table 5.4.1. gives the shares of energy consumption/production of different customer categories in the total amount of energy in the network, for the analysed first week of June. The highest consumption is in the household category, then industry, different small commercial customers, etc. [6].

Table 5.4.1. also gives the assigned c_f - flicker emission coefficient values for all the customer categories. Flicker emission coefficient represents a characteristic emission coefficient giving a linear relationship between flicker emission $P_{st,i}$and the ratio of maximum load (or contractual load) and short circuit capacity in the connection point $\frac{P_{max}}{S_{sc}}$, usually used together with statistical distribution of emission, corresponding to the 99% quantile P_{st} value. For largest industries, flicker emission coefficients were individually estimated and assigned. It must be noted that there are no published values of flicker emission coefficients for majority of the customer categories. Therefore, flicker emission coefficient values were roughly estimated in this research, in order to achieve the match between the model results and the PQ measurements. More measurements of flicker emission coefficients for different customer categories are needed in order to have a more precise model [6].

Table 5.4.1. *Customer category groups in the network, with their share in weekly energy consumption and assigned flicker emission coefficient value*

Customer category	Percentage of total weekly energy	Flicker emission coefficient value
Household	40.27%	12.5
Industry	28.05%	Individual in the range 5 - 24
Small commercial customers	17.29%	12.5
Agriculture	11.08%	12.5
Hot water tanks and night storage heating	4.02%	12.5
Thermal power plant own consumption	1.34%	12.5
Public lighting, mobile phone base stations	0.96%	12.5
Photovoltaics	-2.90%	5
Other distributed generation	-0.11%	2.5
Total	100,00%	

Assigned flicker emission coefficients values correspond to the 99% quantile of the cdf of the flicker emission. This methodology is in line with the present approach for calculating flicker emission coefficients of electric arc furnaces [7]- [23], wind power plants [25]- [26] etc. The P_{st} cdf function used in this research for modelling downstream MV and LV flicker sources is shown in Fig. 5.4.1. It was derived from PQ measurements in the longest feeder in the network, where flicker is dominated from emission of flicker sources in the analysed MV network rather than from background flicker emission. Also, large flicker events, that propagated from the upstream HV network, were removed from the cdf data. The cdf data from Fig. 5.4.1. were normalised with 99% quantile value of flicker, and therefore the graph from Fig. 5.4.1. corresponds with flicker emission coefficients from Table 5.4.1. giving as a result 99% quantile value of flicker [6].

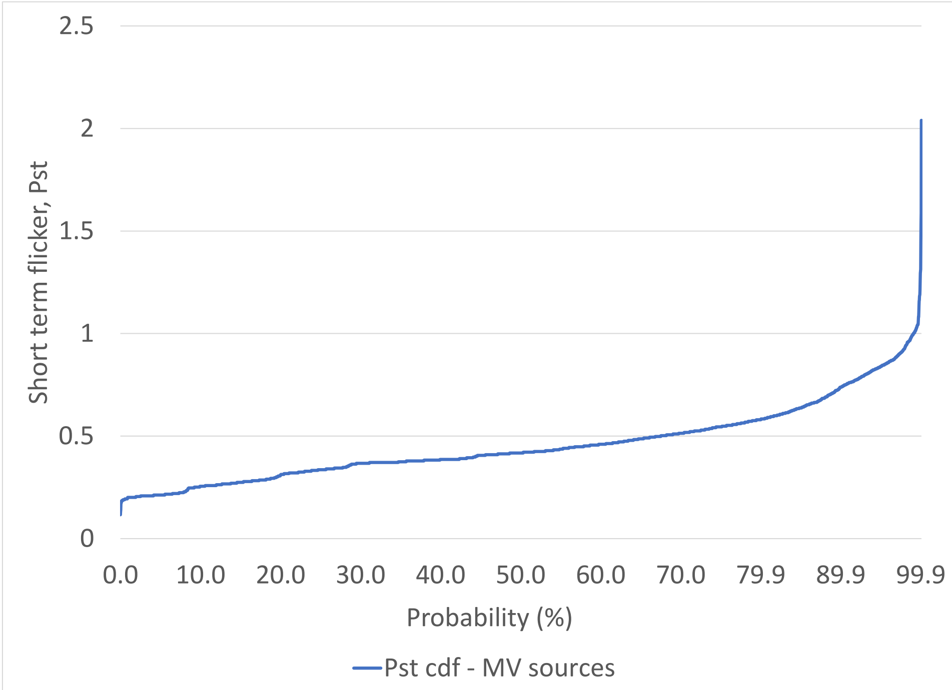

Fig. 5.4.1. *Pst cumulative distribution function (cdf) used for modelling downstream MV and LV flicker sources*

Similar to flicker sources from MV network, Pst cdf curve for background flicker was modelled directly from the PQ measurements. This Pst cdf curve contains large flicker events coming from HV network, and it is shown in Fig. 5.4.2. [6].

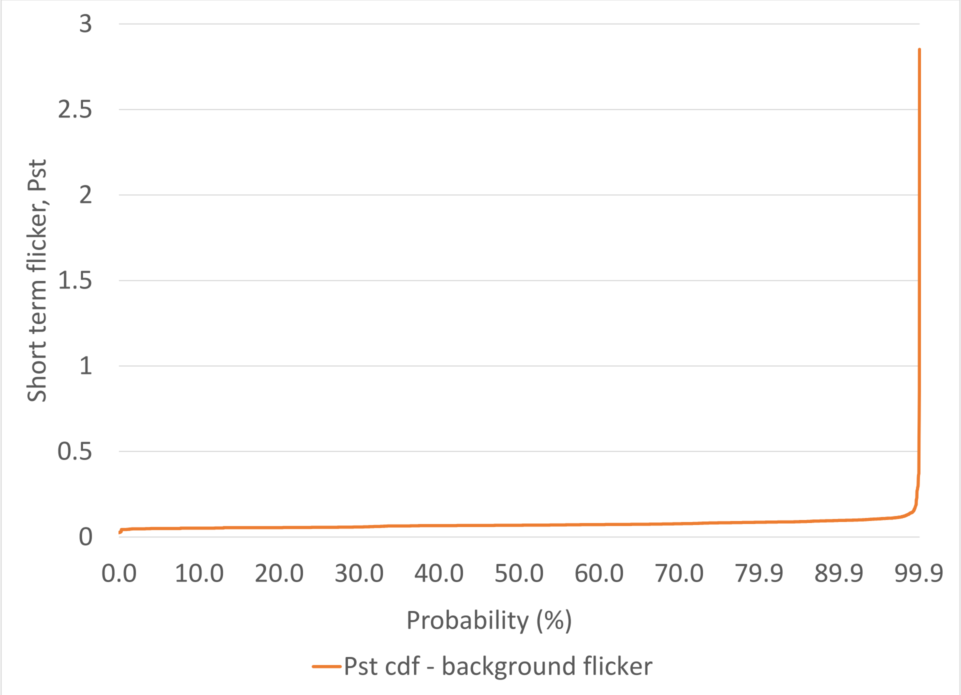

Fig. 5.4.2. *Pst cumulative distribution function (cdf) used for modelling background flicker*

5.4.5 Calculation of Flicker

The total flicker emission for a single flicker sources connected to a node was calculated using the formula 5.4.3.:

$$P_{st,i,n,t} = rand(P_{st}\ cdf) \cdot\ c_{f,n} \cdot \frac{P_{max,i,n,t}}{S_{sc,i}} \quad (5.4.3.)$$

In the equation (5.4.3.), *"i"* represents the number of the node, "n" represents the customer flicker source, and *"t"* is the point in time in one month, while $rand(P_{st}\ cdf)$ provides a random number with a probability distribution according to the data in Fig. 5.4.1. In this way, using (5.4.3.), all the flicker sources for one month are calculated.

Propagation of flicker was calculated taking into account the flicker transfer factor between the individual busses in the network, as shown in the formula 5.4.4. All the individual flicker contributions from all the sources were then summed up using cube summation law for flicker [7], shown in formula 5.4.5.:

:

$$P_{st\ ,j,t} = \sqrt[3]{\sum_{i=1}^{N}(k_{flicker\_i,j} \cdot P_{st,i,n,t})^3} \quad (5.4.4.)$$

where “j” and “i” represent the number of busses and $k_{flicker}$ represents the flicker transfer ratio.

In case of several customers at one node:

$$P_{st\,,j,t} = \sqrt[3]{\sum_{i=1}^{N}(k_{flicker\_i,j} \cdot \sum_{n=1}^{n_i} P_{st,i,n,t})^3} \quad (5.4.5.)$$

Flicker was calculated using two approaches:

a) Every customer was modelled as a flicker source
b) Only one customer per each customer category in every secondary MV/LV transformer station was modelled

Approach b) was tested in order to reduce computation time. Both methods were applied and the results are discussed in the sub-section 6.2.

For all the calculations, one month time frame was chosen. One month of data and calculations is both practical enough from the standpoint of needed one-month measurements to build a model, and also representative enough as a long enough period to characterise and model flicker in the network. For all the calculations, line-line flicker was used and not line-ground, since only line-line measurements of flicker were available. Steps 4-7 were all calculated in MATLAB [6].

5.5 Modelling of Unbalance

5.5.1 Overview of the Modelling Methodology

The main steps of the methodology for modelling unbalance in this research are given below:

1. Model the MV network in a chosen software tool
2. Perform short-circuit calculation for every node individually
3. Export residual voltages in all the nodes resulting from individual short-circuits
4. Based on residual voltages calculate unbalance transfer factors
5. Calculate synthetic load profiles for all LV customers
6. Define current unbalance factors for every characteristic customer category
7. Calculate unbalance voltages from all the individual sources
8. Calculate total unbalance voltage values by summing up unbalance voltages from individual sources using general summation law from IEC 61000-3-13

In this thesis, voltage unbalance is assumed to be caused by unbalanced loads only. Line impedance is assumed to be perfectly balanced.

5.5.2 Short-Circuit Calculation

It was assumed that the negative sequence impedance Z_2 is equal to positive sequence impedance Z_1, and therefore the approach of calculating unbalance transfer factors using short-circuits, similar as for flicker, is valid. The methodology for performing short-circuit calculations is the same as in the case of modelling flicker, presented in more detail in 5.4.2.

5.5.3 Unbalance Transfer Factor

Unbalance transfer factor is equal to voltage transfer factor. Based on residual voltages from short-circuit calculations, unbalance transfer factors were calculated for all the busses, using the formulas (5.5.1.) – (5.5.2.):

$$\Delta u = 1 - u_{residual} \quad (5.5.1.)$$

$$k_{unbalance} = \frac{\Delta u_b}{\Delta u_a} \quad (5.5.2.)$$

with Δu_a being 1 pu (short circuit with fault impedance being zero).

5.5.4 Background Unbalance Voltage

From available PQ measurements in the feeding HV/MV transformer substation, background unbalance voltage at 110 kV was modelled. The values for the analysed month are shown on Fig. 5.5.1.

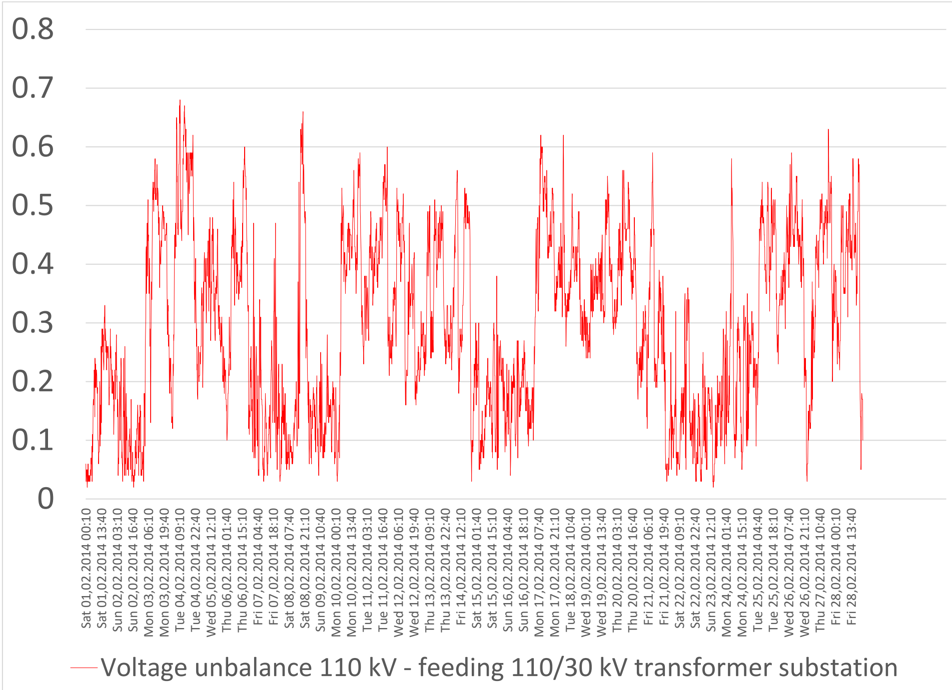

Fig. 5.5.1. *Background voltage unbalance at 110 kV level in the feeding 110/30 kV transformer substation*

5.5.5 Synthetic Load Profiles

This subchapter 5.5.5 was previously published by the author of this thesis in [3].

As for the harmonic load flow, also for the modelling of unbalanced current sources at LV level, weekly load profiles were needed as a necessary part of the methodology. The calculation of synthetic load profiles is the same as in modelling of harmonics part of the thesis, explained in more detail in 5.3.6.1.

5.5.6 Current Unbalance Factor

5.5.6.1 General methodology

Current unbalance factor can be defined as the ratio of negative sequence current to the positive sequence current:

$$c_i = \frac{I_2}{I_1} \qquad (5.5.3.)$$

For this thesis, the following measurement data for current unbalance factor were used to develop the model:

1. Daily 50% quantiles of c_i, for a total of 127 LV networks
2. Weekly ci profiles of 5 LV networks, dominated by different customer categories:

By analysing the available measurement data for current unbalance factors of different customer categories, it was concluded that its trend contains both deterministic and stochastic behaviour. Therefore, a methodology was developed to represent both behaviours in the model, which will be explained in the text of the rest of this subchapter 5.5.6. Due to partly stochastic nature of current unbalance factor, the mission was not to recreate the exact time course of it, but to rather develop a model which would generate current unbalance factor time series, that realistically resembles the behaviour of the measurements.

5.5.6.2 Modelling 50% quantiles of c_i using daily measurements

Using daily 50% quantiles, as a single value representing c_i 10-minute measurements time series of one day consisting of 144 values, two scatterplot graphs were made, one containing the data for all residential grids, and the other one containing the data for small commercial and industry grids. Daily 50% quantiles of ci 10-minute measurements were available for 12 days, for 55 residential grids and 22 grids with small commercial customers. Data for residential grids are shown in Fig. 5.5.2., while data for small commercial and industry grids are shown in Fig. 5.5.3. Every point on a graph represents one daily 50% quantile, and every LV grid is represented with 12 point for 12 available days. It can be concluded that the unbalance factor is lower for LV networks with higher load, which is due to cancellation between different unbalance sources.

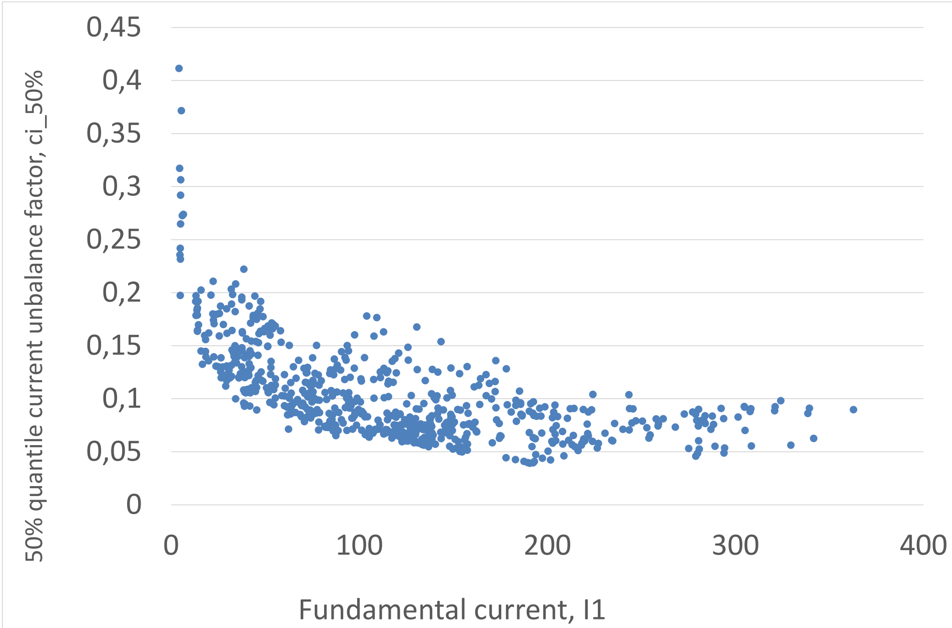

Fig. 5.5.2. *$c_{i\_50\%}$ - daily 50% quantile of current unbalance factor c_i for residential LV grids (12 days, 55 grids)*

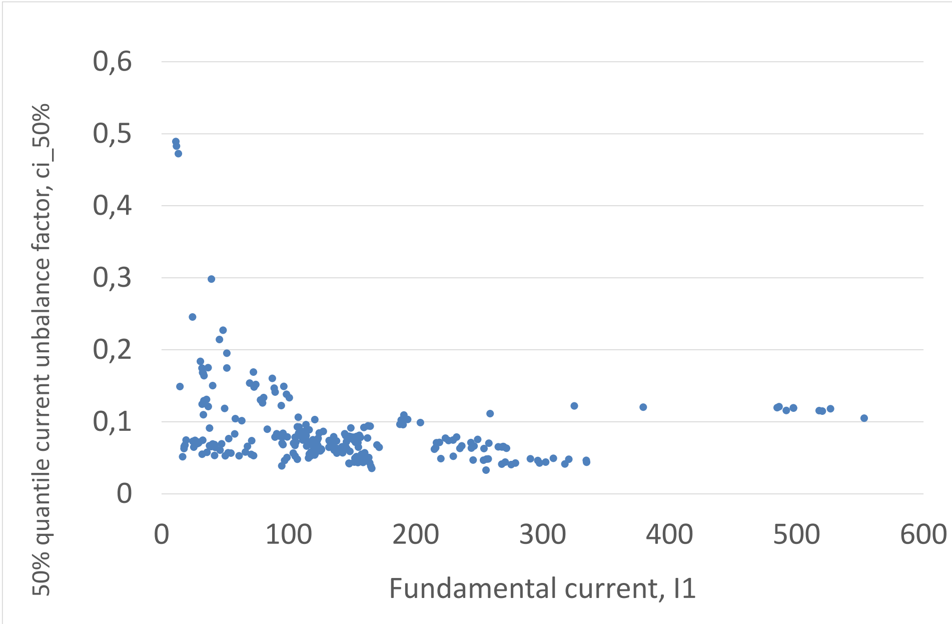

Fig. 5.5.3. *Daily 50% quantile of current unbalance factor c_i for small commercial and industry LV grids (12 days, 22 grids)*

For both graphs, upper and lower envelope were calculated, and they are given in the formulas 5.5.4 – 5.5.7.

Upper envelope for residential LV grids (Fig. 5.5.2.):

$$c_{i\ 50\%\ \mathrm{upper\ envelope}\ (\mathrm{residential})} = -0.071\ln(I_1) + 0.4997 \qquad (5.5.4.)$$

Lower envelope for residential LV grids (Fig. 5.5.2.):

$$c_{i\ 50\%\ \mathrm{lower\ envelope}\ (\mathrm{residential})} = 0.3928\ I_1^{-0.403} \qquad (5.5.5.)$$

Upper envelope for small commercial and industrial LV grids (Fig. 5.5.3.):

$$c_{i\ 50\%\ \mathrm{upper\ envelope}\ (\mathrm{small\ commercial\ and\ industry})} = 1.2524\ I_1^{-0.387} \qquad (5.5.6.)$$

Lower envelope for small commercial and industrial LV grids (Fig 5.5.3.):

$$c_{i\ 50\%\ \mathrm{lower\ envelope}\ (\mathrm{small\ commercial\ and\ industry})} = 0.082\ I_1^{-0.165} \qquad (5.5.7.)$$

In the model, every customer category group at every MV/LV transformer substation was assigned with the magnitude of 50% quantile of current unbalance factor, by using the envelopes 5.5.4. – 5.5.7. of the Figs. 5.5.2. - 5.5.3. The goal was to assign every customer category group with a value between upper and lower envelope. The random number generator decides the chosen distance from upper and lower envelope of the corresponding group (residential or small commercial and industry). Random number generator brings stochasticity to the otherwise deterministic formula and approach. This was done using the following formula 5.5.8.:

$$c_{i\ 50\%} = c_{i\ 50\% upper\ envelope} - rand \cdot (c_{i\ 50\% upper\ envelope} - c_{i 50\%\ lower\ envelope}) \quad (5.5.8.)$$

In the model of this research, $c_{i\ 50\%}$ value determines the magnitude of the current unbalance factor, while the daily/weekly profiles of the current unbalance factor are determined by the part of methodology explained in the next subchapter 5.5.6.3.

5.5.6.3 Modelling weekly c_i profiles using measurements of several LV networks, dominated by different customer categories

For this thesis, five measurements of weekly c_i profiles of different LV networks, dominated by different customer categories, were used:

- Small residential
- Medium residential grid
- Large residential grid
- Small commercial customers
- Large industry

These measurements were used to model weekly c_{i_model} profiles of all the customer categories, and the methodology for this is shown in this subchapter. The methodology is presented and explained in detail for one of the customer categories with available measurements (small commercial customers). For other customer categories, analogous approach was applied.

The starting point of the methodology is the measurement of $c_{i\_measured} = I_2/I_1$, which is shown in Fig. 5.5.4. for one measured week.

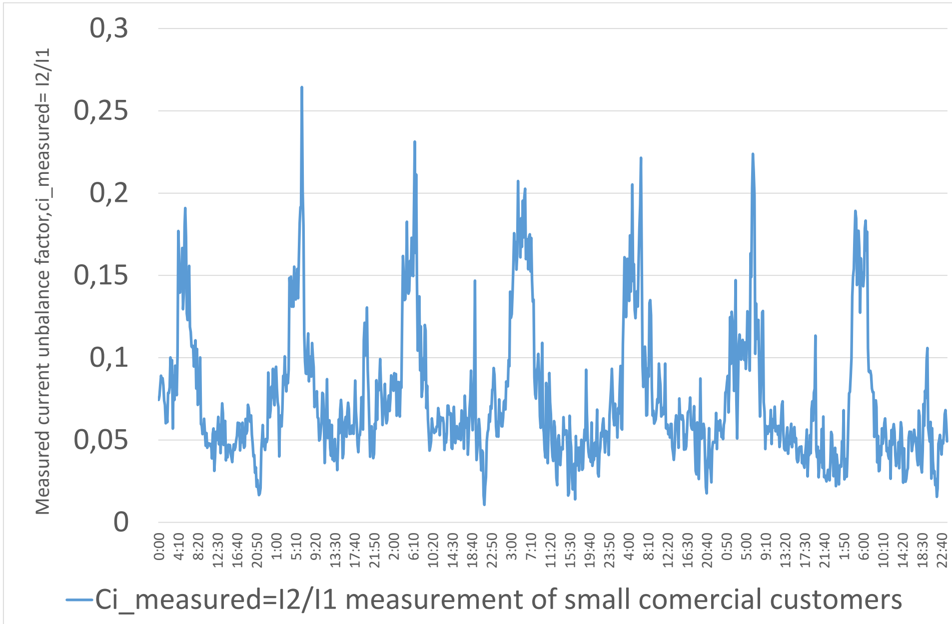

Fig. 5.5.4. *Measurement of* $c_{i\_measured} = I_2/I_1$ *for small commercial customers for one week*

It is clear from the graph 5.5.4. that there is both a deterministic and stochastic behaviour present. Therefore, the measurement data were first filtered in MATLAB, using function based on a moving-average filter principle (using windowsize=20), to extract the deterministic background behaviour, and afterwards residuals were calculated as difference between measured and filtered data to generate the stochastic behaviour.

The measured data of one week were divided in workdays and weekend days, since for some of the categories (especially households) there were differences noticed between current unbalance profiles during workdays and weekend days. Filtered workday profile of $c_{i\_filt} = I_2/I_1$ for small commercial customers is shown in Fig 5.5.5. For weekend days, analogous approach was applied.

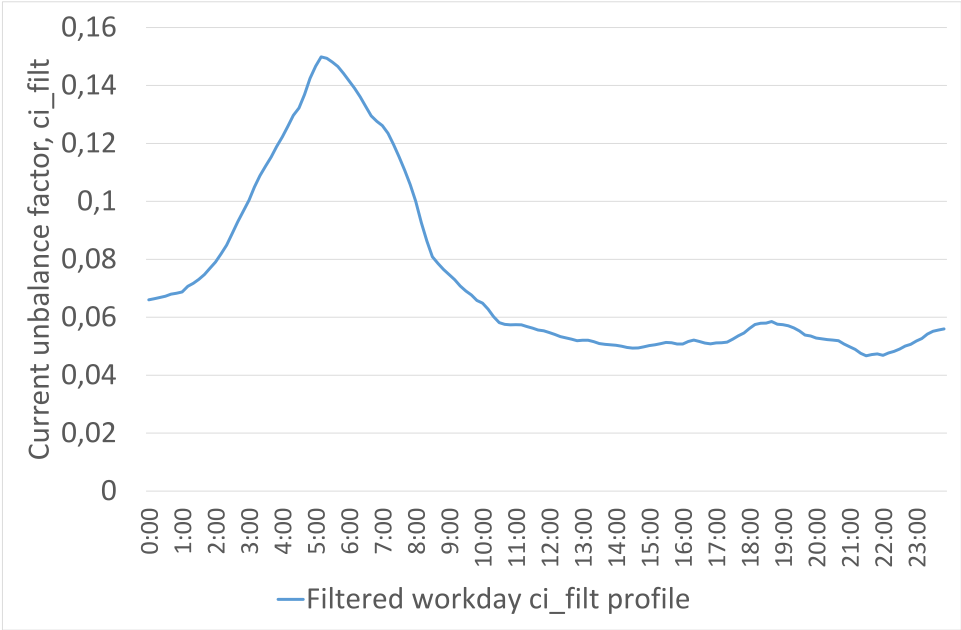

Fig. 5.5.5. *Filtered workday profile of* $ci_{\_filt}$ *for small commercial customers*

The next step is to normalise the current unbalance profile. Normalisation using average value was used in this research. Normalised filtered workday profile of $c_{i\_norm} = I_2/I_1$ for small commercial customers is shown in Fig 5.5.6.

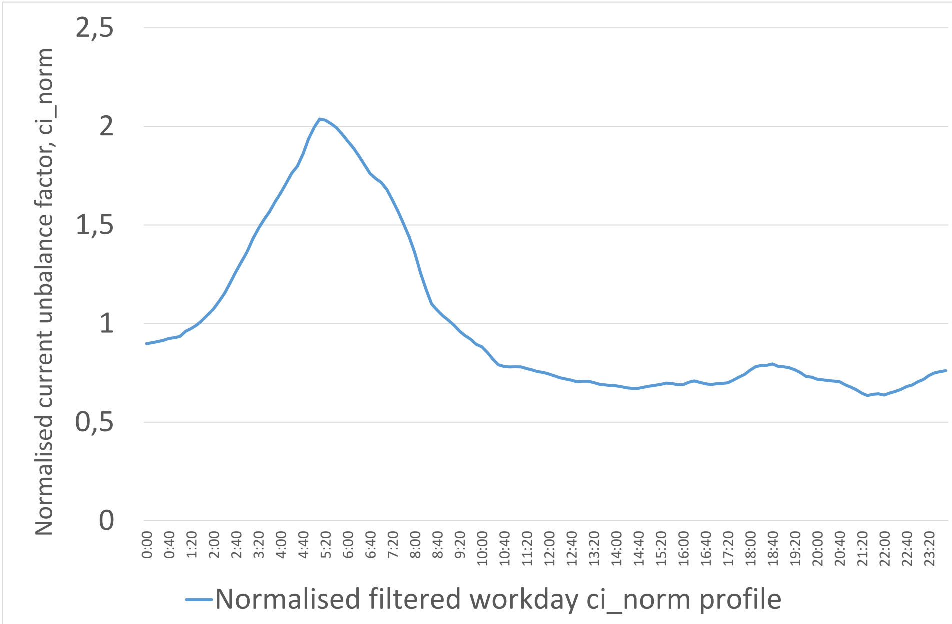

Fig. 5.5.6. *Normalised filtered workday profile of ci_norm for small commercial customers*

Another step is to calculate normalised residuals, by subtracting filtered profile c_{i_filt} from the measured profile $c_{i\_measured}$, and normalising it. Normalisation with average value was used in this research. Normalised residual cdf graph of $c_{i\_res} = I_2/I_1$ for small commercial customers is shown in Fig 5.5.7.

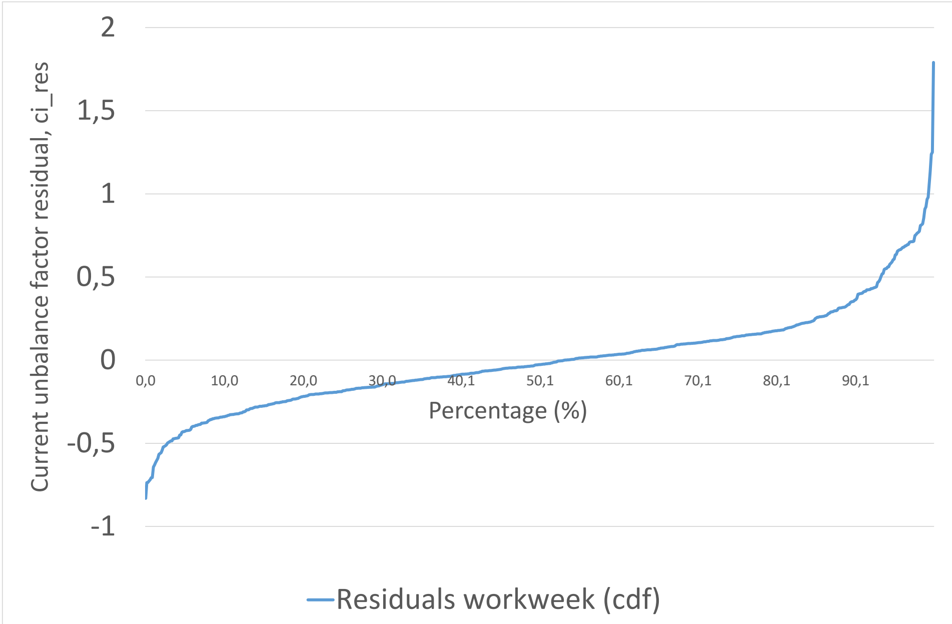

Fig. 5.5.7. *Normalised residual cdf graph of c_{i_res} for small commercial customers*

Normalised filtered workday profile c_{i_norm} was combined with normalised residual cdf graph c_{i_res} to create an individual final c_{i_model} generated current unbalance profile for every customer group belonging to small commercial customers category. In this calculation of final generated current unbalance profiles c_{i_model}, normalised filtered weekly profile c_{i_norm} was used always as it is, while for different customers random sampling from normalised residual cdf graph c_{i_res} ensured stochasticity and difference between behaviour of different customers. Thus, both deterministic and stochastic behaviour of current unbalance profile was successfully modelled. An example of final generated c_{i_model} weekly current unbalance profile is shown in Fig. 5.5.8., and it can be seen that it is very similar to measured profile from Fig. 5.5.4.

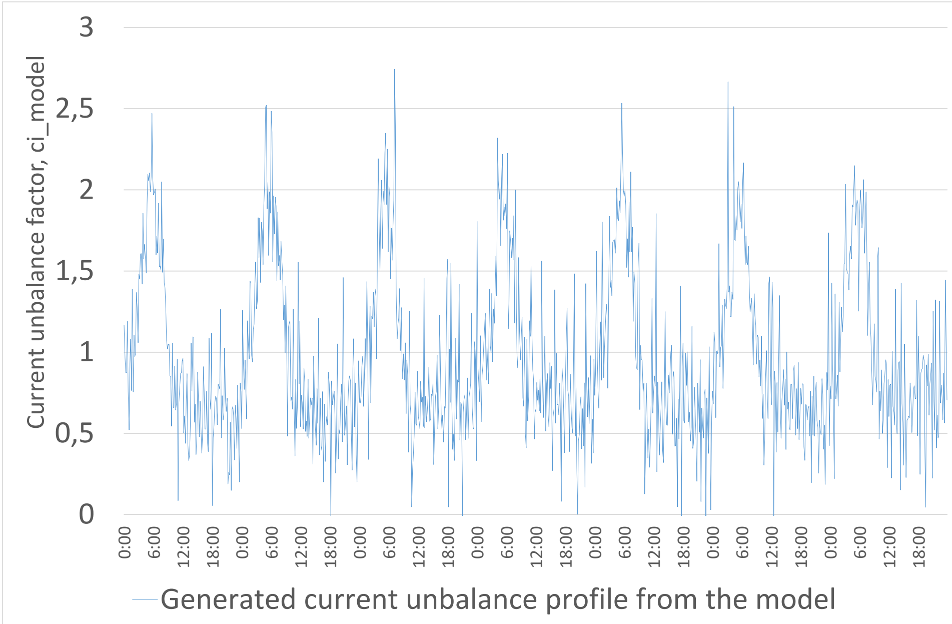

Fig. 5.5.8. *Final generated current unbalance profile* $c_{i\_model} = I_2/I_1$ *from the model, for small commercial customers for one week*

5.5.6.4 Assigning current unbalance factor data to different customer categories

All the customer categories in this research were assigned both with one of the 50% quantile groups and weekly final generated current unbalance profile c_{i_model}, which is presented in Table 5.5.1. Since for some customer categories data about current unbalance factors were not available in the published literature nor in the available measurements, available measurements of the most similar customer category were used to cover these customer categories. Therefore, agriculture, night storage heating and hot water tanks, public lighting and photovoltaics customer categories were assigned with residential current unbalance group, while thermal power plant own consumption was assigned with large industry customer group. Also, mobile phone base stations and other distributed generation were assumed to have no current unbalance emission.

Table 5.5.1. *Customer categories in the network, with their share in weekly energy consumption and assigned current unbalance factor 50% quantile groups and weekly profiles*

Customer category	Customer category code	Percentage of total weekly energy	50% quantile group	Weekly c_{i_model} profile
Household	H0	40.27%	Residential	Residential (small, medium and large)
Industry	Not assigned	28.05%	Small commercial and industry	Large industry
Small commercial customers	G0-G6	17.29%	Small commercial and industry	Small commercial
Agriculture	L0-L2	11.08%	Residential	Residential (small)
Night storage heating and hot water tanks	ULA-ULF, U1-U2	4.02%	Residential	Residential (small)
Thermal power plant own consumption	Not assigned	1.34%	Small commercial and industry	Large industry
Public lighting	B1	0.36%	Residential	Residential (small)
Mobile phone base stations	G7	0.6%	No unbalance emission	No unbalance emission
Photovoltaics	E1	-2.90%	Residential	Residential (small)
Other distributed generation	E0	-0.11%	No unbalance emission	No unbalance emission
Total		100.00%		

5.5.7 Calculation of Unbalance

Voltage unbalance from individual current unbalance sources was calculated using the formula [92]:

$$\frac{U_{2,i,n,t}}{U_{1i,,n,t}} = c_{u,i,n,t} = \frac{S_{i,n,t}}{S_{SC,i}} c_{i,model,,n,t} \cdot c_{i,50\%,n} \qquad (5.5.9.)$$

In the equation (5.5.9), “i” represents the number of the node, “n” represents the customer unbalance source, while “t” is the point in time in one month.

Current unbalance factor $c_{i,t}$ is calculated by multiplying the magnitude of the current unbalance factor $c_{i,model,,n,t}$, calculated according to subchapter 5.5.6.2, with the weekly current unbalance profile $c_{i,50\%,n}$, calculated according to subchapter 5.5.6.3.

Propagation of unbalance was calculated taking into account the unbalance transfer factor between the individual busses in the network, using the following formula 5.5.10. For summation of voltage unbalances caused by different unbalance current sources, general summation law from the standard IEC 61000-3-13 [93] was used, where $\alpha = 1{,}4$ is an indicative value of exponent for the summation of general unbalanced installations.

.

$$:\frac{U_{2(ji)}}{U_{1\,(ji)}} = \sqrt[\alpha]{\sum_{i=1}^{N}(k_{unbalance\,(ji)} \cdot \frac{U_{2\,(ii)}}{U_{1\,(ii)}})^{\alpha}}$$

Where "j" and "i" represent the number of busses and $k_{unbalance}$ represents the unbalance transfer ratio.

In case of several customers at one node:

$$\frac{U_{2(ji)}}{U_{1\,(ji)}} = \sqrt[\alpha]{\sum_{i=1}^{N}(k_{unbalance\,(ji)} \cdot \sum_{n=1}^{n_i} \frac{U_{2\,(ii)}}{U_{1\,(ii)}})^{\alpha}} \quad (5.5.13.)$$

Vector summation of voltage unbalances due to different sources was not done in this research, due to unavailability of the measurement data for this task and due to additional uncertainties that this approach would bring. Approach from standard IEC 61000-3-13 [93] was used instead.

The results of modelling of unbalance were not verified with measurements due to unavailability of the correct measurements.

5.6 Voltage Dips Consideration

This subchapter explains the methodology of considering voltage dips in the overall algorithm of optimal PQ monitor placement. Before presenting the approach, it should be explained how voltage dips are propagated and tripped by protection relays and isolated by circuit breakers in radial MV distribution networks. In such networks, feeding HV/MV transformer substation is usually equipped with circuit breakers and protection relays installed in all the MV feeder cabinets. If there are no more circuit breakers in the network, every short-circuit gets tripped by one of the circuit breakers in the feeding HV/MV transformer substation. In this case, every voltage dip is actually followed by an interruption in all the nodes of the faulty feeder, which can be registered by a PQ monitor at the MV busbars of the feeding HV/MV transformer substation. For the rest of the healthy feeders, voltage dip experienced at the MV busbars of the feeding HV/MV transformer substation is propagated with the same value until the end of all the healthy feeders, since it is a radial distribution network, and this can also be registered by a PQ monitor at the MV busbars of the feeding HV/MV transformer substation. Therefore, in this case when circuit breakers are only installed at the feeding HV/MV transformer substation, only one PQ monitor at the main MV busbar in the feeding HV/MV transformer substation is enough to register all the voltage dips in the radial MV distribution network.

However, in the analysed network, there is one circuit breaker in the MV feeder (shown in Fig. 5.6.1.) and it protects a small portion of the green feeder 2. Therefore, in this network PQ monitor installed at the feeding HV/MV transformer substation does not register 100% of voltage dips that occur in the analysed network, more specifically some information is lost on the green feeder 2.

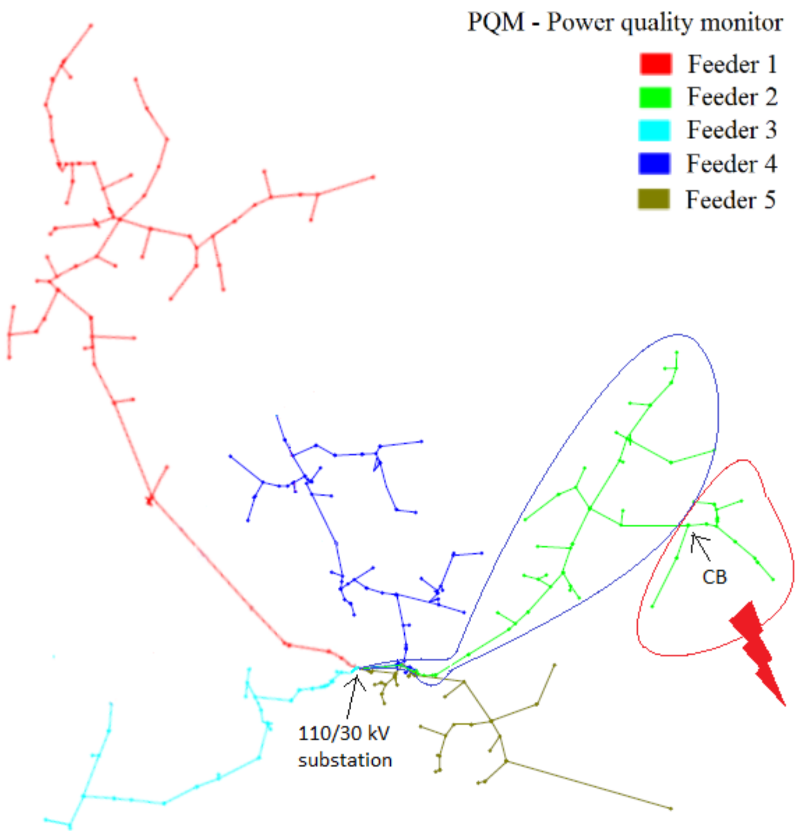

Fig. 5.6.1. *Network diagram with zones before (blue) and after (red) the circuit breaker installed at the green feeder 2*

In order to calculate how much information on voltage dips is lost if no PQ monitors are installed on the green feeder 2, a simple methodology was applied. First factor for information loss is that there are faults causing voltage dips that are not properly monitored, and these are the faults tripped by the circuit breaker installed in the green feeder 2. Explained more in detail, faults behind the circuit breaker cause the circuit breaker to trip, and the tripped part of the feeder (red zone on Fig.

5.6.1.) experiences an interruption. At the same time, the healthy part of the feeder (blue zone on Fig. 5.6.1.) before the circuit breaker experiences a voltage dip, which is the second factor for information loss if there are no PQ monitors in that feeder. In order to calculate the information loss, following formulas are applied:

$$faults\ with\ information\ loss\ (\%) = \frac{lenght\ of\ overhead\ lines\ after\ the\ CB\ (km)}{total\ length\ of\ overhead\ lines\ in\ the\ network\ (km)} \quad (5.6.1.)$$

$$information\ loss\ for\ faults\ after\ CB\ (\%) = \frac{no.\ of\ transformer\ substations\ before\ CB}{no.\ of\ transformer\ substations\ in\ the\ network} \quad (5.6.2.)$$

$$total\ information\ loss\ (\%) = faults\ with\ information\ loss\ (\%) \times information\ loss\ for\ faults\ after\ CB\ (\%) \quad (5.6.3.)$$

To summarise, total information loss is the multiplication of the percentage of faults that are not monitored completely (formula 5.6.1.), calculated as a share of overhead lines length, and the percentage of information loss for these faults, represented by the share of transformer substations that experience voltage dips that are not registered properly (formula 5.6.2.).

The simple methodology presented in this subchapter is especially useful to assess the need for installation of PQ monitors to monitor voltage dips in the following MV distribution networks:

- MV distribution networks with circuit breakers only installed in the feeding HV/MV transformer substation
- MV distribution networks with low number of circuit breakers apart from the circuit breakers installed in the feeding HV/MV transformer substation

If the information loss is not negligible, and there are more circuit breakers on the MV feeders, a methodology presented in [59] can be used. The paper [59] presents a method to placement of power quality monitors (PQMs) by using the multivariable regression (MVR) model, the Cp and R^2 statistical indices. Fault data in each bus, initially in this method, is collected and then the correlation coefficient which show the relationship between buses during system disturbances are calculated, based on which two or three buses with the highest correlation coefficient values are identified. Based on the results, these buses are considered as the most sensitive buses in the system. The identified bus voltages are then considered as independent variables in the developed MVR model to estimate the other bus voltages. Two or three buses that have maximum and minimum frequency of the calculated correlation coefficient, Cp and R^2, are selected and then the appropriate number and placement of PQMs is then determined based on the lowest value of the Cp and a suitable value of the R^2 [59]. The approach in [59] can be integrated with this PhD research by way of first modelling faults in all the busses and collecting the data which serves as an input for regression (MVR). The difference is that:

i) The regression (MVR) coefficients should be calculated and not the correlation coefficient and

ii) The criteria for choosing the PQM locations is only R^2 and not Cp and R^2.

Of course, another possible approach is to install a PQ monitoring device behind the circuit breaker, which would give the information about the outage behind the circuit breaker and a range for the voltage dip in front of the circuit breaker, which is limited by the dip behind the circuit breaker (prior tripping) and the dip at the HV/MV station.

5.7 MVR Optimal Placement of PQ Monitors

5.7.1 General Approach

This subchapter explains the methodology for optimal placement of PQ monitors. In this thesis, linear regression is used to establish linear relationships between time series (weekly or monthly) of PQ parameters for different nodes in the network. Different choice criteria are used to choose the optimal minimal number of PQMs. MATLAB was used in this research to implement the methodology. The main steps of the methodology for optimal PQ monitor placement are given below:

1. Step 1: Import the results of modelling of PQ parameters (harmonics, flicker, unbalance) for a longer time period (one week or month)
2. Step 2: In every iteration a complete MVR calculation for all the busses is done, for considered PQM configuration and for all three PQ parameters separately
3. Step 3: At the end of the iteration, the results from different PQ parameters are combined and joint stopping and choice criteria for PQ monitors are applied in order to find optimal locations of PQ monitors

Step 1 is done only once at the beginning, while steps 2 and 3 are calculated in iterations until optimal PQ placement configuration is reached.

5.7.2 Step 1: Import of PQ Parameter Modelling Results

Results of modelling of PQ parameters in the analysed network, for longer periods of time (week, month) serve as an input to the MVR calculation. Modelling of harmonics, flicker and unbalance is explained in the previous subchapters (5.3, 5.4 and 5.5). Results for all the nodes in the network are used.

5.7.3 Step 2: Complete MVR Calculation

MVR has been used to explain the relationships of PQ parameters in every node in the network based on configuration of one or several PQ monitors. Forward selection method is used in every iteration to build a configuration of PQ monitors, i.e. PQ monitors are added to the configuration one by one in steps starting from zero PQMs. In this step one PQM is added in every iteration, with complete MVR calculation performed for every possible location of that PQM in the network. Next step 3 is used to choose the optimal one PQM location from all the nodes. MVR has been calculated for every PQ parameter before applying the choice criteria.

5.7.4 Step 3: Goodness of Fit Criteria

Implementation of different goodness of fit choice criteria for PQM locations was tested (R^2, MSE, AIC, BIC, Mellow's Cp), and R^2 has been chosen as the most suitable criterion. R^2 is easy to understand, comprehend and physically link with real life state of PQ, since it represents the variability explained by the regression model. E.g. R^2=0.9 represents a model where 90% of variability is explained by the regression model and 10% is not explained. In this way used of the model can easily comprehend the goodness of fit of the model. In this research, two R^2 criteria were applied, one R^2_{min} as a model stopping criteria and other R^2_{avg} for choosing PQM locations:

1. R^2_{min} - Minimum variability explained by the model as a stopping criterion for the model

R^2_{min} = 0.9 is the minimum variability explained by the model, which is used as a stopping criteria for the PQM placement model. R^2_{min} is the minimum value of R^2 among all the PQ parameters and all the nodes. This stopping criteria needs to be satisfied for every node and for every PQ parameter for the iterative algorithm to be stopped. It is assumed that 0.9 is a reasonable value but it can be adapted easily if necessary. This criterion ensures adequate minimum observability of the complete network i.e. all its busses and all the PQ parameters, and PQ monitors are added in a forward selection method, until this criterion is met for all the PQ parameters and all the nodes in the networks. When all the busses are monitored above this threshold, the adding of PQMs is stopped.

2. R^2_{avg} - Weighted average criterion for choosing the PQM locations

PQM locations are among different possible locations chosen based on a weighted average of R^2_{avg}, representing the average value of R^2 for complete network (all the nodes) and all the PQ parameters. The formula for calculating is R^2_{avg}:

$$R^2_{avg,i} = w_5 w_h R^2_{h5} + w_7 w_h R^2_{h7} + w_f R^2_f + w_u R^2_u \quad (5.7.1.)$$

$$R^2_{avg,i} = \sum_{i=1}^{N} R^2_{avg,i} \Big/ N$$

where:

w_5=0.5, w_7=0.5

w_h=0.2, w_f=0.5, w_u=0.3

N – number of nodes

are the weighting factors for two analysed harmonics (w_5 and w_7) and weighting factor for harmonics (w_h), flicker (w_f) and unbalance (w_u). Weighting factors for different PQ parameters were defined based on the importance of PQ parameters and closeness of their values in the analysed to the EN 50160 limits. Therefore, flicker has the highest value as a parameter which occasionally exceeds the limits, followed by unbalance and harmonics. It was assumed that both harmonics (5th and 7th) have the same impact. This distribution of the choice criteria can of course be defined according to the preferences of DSO. It's evident that in this way there will be different weighting factors in different grids, depending on the actual PQ situation. Alternatively, regulation authorities could define general weighting factors. They could be based for instance on economic consequences of violated PQ limits.

One advantage of the used method is that after the MVR calculation, coefficients are obtained to explain the behaviour in all the nodes in the network based on the chosen PQM configuration. This means that after the PQM configuration is installed in the network, an almost complete observability of all the network nodes can be achieved.

In this research, optimisation algorithms were not used as a part of the methodology, since only few monitors were needed to monitor the whole network. Generally, if only a small number of monitors are needed, optimisation is not necessary, since the optimal solution can be achieved by forward selection method with reasonable computational work time to solve the problem. However, for larger networks, optimisation in a huge solution space might be necessary.

In such case when more monitors are needed, works of other researchers can be used, e.g. work [10], that used genetic algorithm and Mellow's Cp to find the optimal solution, which can be integrated with the work of this PhD thesis. The study [10] presents a method to determine the optimal number and placement of power quality monitors (PQMs) in power systems by using genetic algorithm and Mallow's Cp. Mallow's Cp is a statistical criterion for selecting among many alternative subset regressions. In the conventional monitor reach area based (MRA) method, this procedure helps to avoid the dependency of set voltage sag threshold values of PQMs. In the proposed Genetic Algorithm Cp (GACp) method, the fitness function for problem modelling aims to minimize allocated monitors and minimize the difference between the Mallow's Cp and the number of variables used for the multivariable regression model during estimation of unmonitored buses. After obtaining the optimal placements of PQMs by using the GACp method, the observability and redundancy of the monitors are tested to further reduce the redundant PQMs. Using the DIgSILENT Power Factory software the IEEE 30 bus test system is simulated to validate the proposed method. The simulated results show that the GACp method requires only two PQMs to observe all voltage sags that may appear at each bus in the test system without redundancy [10]. The way to integrate the work of [10] with this PhD research is to add genetic algorithm on top of the methodology used in this PhD thesis.

5.7.5 Performed optimal PQM location calculations

In this thesis, four different results of MVR algorithm were calculated and compared:

1) MVR algorithm defines PQM locations
   This run calculated the PQM locations as given exactly by MVR, without any interventions in terms of fixing some solutions beforehand
2) 1st location is fixed, MVR algorithm defines the rest of PQM locations
   This run calculated the PQM locations in a way that the 1st location is fixed beforehand (MV busbars of feeding HV/MV transformer substation) while the 2nd location is calculated by MVR
3) Current PQM configuration in the analysed network
   This run calculates the MVR parameters for a configuration of existing two PQM monitors in the network
4) Global optimum solution
   This run calculates the true global optimum solution by choosing the best solution among all the possible PQM configurations

6 APPLICATION ON A REAL MV DISTRIBUTION GRID

6.1 Modelling of Harmonics

The large parts of this subchapter 6.1 were previously published by the author of this thesis in [3].

In this section the results of harmonic the load flow simulations, performed in the chosen software tool by using the methodology explained in subsection 5.3, are presented and compared with measurements from existing PQ monitors. The results are presented in Figs. 6.1.1. – 6.1.4. with the following line notation [3]:

- Measurements from existing PQ monitors (blue solid line)
- Results of simulations with modelling of harmonic source models according to the IEC 61000-3-6 summation law (red dotted line)
- Results of simulations with modelling of harmonic source models using complex phasors (green dashed line)

The results of the 5th and 7th harmonic voltages are presented for two sites [3]:

- Site 1: 110/30 kV substation – 30 kV bus (PQM 5, 6)

- Site 2: 30/0.4 kV substation – Feeder 1 – 30 kV bus (PQM 1)

The results for other sites in the analysed network are not presented in this thesis, since a great similarity in their trend with the two presented sites was noticed. It was observed that the voltage harmonics have the lowest value at the 30 kV buses of primary 110/30 kV substation (site 1), due to the highest short circuit capacity, and increase on the 30 kV feeders. The harmonic voltages have the highest value, among sites with PQ measurement, on the analysed site 2. The position of the analysed sites in the network can be seen from Fig. 5.2.2. in section 5.2.1. [3].

Results for site 1 are shown in Figs. 6.1.1. – 6.1.2., while the results for site 2 are shown in Figs. 6.1.3. – 6.1.4. The magnitudes of the harmonic voltages for site 2 are noticeably higher than the magnitudes for site 1, but the weekly trend is very similar between the two sites. It can be seen that the results of the simulations have a rather good match with the measurement results for both sites and for both the 5th and the 7th harmonic voltages, with the exception of the 7th harmonic in the method using complex phasors. Comparing to the PQ measurements, the results of the method according to the IEC 61000-3-6 summation law are in total better than the results of the method using complex phasors [3].

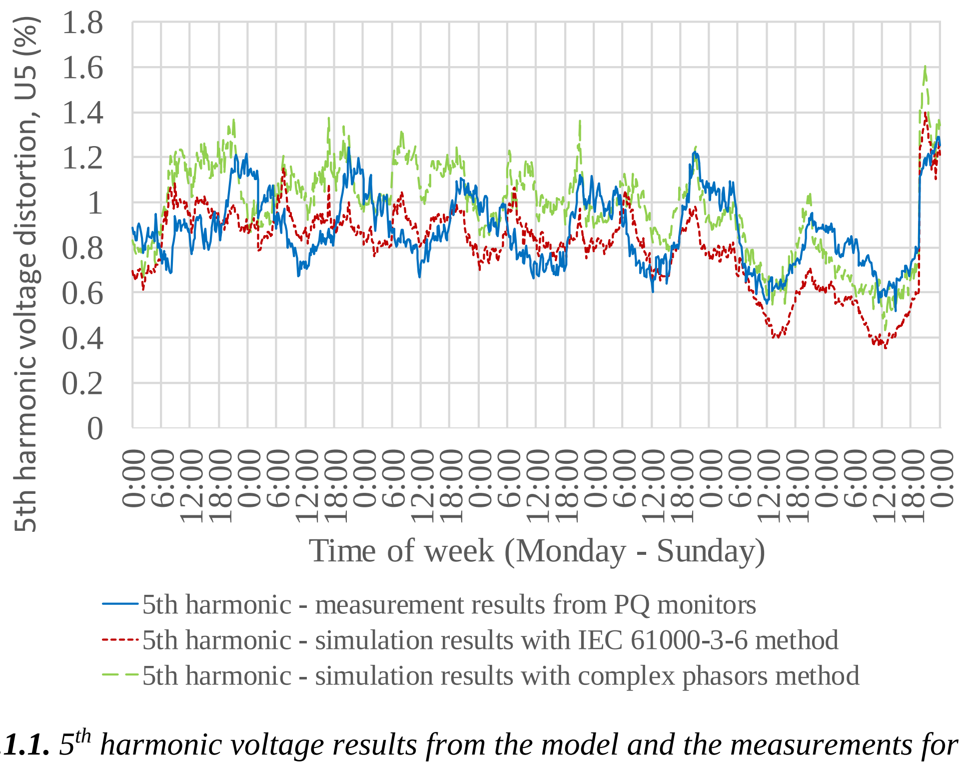

Fig. 6.1.1. *5th harmonic voltage results from the model and the measurements for site 1*

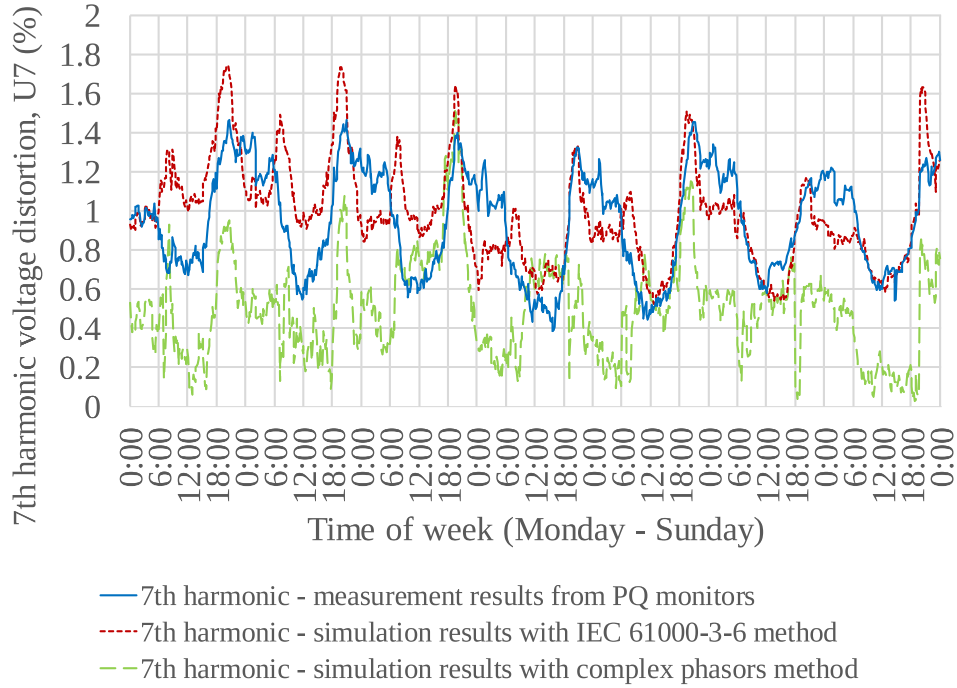

Fig. 6.1.2. *7th harmonic voltage results from the model and the measurements for site 1*

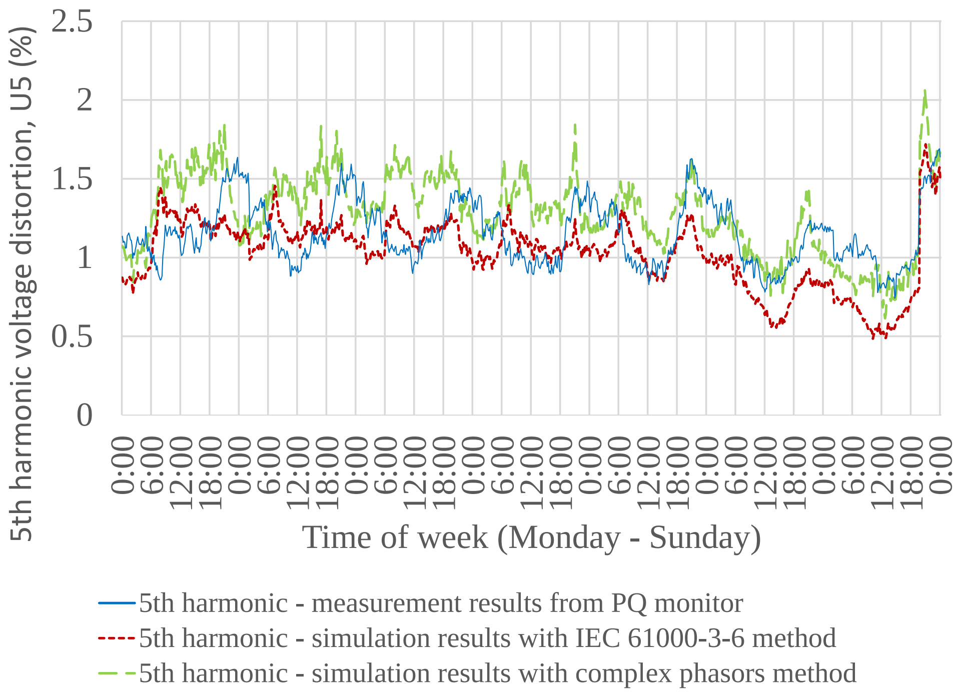

Fig. 6.1.3. *5th harmonic voltage results from the model and the measurements for site 2*

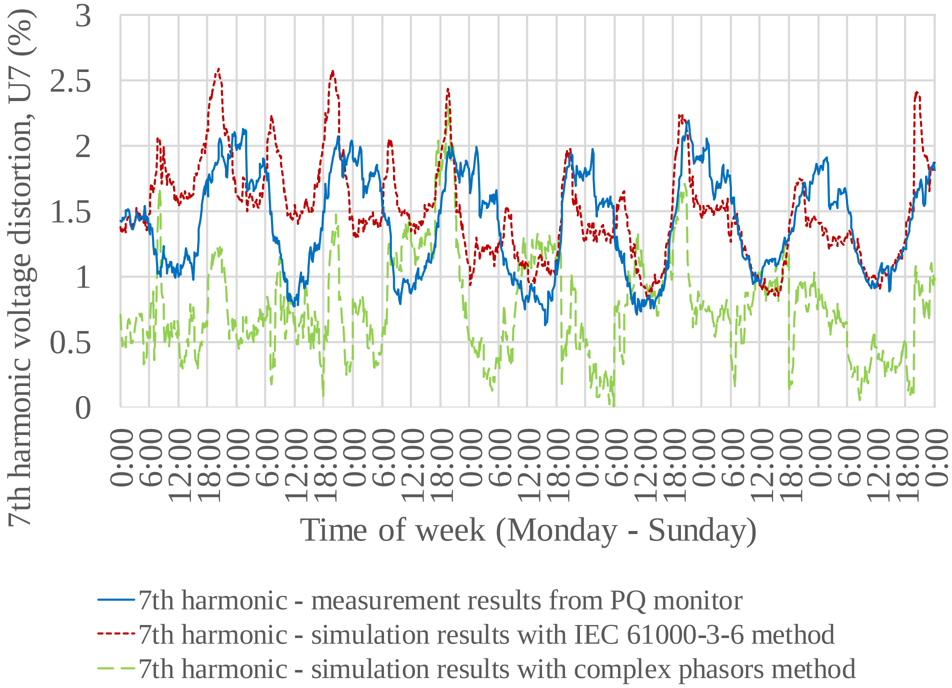

Fig. 6.1.4. *7^th^ harmonic voltage results from the model and the measurements for site 2*

In order to statistically quantify the results presented in Fig. 6.1.1. – 6.1.4. and compare them, different percentage quantiles (50%, 90%, 95%, 99%) were calculated for all the presented results. These quantiles are given in Table 6.1.1. for site 1 and in Table 6.1.2. for site 2. The quantiles also prove that the simulations have provided rather good results compared to the measurements. The quantiles also show that the results of the method according to the IEC 61000-3-6 summation law are noticeably better than the results of the method using complex phasors [3].

Table 6.1.1. *Statistical voltage harmonic quantiles of the results of the simulations and the measurements for site 1*

	Quantile			
Result	50%	90%	95%	99%
5th harmonic voltage				
PQ monitors measurements	0.86	1.10	1.15	1.23
Simulations - IEC 61000-3-6	0.83	0.98	1.03	1.27
Simulations - complex phasors	0.99	1.20	1.25	1.41
7th harmonic voltage				
PQ monitors measurements	0.97	1.29	1.35	1.42
Simulations - IEC 61000-3-6	0.96	1.34	1.50	1.71
Simulations - complex phasors	0.50	0.79	0.95	1.30

Table 6.1.2. *Statistical voltage harmonic quantiles of the results of the simulations and the measurements for site 2*

	Quantile			
Result	50%	90%	95%	99%
5th harmonic voltage				
PQ monitor measurements	1.12	1.44	1.52	1.62
Simulations - IEC 61000-3-6	1.06	1.26	1.31	1.57
Simulations - complex phasors	1.29	1.59	1.65	1.84
7th harmonic voltage				
PQ monitor measurements	1.44	1.90	1.98	2.11
Simulations - IEC 61000-3-6	1.45	2.01	2.23	2.53
Simulations - complex phasors	0.71	1.24	1.36	2.01

The following paragraphs present the results of harmonic voltage propagation in the analysed large real MV distribution network. The propagation of harmonic voltages is expressed in this research as a ratio between the values of harmonic voltages at different nodes on MV feeders (location of PQM 1, 2, 3, 4 – Fig. 5.2.2.) and at the primary 110/30 kV transformer substation (location of PQM 5 – Fig. 5.2.2.) [5]:

$$r_{Uh} = \frac{Uh_{PQM\,X}}{Uh_{PQM\,5}} \quad (6.1.1.)$$

The results for the two harmonic source modelling methods are firstly presented as weekly trends of ratio between the node with PQM 1 installed (node with the highest harmonic values among all nodes with PQMs) and the 30 kV bus at the primary 110/30 kV substation (PQM 5). Fig. 6.1.5. presents the ratios of 5th harmonic voltage, while Fig. 6.1.6. presents the ratios of 7th harmonic voltage. As can be seen from Figs. 6.1.5. and 6.1.6., the results of the simulations show a very good match with the measurements. The only results that are not presented are the 7th harmonic voltages for the method of modelling using complex phasors, since this method is much more sensitive to input data uncertainty, which is often to be expected when large distribution networks are analysed [5].

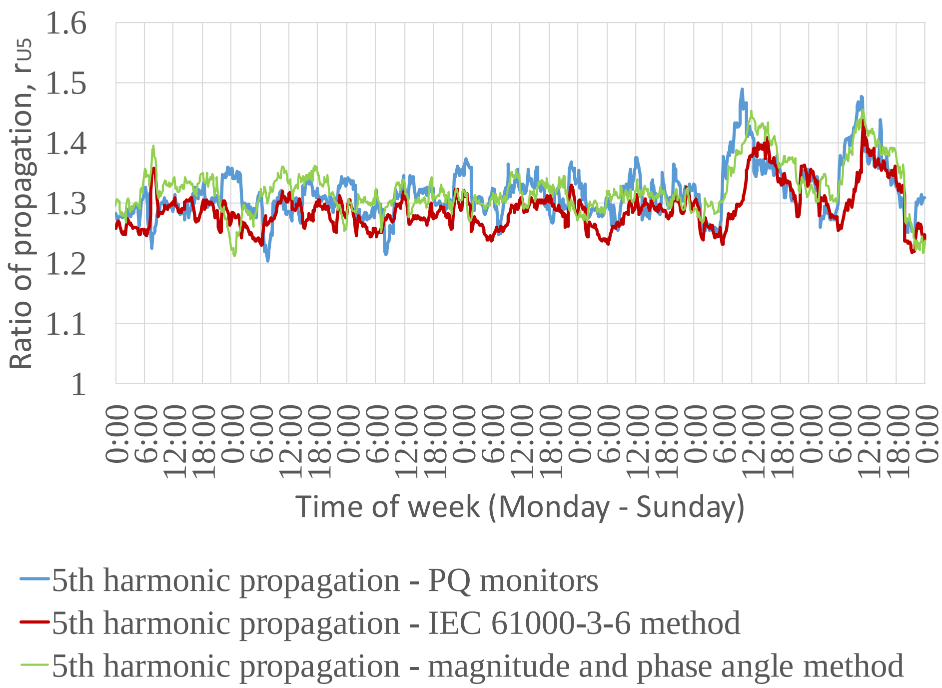

Fig. 6.1.5. *Ratios of 5th harmonic voltage from PQ measurements and simulations (between node of PQM 1 and node of PQM 5 - Fig. 5.2.2.)*

The time characteristic of the ratios is statistically analysed and presented as 95% quantiles, between all the nodes in MV feeders with PQMs installed (PQM 1, 2, 3, 4 - Fig. 5.2.2.) and 30 kV bus at 110/30 kV substation (PQM 5 - Fig. 5.2.2.). The results are shown in Table 6.1.3., and it can be seen that a very good match between the measurements and the simulations was achieved for both modelling approaches [5].

Table 6.1.3. Ratios of 95% quantiles of harmonic voltages from PQ measurements and simulations

	PQM 3	PQM 2	PQM 4	PQM 1
<u>5th harmonic</u>				
PQ measurements	1.02	1.05	1.02	1.32
IEC 61000-3-6 method	1.01	1.03	1.06	1.28
Complex phasor method	1.01	1.03	1.06	1.32
<u>7th harmonic</u>				
PQ measurements	1.02	1.04	1.06	1.47
IEC 61000-3-6 method	1.01	1.02	1.07	1.49

The errors between the simulations and the measurements are assessed by mean absolute error (MAE) and mean absolute percentage error (MAPE). The errors are calculated both for the ratio and the time characteristic of the magnitudes of harmonic voltages. The errors are calculated for weekly time series of all the analysed nodes with PQMs [5].

MAE errors for the ratios are between 0.006 and 0.051 for 5^{th} harmonic and 0.007 and 0.046 for 7^{th} harmonic, while the MAPE errors are in the range between 0.6% and 6.2% for 5^{th} harmonic and 0.7% and 3.1% for 7^{th} harmonic. For time characteristics of the magnitudes of harmonic voltages, MAE errors are between 0.15% and 0.23% for 5^{th} harmonic and 0.19% and 0.32% for 7^{th} harmonic, while the MAPE errors are in the range between 17.8% and 22,4% for 5^{th} harmonic and 21.5% and 24.3% for 7^{th} harmonic. These ranges cover both modelling approaches [5].

Even though the errors for the ratios are rather small, the errors for the time characteristics of the magnitudes of harmonic voltages point out that the perfect match between the measurements and the simulations was is achieved. The errors come from the differences in weekly trends between the measurements and the simulations. The exact reproduction of the weekly trend is very challenging and comes from many uncertainties related to modelling the enormous number of harmonic sources and their behaviour during the course of one week [5].

However, as for the optimal placement of PQM, the correct simulation of the propagation is much more important than reproducing exact weekly trends, the envisaged accuracy of the simulations with respect to the goal has been fully achieved [5].

In Figs. 6.1.7. – 6.1.8. scatter plots of 5^{th} harmonic voltage values, for all the nodes in the network with PQM installed, are shown from PQM measurements and IEC 61000-3-6 method model results respectively. Same figures for 7^{th} harmonic are shown in Fig. 6.1.9. – 6.1.10. It is evident from the figures that the clouds of 5^{th} and 7^{th} harmonic propagation are very similar between the

PQM measurements and the IEC 61000-3-6 method model, which is another confirmation of the validity of the model.

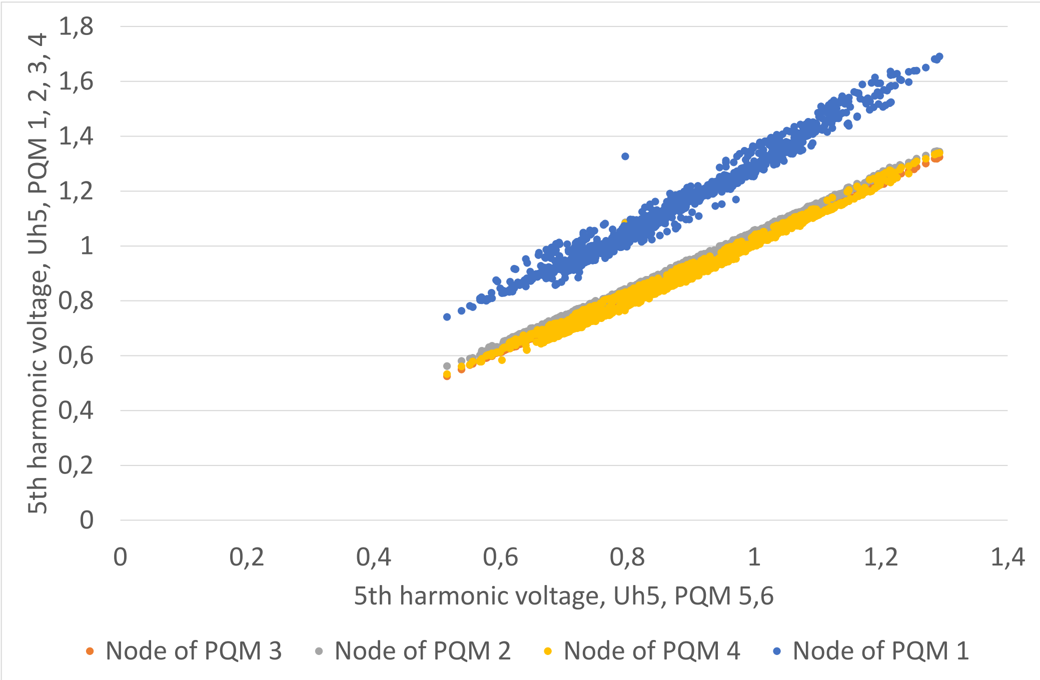

Fig. 6.1.7. *Scatter plots of 5th harmonic voltage values from PQM measurements, for all the nodes in the network with PQM installed*

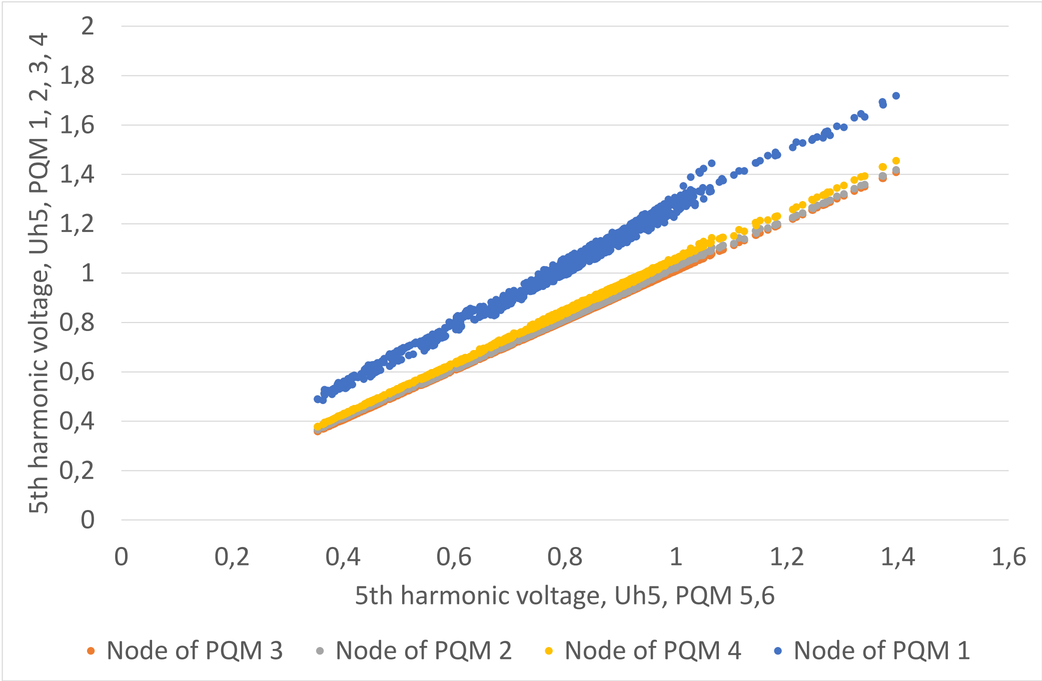

Fig. 6.1.8. *Scatter plots of 5th harmonic voltage values from the IEC 61000-3-6 method model, for all the nodes in the network with PQM installed*

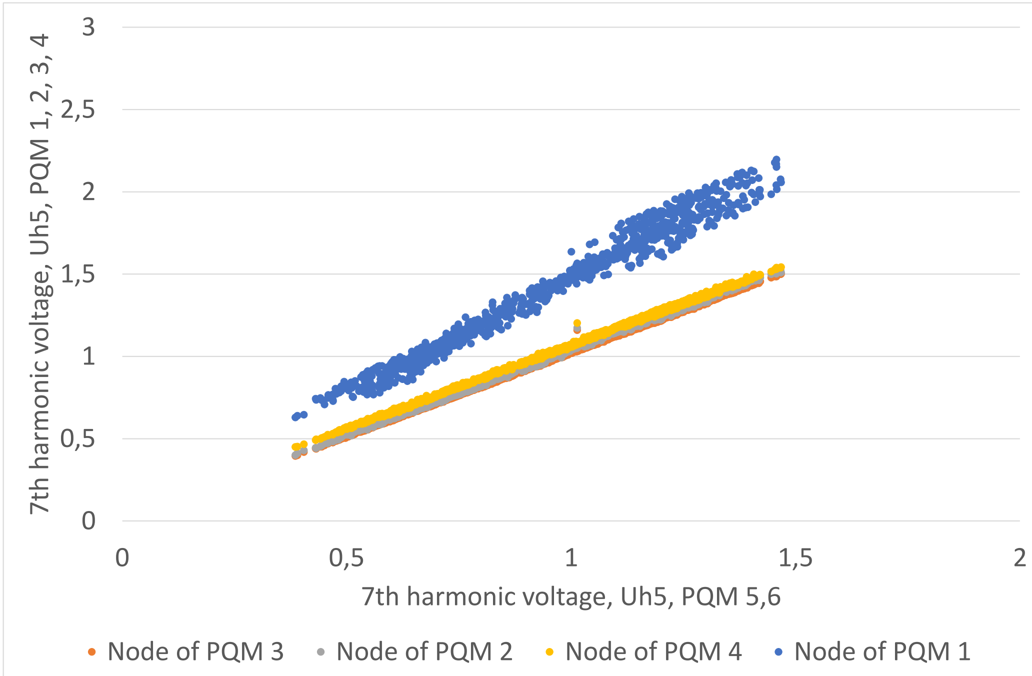

Fig. 6.1.9. *Scatter plots of 7th harmonic voltage values from PQM measurements, for all the nodes in the network with PQM installed*

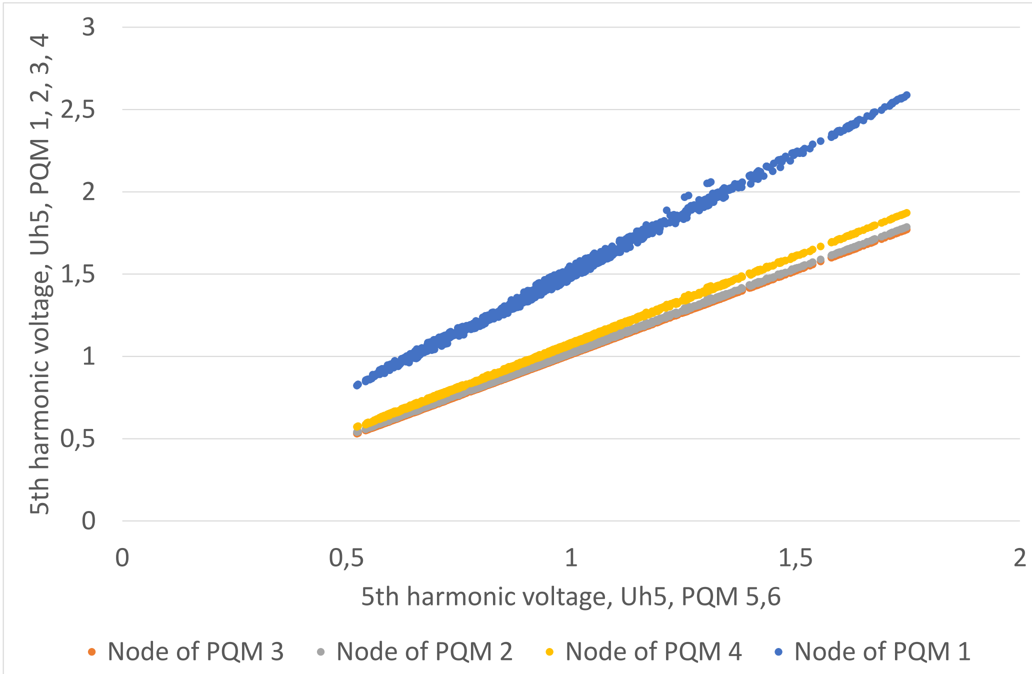

Fig. 6.1.10. *Scatter plots of 7th harmonic voltage values from the IEC 61000-3-6 method model, for all the nodes in the network with PQM installed*

Another merit of the validity of the model, presented in this thesis, is the comparison of coefficients of determination R^2,obtained after linear regression. The R^2 is the measure of variability explained by linear regression model. Tables 6.1.4. and 6.1.5. present the R^2 of the PQ measurements and the IEC 61000-3-6 method model respectively, for busses with PQM installed. From Tables 6.1.4. and 6.1.5. a great similarity can be seen, which is another confirmation of the validity of the model.

Table 6.1.4. *Coefficient of determination R2 for the PQ measurement results, for all the nodes with PQM installed*

Node	Node of PQM 5,6	Node of PQM 3	Node of PQM 4	Node of PQM 2	Node of PQM 1
Node of PQM 5,6	1,0000	0,9996	0,9875	0,9964	0,9749
Node of PQM 3	0,9996	1,0000	0,9877	0,9966	0,9748
Node of PQM 4	0,9875	0,9877	1,0000	0,9941	0,9738
Node of PQM 2	0,9964	0,9966	0,9941	1,0000	0,9781
Node of PQM 1	0,9749	0,9748	0,9738	0,9781	1,0000

Table 6.1.5. *Coefficient of determination R2 for the IEC 61000-3-6 method model results, for all the nodes with PQM installed*

Node	Node of PQM 5,6	Node of PQM 3	Node of PQM 4	Node of PQM 2	Node of PQM 1
Node of PQM 5,6	1,0000	1,0000	0,9991	0,9993	0,9918
Node of PQM 3	1,0000	1,0000	0,9993	0,9996	0,9924
Node of PQM 4	0,9991	0,9993	1,0000	0,9998	0,9939
Node of PQM 2	0,9993	0,9996	0,9998	1,0000	0,9937
Node of PQM 1	0,9918	0,9924	0,9939	0,9937	1,0000

In order to test the sensitivity of the simulation results, for the two used methods, to the uncertainties in the input data, a sensitivity analysis has been done. Table 6.1.6. shows the list and values of the key input parameters of the models, that have been taken for the sensitivity analysis. Sensitivity analysis for the method according to IEC 61000-3-6 summation law takes into account only input parameters no. 3 and no. 4, while the sensitivity analysis of the method with both magnitudes and phase angles modelled takes into account all the input parameters from Table 6.1.6.

Table 6.1.6. *Values of the simulation models input parameters taken for sensitivity analysis*

No.	Input parameter	Values in subsection 5.3	Values for sensitivity analysis
1.	Background harmonic voltage source phase angles taken as fixed	5^{th}: Fig. 5.2.4. 7^{th}: Fig. 5.2.4.	5^{th}: 75° 7^{th}: 110°
2.	Background harmonic voltage source phase angle variability	5^{th}: Fig. 5.2.4. 7^{th}: Fig. 5.2.4.	5^{th}: Fig. 5.2.4. ± 30° 7^{th}: Fig. 5.2.4. ± 45°
3.	Distribution of three office harmonic current source models	Uniform	Three scenarios (80/10/10%, 10/80/10%, 10/10/80%)
4.	Percentage of motors with VSDs for industry customers	30%	15% - 45%
5.	Harmonic emission of three-phase rectifier	No harmonic voltage pre-distortion	For U_5 = 3% and φ_{U5}=220°: I_5: +35% I_7: +24%
6.	Harmonic emission of three-phase rectifier	All rectifiers operate under nominal load	Rectifiers under 50% load: I_5(%): +50% I_7(%): +50%

Input parameters no. 1 and no. 2 take into account the uncertainties related to background harmonic voltage source model phase angles. Input parameter no. 1 models background harmonic voltage source model phase angles as fixed, while input parameter no. 2 models additionally a potential variability by shifting the phase angles in two scenarios by ± 30° (5th harmonic) and ± 45° (7th harmonic). Input parameter no. 3 models different distributions of three office harmonic current source models used in the model. These different distributions are modelled in three scenarios of domination for each harmonic current source model in the ratios 80/10/10%, 10/80/10% and 10/10/80%. Input parameter no. 4 takes into account the uncertainty regarding the estimated value of percentage of motors with VSDs for industry customers, and models these values in two scenarios with 15% and 45% values. Input parameters no. 5 and no. 6 deal with uncertainty related to harmonic emission of three-phase rectifier with dc-link inductance and capacitance, according to the results of [84]. Input parameter no. 5 models the impact of harmonic voltage pre-distortion of U_5 = 3% and φ_{U5}=220°, which result in I_5: +35% and I_7: +24%. Also, input parameter no. 6 models the harmonic emission of three-phase rectifier under 50% load, which results in I_5: +50% and I_7: +50%. For input parameter no. 6 two scenarios were tested, with harmonic emission of 100% and 50% of rectifiers operating under 50% load.

Results of the sensitivity analysis are shown in Figs. 6.1.11. – 6.1.12. for method according to IEC 61000-3-6 summation law and in Figs. 6.1.13. – 6.1.14. for method with both magnitudes and phase angles modelled. Results are shown only for site 1, as the most representative bus. The results colored in green zone on Figs. 6.1.11. – 6.1.14. represent a range between minimum and maximum value, obtained by varying all the input parameters from Table 6.1.6.

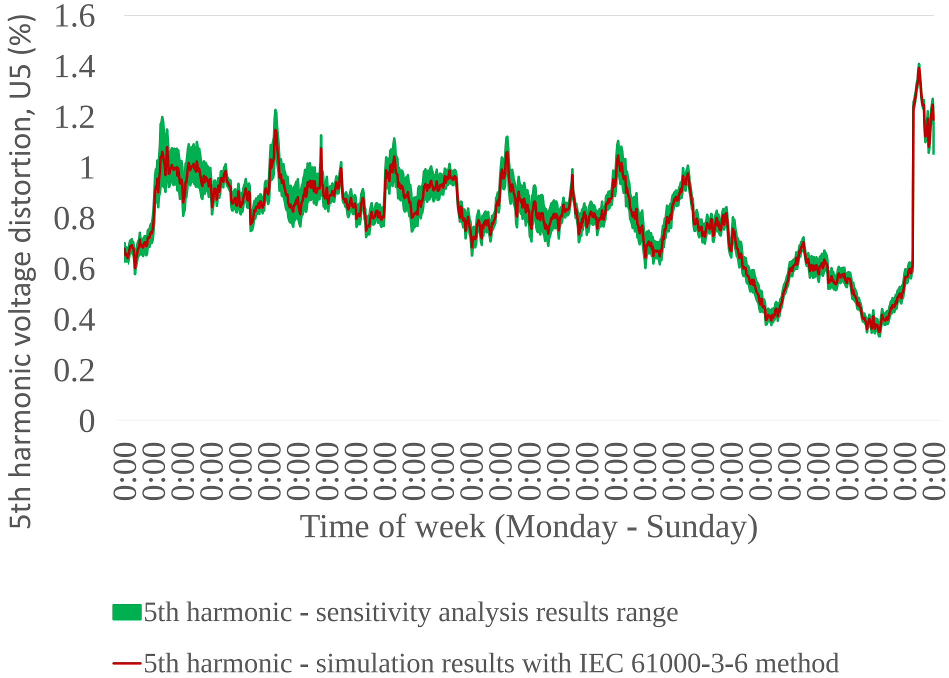

Fig. 6.1.11. *Sensitivity analysis results for 5th harmonic and method according to IEC 61000-3-6 summation law*

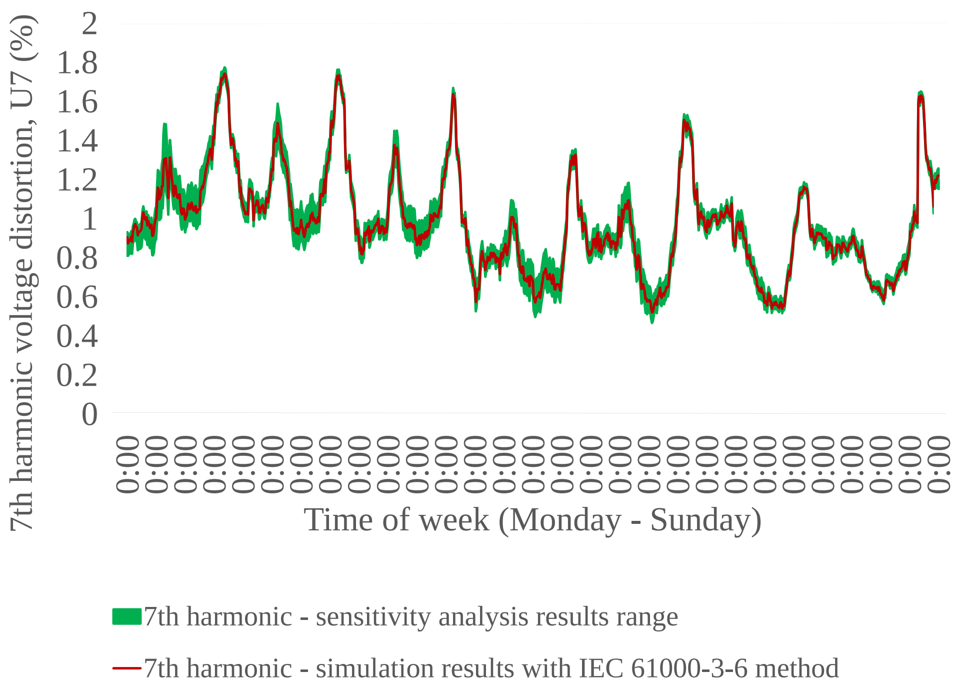

Fig. 6.1.12. *Sensitivity analysis results for 7th harmonic and method according to IEC 61000-3-6 summation law*

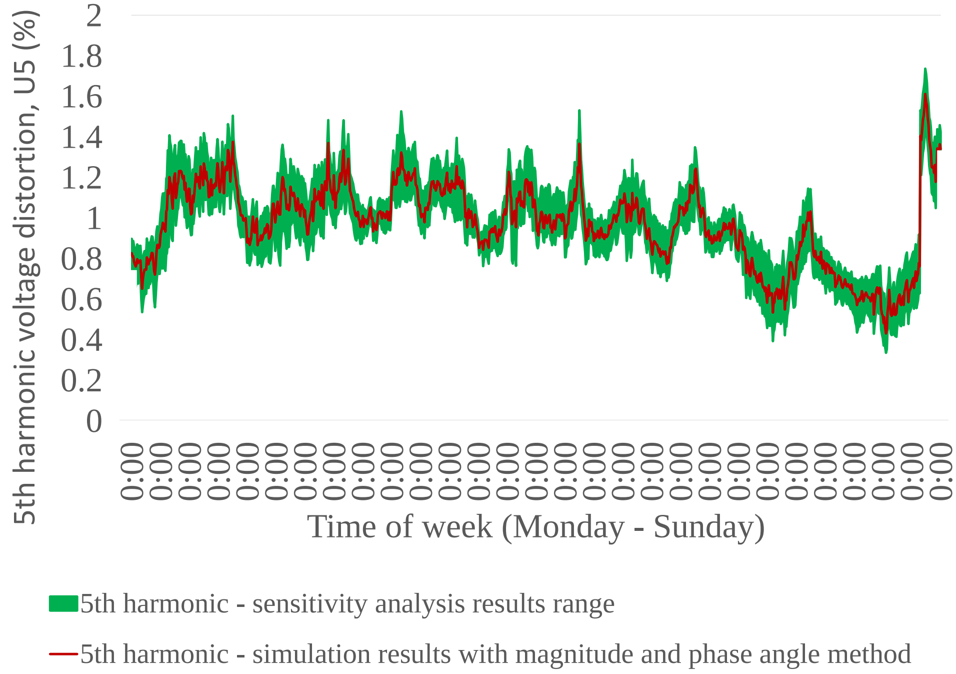

Fig. 6.1.13. *Sensitivity analysis results for 5th harmonic and method with both magnitudes and phase angles modelled*

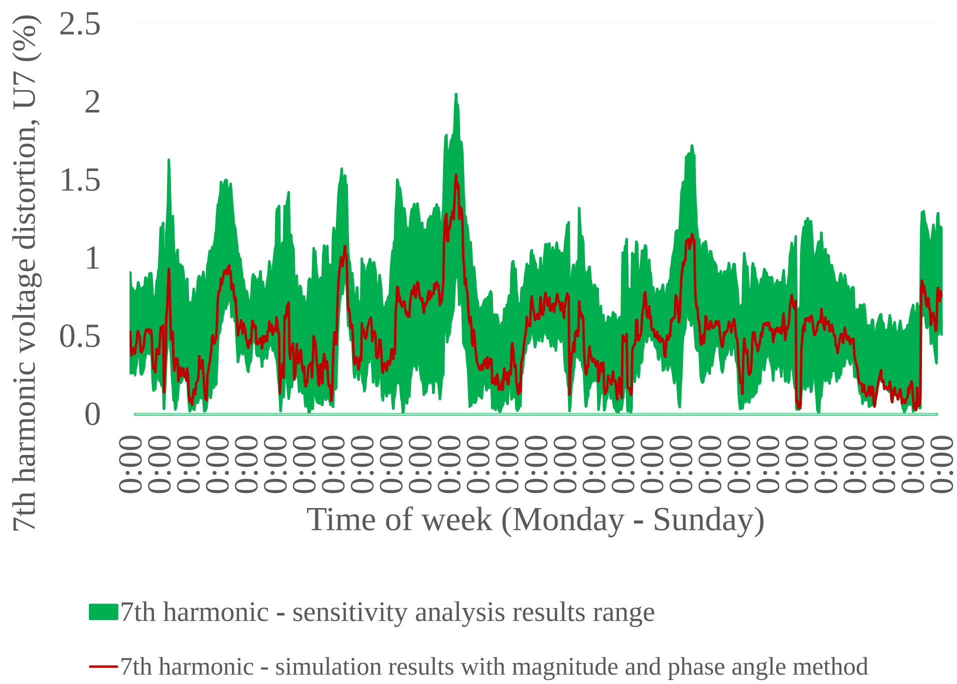

Fig. 6.1.14. *Sensitivity analysis results for 7th harmonic and method with both magnitudes and phase angles modelled*

As it can be clearly seen from Figs. 6.1.11. – 6.1.14., the method according to IEC 61000-3-6 has narrower green zone of sensitivity analysis results range and is therefore less sensitive to input data uncertainties. More detailed insight into sensitivity analysis of method with both magnitude and phase angle modelled revealed that this method is most sensitive to background harmonic voltage source phase angle variations, which can be attributed to large share of background harmonic distortion in the total harmonic distortion.

6.2 Modelling of Flicker

The large parts of this subchapter 6.2 were previously published by the author of this thesis in [6].

In Fig. 6.2.1. the PQ measurement results are shown for the node of PQM 1 for one month, while Fig. 6.2.2. presents the results of the model for the same month and node. Comparing these two graphs, we can see a great similarity between the results of the model and the measurements. This is therefore a verification of the validity of the model results. The majority of the flicker values throughout the month lay in the range 0.05 - 0.25 for both the measurements and the model. The largest flicker event in the measurements time series is P_{st}=2.69, but the y-axis in both graphs is shown only until the value of P_{st} = 1, for the sake of easier comparison. The large flicker events do not match in time because the model inserts stochasticity through the use of cdf curves in modelling background flicker (Fig. 5.4.2.), but the frequency of occurrence of the large flicker events is the same in the measurements and the model [6].

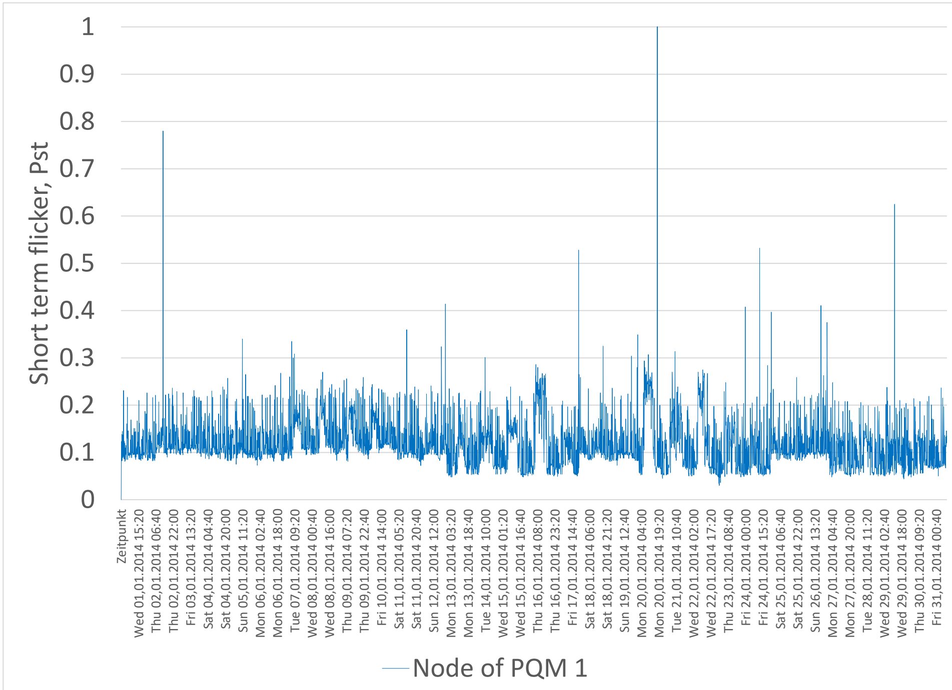

Fig. 6.2.1. *Monthly Pst graph for the node of PQM 1 - measurements*

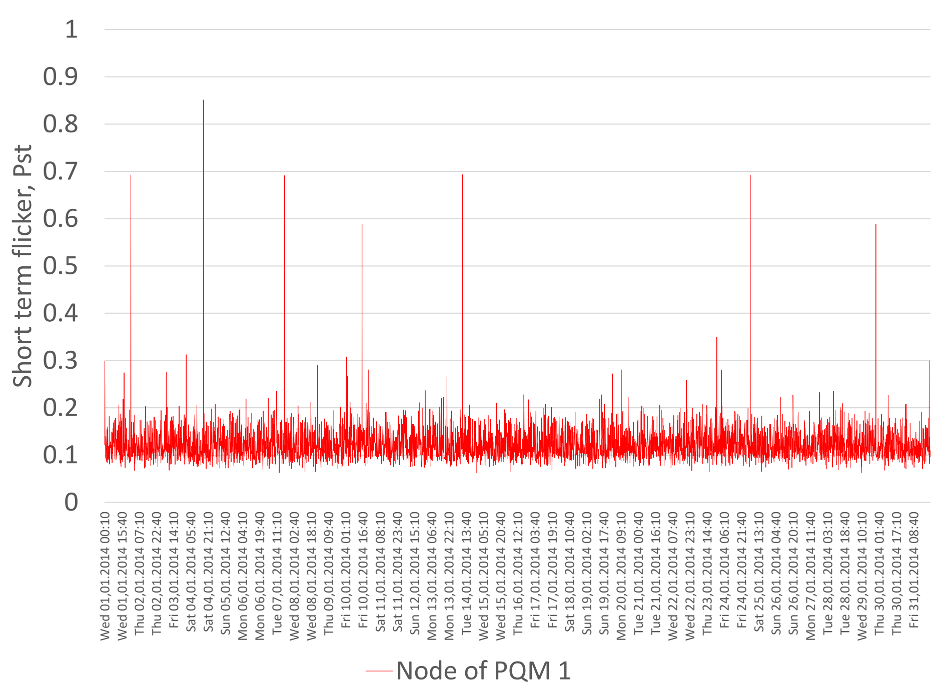

Fig. 6.2.2. *Monthly Pst graph for the node of PQM 1 – measurements – results of the model*

In order to present the propagation of the flicker throughout the network, both in measurement and model results, scatter plot graphs are made and shown in Fig. 6.2.3. and Fig. 6.3.4. Scatter plots for the measurements are shown in Fig. 6.2.3., while Fig. 6.2.4. shows scatter plots for the results of the model. All scatter plots represent the propagation of flicker between the main transformer substation (PQM 5 – 30 kV – x axis) and the feeders (PQM 1, 2, 3, 4 – y axis). For better comparison, only flicker values below $P_{st} = 1$ are shown, Fig. 6.2.3. and Fig. 6.2.4. show a great similarity between the scatter plot clouds of data points, which again confirms the validity of the model [6].

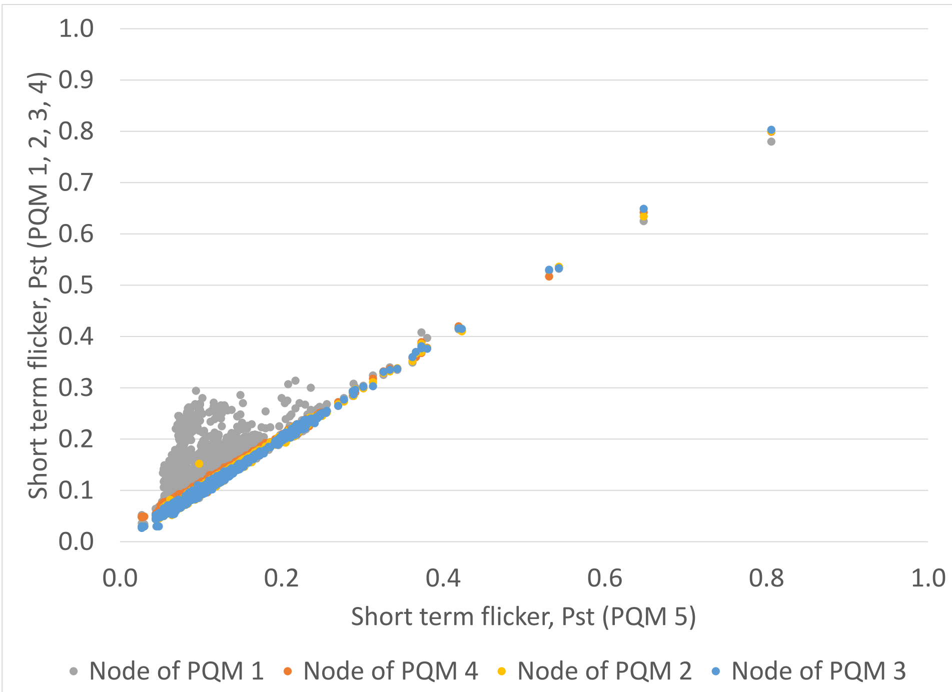

Fig. 6.2.3. *Scatter plots of PQ measurements for all the nodes in the network with PQM installed*

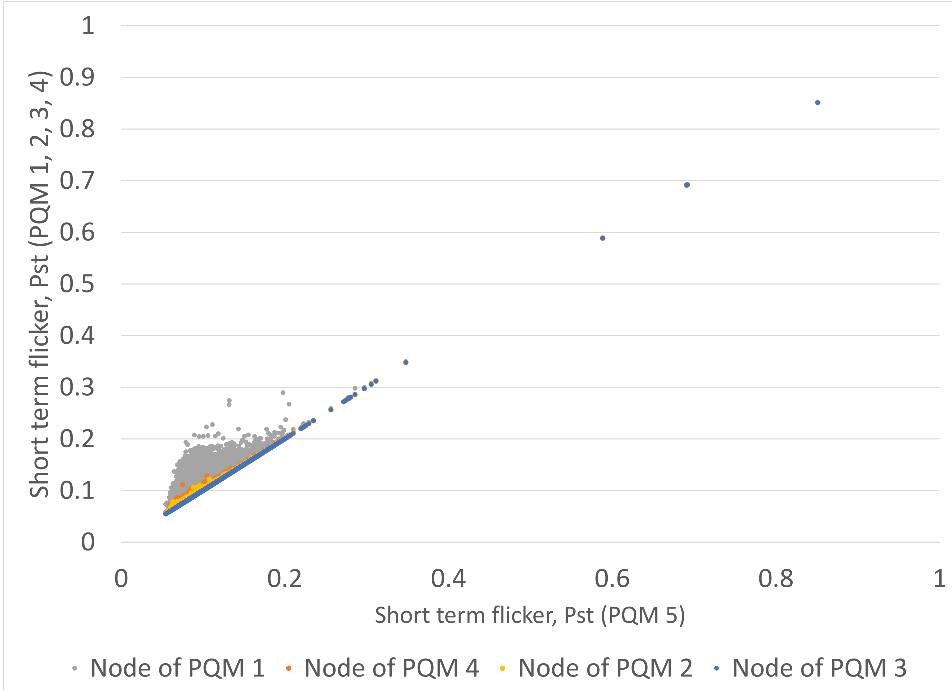

Fig. 6.2.4. *Scatter plots of model results for all the nodes in the network with PQM installed*

By analysing the results more in detail, it has been concluded that the dominant impact on flicker values comes from the largest industrial customers. The reason is their large P_{max} – maximum power, which leads to higher current variations and hence higher flicker in the network. Also, for some of the industries, higher flicker emission coefficients than for the other customer categories were assigned in order to match the measurements. The consequence of dominant industry impact is also that the results are very similar for both flicker modelling approaches noted in subsection 5.4.5.:

a) Every customer was modelled as a flicker source
b) Only one customer per each customer category in every secondary MV/LV transformer station was modelled

Both modelling approaches lead to very similar result. The explanation is that the flicker values are, due to cubic summation law, dominated by individual large industries, rather than by smaller customers that come in groups in MV/LV transformer substations (households, small commercial customers etc.) modelled in approach b) [6].

In order to statistically quantify the results presented in Fig. 6.2.1. – 6.2.2. and compare them, different percentage quantiles (50%, 90%, 95%, 99%) were calculated for all the presented results. These quantiles are given in Table 6.2.1. for node with PQM 5,6 and node of PQM 1. The quantiles also prove that the simulations have provided rather good results compared to the measurements.

Table 6.2.1. *Statistical flicker quantiles of the results of the measurements and the simulations for nodes with PQM 5,6 and PQM 1*

	Quantile			
Result	50%	90%	95%	99%
Node of PQM 5,6				
PQ measurements	0,10	0,14	0,20	0,23
Model results	0,10	0,15	0,16	0,20
Node of PQM 1				
PQ measurements	0,11	0,19	0,22	0,26
Model results	0,12	0,16	0,18	0,21

The results of flicker propagation in the analysed large real MV distribution network are presented below. The propagation of flicker is expressed in this research as a ratio between the values of flicker at different nodes on MV feeders (location of PQM 1, 2, 3, 4 – Fig. 5.2.2.) and at the primary 110/30 kV transformer substation (location of PQM 5 – Fig. 5.2.2.):

$$\mathrm{r_f} = \frac{\mathrm{Pst_{PQM\,X}}}{\mathrm{Pst_{PQM\,5}}} \qquad (6.2.1.)$$

The results for the flicker model are presented in Fig. 6.2.5. as weekly trend of ratio between the node with PQM 1 installed (node with the highest flicker values among all nodes with PQMs) and the 30 kV bus at the primary 110/30 kV substation (PQM 5). As can be seen from Figs. 6.2.5. the results of the simulations do not show a very good match with the measurements. The reason is the stochasticity of flicker because of which peaks of higher flicker values happen in different times between the measurements and the model. Achieving temporal element match was not the priority of this research, but rather was a relatively good propagation, proven by other graphs and tables in this subchapter.

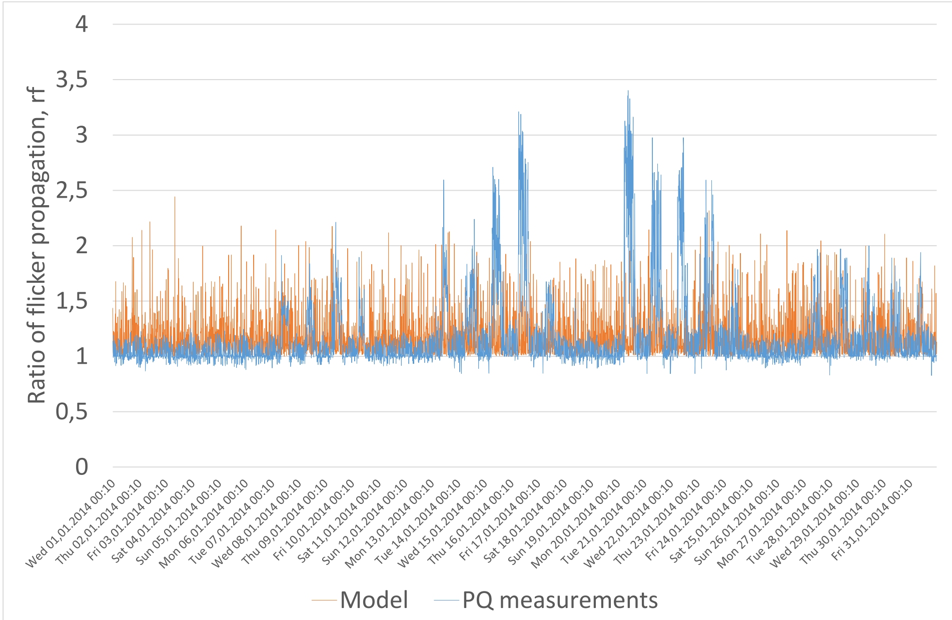

Fig. 6.2.5. *Transfer ratios of flicker from PQ measurements and simulations (between node of PQM 1 and node of PQM 5 - Fig. 5.2.2.)*

The time characteristic of the ratios is statistically analysed and presented as 95% quantiles, between all the nodes in MV feeders with PQMs installed (PQM 1, 2, 3, 4 - Fig. 5.2.2.) and 30 kV bus at 110/30 kV substation (PQM 5 - Fig. 5.2.2.). The results are shown in Table 6.2.2., and it can be seen that a very good match between the measurements and the simulations was achieved.

Table 6.2.2. Ratios of 95% quantiles of flicker from PQ measurements and simulations

	PQM 3	PQM 4	PQM 1	PQM 2
PQ measurements	1,00	1,01	1,10	0,99
Model results	1,00	1,00	1,09	1,00

Another merit of the validity of the model, presented in this thesis, is the comparison of coefficients of determination R^2,obtained after linear regression. The R^2 is the measure of variability explained by linear regression model. Tables 6.2.3. and 6.2.4. present the R^2 of the flicker PQ measurements and the method model respectively, for busses with PQM installed. From Tables 6.2.3. and 6.2.4. a great similarity can be seen, which is another confirmation of the validity of the model.

Table 6.2.3. *Coefficient of determination R^2 for the flicker PQ measurement results, for all the nodes with PQM installed*

Node	Node of PQM 5,6	Node of PQM 3	Node of PQM 4	Node of PQM 2	Node of PQM 1
Node of PQM 5,6	1,0000	0,9980	0,9935	0,9971	0,7873
Node of PQM 3	0,9980	1,0000	0,9931	0,9969	0,7867
Node of PQM 4	0,9935	0,9931	1,0000	0,9939	0,8066
Node of PQM 2	0,9971	0,9969	0,9939	1,0000	0,7912
Node of PQM 1	0,7873	0,7867	0,8066	0,7912	1,0000

Table 6.1.5. *Coefficient of determination R^2 for the flicker method model results, for all the nodes with PQM installed*

Node	Node of PQM 5,6	Node of PQM 3	Node of PQM 4	Node of PQM 2	Node of PQM 1
Node of PQM 5,6	1,0000	1,0000	0,9965	0,9990	0,7859
Node of PQM 3	1,0000	1,0000	0,9965	0,9990	0,7859
Node of PQM 4	0,9965	0,9965	1,0000	0,9955	0,7845
Node of PQM 2	0,9990	0,9990	0,9955	1,0000	0,7859
Node of PQM 1	0,7859	0,7859	0,7845	0,7859	1,0000

6.3 Modelling of Unbalance

In Fig. 6.3.1. the results of the model of unbalance are shown, during the analysed month of February. Results are shown for two nodes in the network:

- Node of PQM 1 (longest feeder in the network)
- Node of PQM 7,8 (110 kV) – feeding 110/30 kV substation

The results in Fig 6.3.1. show the increase of the unbalance voltage downstream the network towards the longest feeder, which is expected due to the impact of LV current unbalance sources. The increase is especially visible on some of the peaks in the lines.

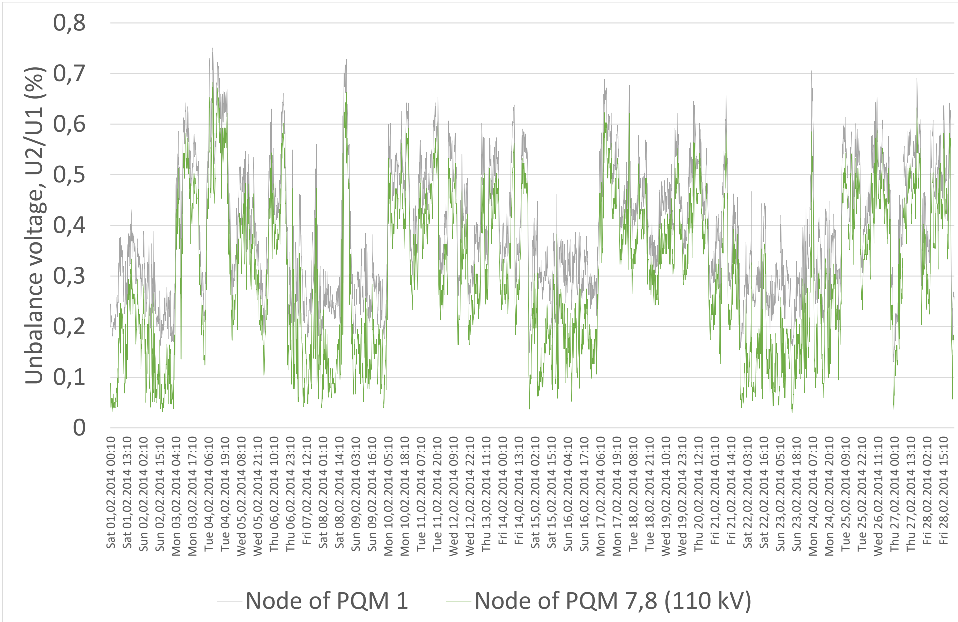

Fig. 6.3.1. *Voltage unbalance during the analysed month for nodes of PQM 1 and PQM 7,8 (110 kV)*

In order to present the propagation of the unbalance voltages throughout the network, scatter plot graph is made and shown in Fig. 6.3.2. Scatter plot represents the propagation of unbalance voltage between the main transformer substation (PQM 5 – 30 kV – x axis) and the feeders (PQM 1, 2, 3, 4 – y axis). It can be noticed that the scatter plot cloud is widest for feeder with PQM 1, which is a consequence of stochastic behaviour of customers and long lines and their impedances.

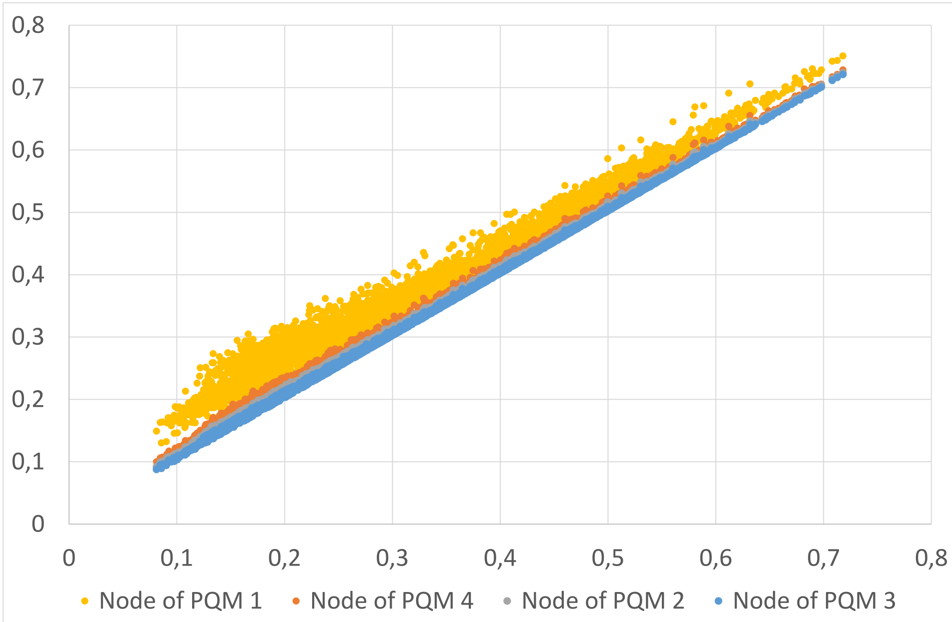

Fig. 6.3.2. *Scatter plot of unbalance voltage model results for all the nodes in the network with PQM installed*

In order to statistically quantify the results presented in Fig. 6.3.2., different percentage quantiles (50%, 90%, 95%, 99%) were calculated for all the presented results. These quantiles are given in Table 6.2.1. for node with PQM 5,6 and node of PQM 1.

Table 6.3.1. *Statistical voltage unbalance quantiles of the results of the simulations for nodes with PQM 5,6 and PQM 1*

	Quantile			
Result	50%	90%	95%	99%
Node of PQM 5,6				
Model results	0,33	0,53	0,57	0,63
Node of PQM 1				
Model results	0,38	0,57	0,61	0,67

The results of unbalance voltage propagation in the analysed large real MV distribution network are presented below. The propagation of voltage unbalance is expressed in this research as a transfer ratio between the values of voltage unbalance at different nodes on MV feeders (location of PQM 1, 2, 3, 4 – Fig. 5.2.2.) and at the primary 110/30 kV transformer substation (location of PQM 5 – Fig. 5.2.2.):

$$r_u = \frac{u2/u1_{\mathrm{PQM\,X}}}{u2/u1_{\mathrm{PQM\,5}}} \quad (6.3.1.)$$

The results for the unbalance voltage model are presented in Fig. 6.3.3. as weekly trend of transfer ratio between the node with PQM 1 installed (node with the highest flicker values among all nodes with PQMs) and the 30 kV bus at the primary 110/30 kV substation (PQM 5).

Fig. 6.2.5. *Ratios of unbalance voltages from simulations (between node of PQM 1 and node of PQM 5 - Fig. 5.2.2.)*

The time characteristic of the ratios is statistically analysed and presented as 95% quantiles, between all the nodes in MV feeders with PQMs installed (PQM 1, 2, 3, 4 - Fig. 5.2.2.) and 30 kV bus at 110/30 kV substation (PQM 5 - Fig. 5.2.2.). The results are shown in Table 6.3.2.

Table 6.3.2. Ratios of 95% quantiles of flicker from simulations

	PQM 3	PQM 4	PQM 1	PQM 2
Model results	1,00	1,00	1,09	1,00

Also, the coefficients of determination R^2, obtained after linear regression, are presented in Table 6.3.3. The R^2 is the measure of variability explained by linear regression model.

Table 6.3.3. *Coefficient of determination R^2 for the unbalance voltage method model results, for all the nodes with PQM installed*

Node	Node of PQM 5,6	Node of PQM 3	Node of PQM 4	Node of PQM 2	Node of PQM 1
Node of PQM 5,6	1,0000	0,9997	0,9986	0,9994	0,9840
Node of PQM 3	0,9997	1,0000	0,9994	0,9999	0,9872
Node of PQM 4	0,9986	0,9994	1,0000	0,9997	0,9912
Node of PQM 2	0,9994	0,9999	0,9997	1,0000	0,9889
Node of PQM 1	0,9840	0,9872	0,9912	0,9889	1,0000

The results of the model were not verified with PQ measurements, due to unavailability of correct PQ measurements for this PQ parameter. Therefore, this chapter did not include the results of unbalance voltage measurements.

6.4 Voltage Dips Consideration

According to the simple methodology presented in subchapter 5.6, total information loss was calculated when no PQ monitors are installed in the MV feeders (except at the main busbar in the feeding HV/MV transformer substation), and the results are presented in Table 6.4.1. The results of formula 5.6.1. show that for 6.04% of faults there is an information loss. For this portion of faults, there is an information loss of 17.57% of transformer substations not monitored correctly, as calculated by formula 5.6.2. Total information loss is the multiplication of these two percentages and according to the formula 5.6.3. total information loss is 1.06%.

Table 6.4.1. *Calculation of information loss if no PQ monitors are installed in the MV feeders to monitor voltage dips*

Variable	Value	Unit	Formula
Length of overhead lines after the CB	9.2	km	
Total length of overhead lines in the network	152.2	km	
Faults with information loss	6.04	%	5.6.1.
Number of transformer substations before CB	26		
Number of transformer substations in the network	148		
Information loss for faults after CB	17.57	%	5.6.2.
Total information loss	1.06	%	5.6.3.

Since total information loss if no PQ monitors are installed in the MV feeders to monitor voltage dips is only 1,06%, there is no economic justification to install PQ monitor in the green feeder 2 to monitor voltage dips (Figure 5.6.1.). Therefore, this simple methodology for considering voltage dips, presented in this thesis, proved to be useful for an analysed network, which has a low number of circuit breakers in MV feeders, apart from the circuit breakers at the MV cabinet in the feeding HV/MV transformer substation.

6.5 MVR Optimal Placement of PQ Monitors

In this thesis, four different results of MVR algorithm were calculated and compared:

1) MVR algorithm defines PQM locations
2) 1st location is fixed, MVR algorithm defines the rest of PQM locations
3) Current PQM configuration in the analysed network
4) Global optimum solution

1) MVR algorithm defines PQM locations

This is the solution calculated entirely by the MVR algorithm, according to the methodology presented in this thesis. The chosen PQM configuration is shown in Fig. 6.5.1.

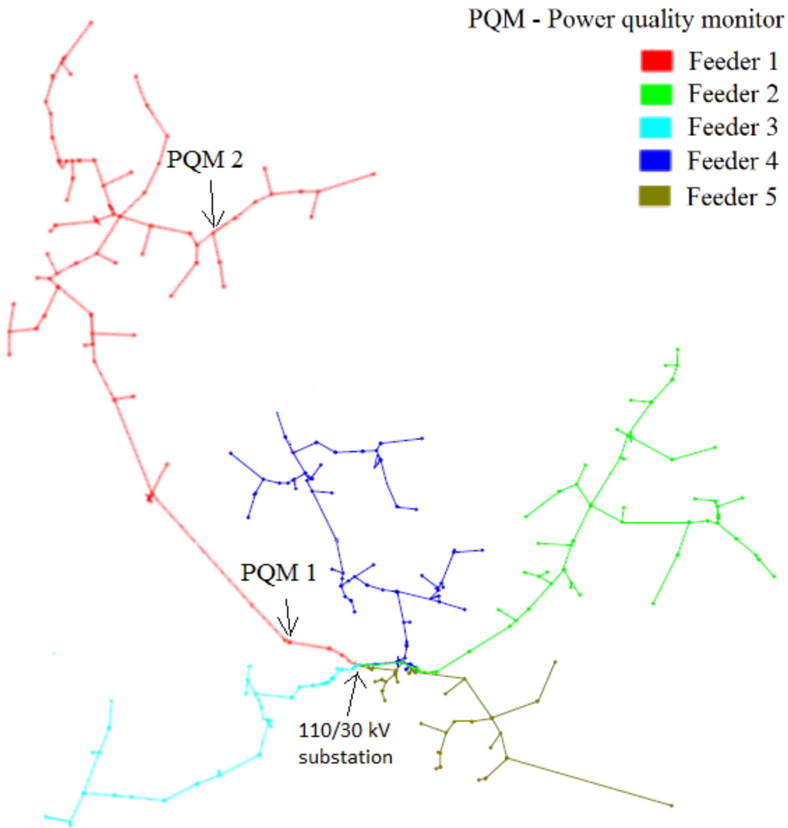

Fig. 6.5.1. *Geographical diagram of analysed MV network with locations of PQMs chosen by MVR algorithm*

For this PQM configuration, average and minimum coefficient of determination is:

$$\mathbf{R^2_{avg}=0{,}9995,\ R^2_{min}=0{,}9964}$$

It is evident that the network will be covered with great confidence with the suggested PQM configuration, since values of R^2_{avg} and, R^2_{min} are rather very high.

2) *<u>1st location is fixed, MVR algorithm defines the rest of PQM locations</u>*

This solution strives to be the most practical, with first PQM location set to be at the 30 kV busbars of the feeding 110/30 kV substation. This location is very much logical, since it represents the most important node of the 30 kV network, from which a huge portion of the network can be monitored. The second PQM location is chosen by MVR. PQM configuration is shown in Fig.6.5.2.

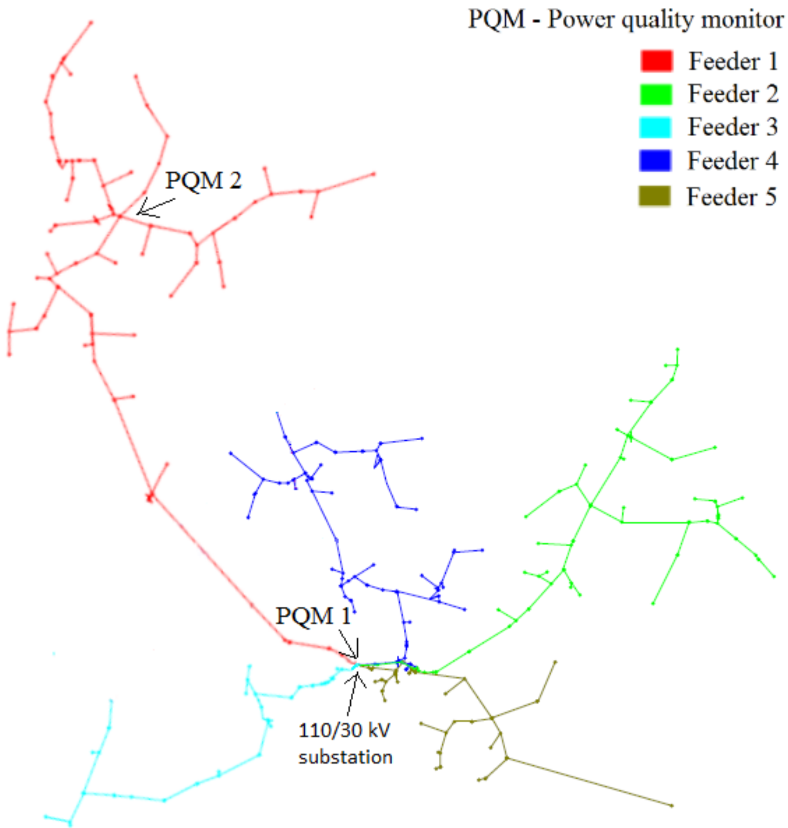

Fig. 6.5.2. *Geographical diagram of analysed MV network with locations of PQMs with 1st PQM location fixed and 2nd location chosen by MVR algorithm*

For this PQM configuration, average and minimum coefficient of determination is:

$$\mathbf{R^2_{avg}=0{,}9995,\ R^2_{min}=0{,}9965}$$

It can be sen that the values of R^2_{avg} and, R^2_{min} are very similar to the configuration entirely suggested by MVR. Therefore not much of the observability will be lost if this configuration is chosen as the final solution. Feeding 110/30 kV is already a location of PQM in existing configuration and it is easier not to change it.

3) *Current PQM configuration in the analysed network*

Current PQM configuration in the analysed network is consisted of 8 PQMs, where PQMs are installed in 4 out of 5 feeders. Current configuration of PQMs is shown in Fig. 6.5.3.. It is analysed here if only 2 PQMs are needed to monitor the analysed MV network with high confidence. The two proposed PQMs are:

i) PQM 1 in the feeding 110/30 kV transformer substation
ii) PQM 2 in the longest (red) feeder

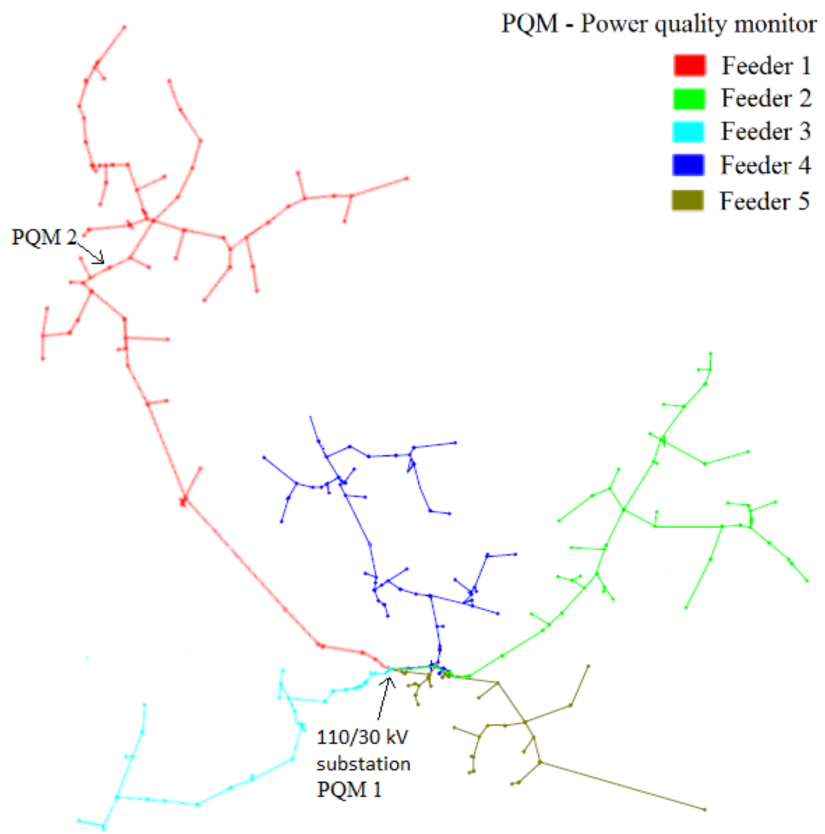

Fig. 6.5.3. *Geographical diagram of analysed MV network with feeder colouring and existing locations of PQMs*

For this PQM configuration, average and minimum coefficient of determination is:

$$\mathbf{R^2_{avg}=0{,}9995,\ R^2_{min}=0{,}9965}$$

which proves that only 2 PQMs from the current configuration are enough to monitor the complete network with high confidence. This proves that the presented MVR algorithm gives significantly less number of monitors than the existing configuration calculated using [28]. In similar manner, existing configurations of PQMs can be checked for other networks to analyse if they cover the network sufficiently.

4) <u>*Global optimum solution*</u>

Global optimum solution was obtained by calculating all the possible solutions with 2 PQMs (for 150 MV busses it is a total of 150^2=22.500 solutions), and choosing the best solution based on R^2 criterion. The graphical representation of the solution in shown in Fig. 6.5.4.

The need for a global optimum solution comes from the fact that MVR method chooses the first PQM that is optimal for configuration of only one PQM. The second PQM is chosen as an optimal solution, but when the first PQM is already chosen and fixed. This does not mean therefore that the combination of the two chosen PQMs is optimal.

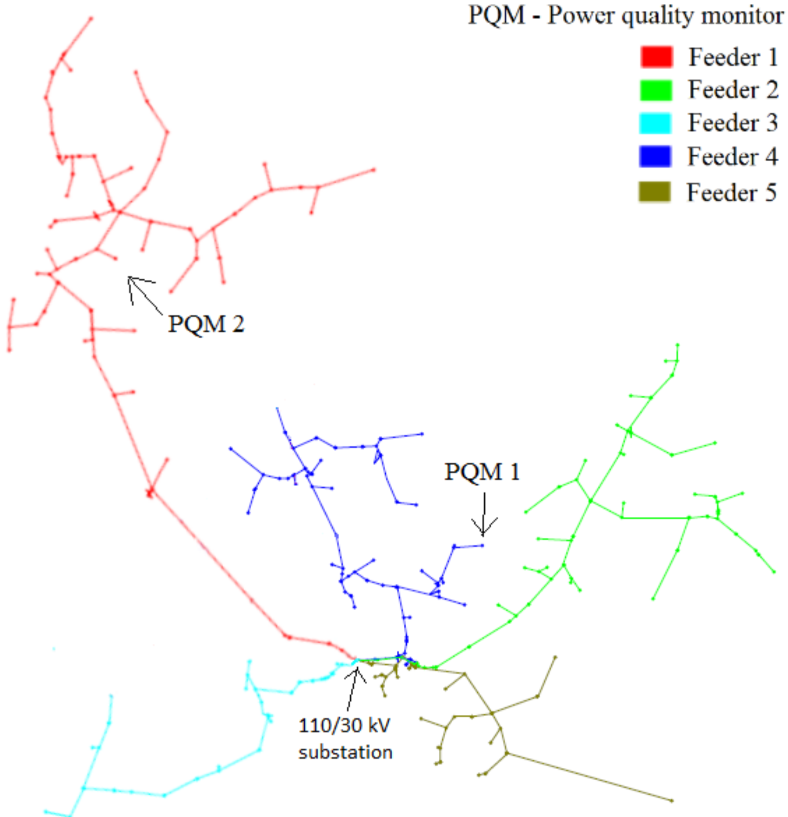

Fig. 6.5.4. *Geographical diagram of analysed MV network with feeder colouring and global optimum solution of locations of PQMs*

For this PQM configuration, average and minimum coefficient of determination is:

$$\mathbf{R^2_{avg}=0{,}9996,\ R^2_{min}=0{,}9975,}$$

We can notice that there is only a slight difference between all the other best solutions presented and the global optimum (only slightly better). Therefore there is a question if we need an optimisation algorithm for such a network. Regardless of the small differences between the solution, MVR algorithm placed the second PQM 2 just near the major flicker source in the network (construction company).

General comments on presented solutions

Generally, the first PQM is chosen near the feeding 110/30 kV substation, since the PQM monitor in such node covers the largest part of the network with very high R^2_{avg} and R^2_{min} values of the choice criteria. The second PQM is chosen to be at some node of red Feeder 1, which is the only feeder which is not covered by satisfactory high values of R^2_{avg} and R^2_{min} using the first PQM location near the feeding 110/30 kV substation.

Analysing more in detail the regression coefficients, it can be concluded that for the majority of the network (all feeders except the Red feeder), the b1 coefficients show that PQM 1 monitor is used to cover this part of the network (Green, Blue, Light blue, Brown feeders). For the rest of the network (Red feeder), PQM 2 is used to cover this remaining part of the network, which is depicted by dominant b2 coefficient. For the busses in between the zones of PQM 1 and PQM 2, both b1 and b2 regression coefficients have significant value. This confirms the fact that the linear regression works on the principal of similarity, where the node with more similarity in behavior are used to explain the state of PQ.

Generally, values of R^2 are very high in all the solutions, but still below 1. It needs to be commented that R^2=1 should not be expected from the PQM configuration, since perfect observability needs not to be achieved. There is always a margin of variability no explained that is accepted by the model, and in this research R^2_{min}=0,8 was set, where different values of R^2_{min} can be set by the DSO in the project. Different values of R^2_{min} can lead to higher number of PQM needed to cover the network with this criterion set.

Heat maps

In order to compare different solutions and show how close different solutions are in terms of choice criterion, heat maps are drawn and presented. The following heat maps are presented:

- 1st location fixed (110/30 kV transformer substation), heat map represents results for 2nd choice of PQM location for $\mathbf{R^2_{average}}$ as choice criteria (Fig. 6.5.5.)
- 1st location chosen by MVR, heat map represents results for 2nd choice of PQM location for $\mathbf{R^2_{average}}$ as choice criteria (Fig. 6.5.6.)

The heat maps for R^2_{min} are not shown because of their great similarity to the graphs of $R^2_{average}$.

Fig 6.5.5. shows the choice criteria $R^2_{average}$ for the case where the 1st location is fixed (110/30 kV transformer substation), and heat map presents the results for 2nd choice of PQM location. We can see that a very good result can be achieved by locating 2nd PQM anywhere on the longest feeder in the upper part of the network, and there are a considerable number of good solutions with similar $R^2_{average}$. The solutions are noticeably worse if the 2nd location is chosen in the remaining part of the network. The explanation is based on the fact that linear regression rests on the principle of similarity. PQM in feeding 110/30 kV transformer substation captures the behavior in the lower part of the network, and adding of 2nd monitor from that region does not contribute much (red part). Longest feeder in the upper part of the network has characteristic behavior not captured by the 1st monitor, and therefore 2nd monitor is needed in their part of the network.

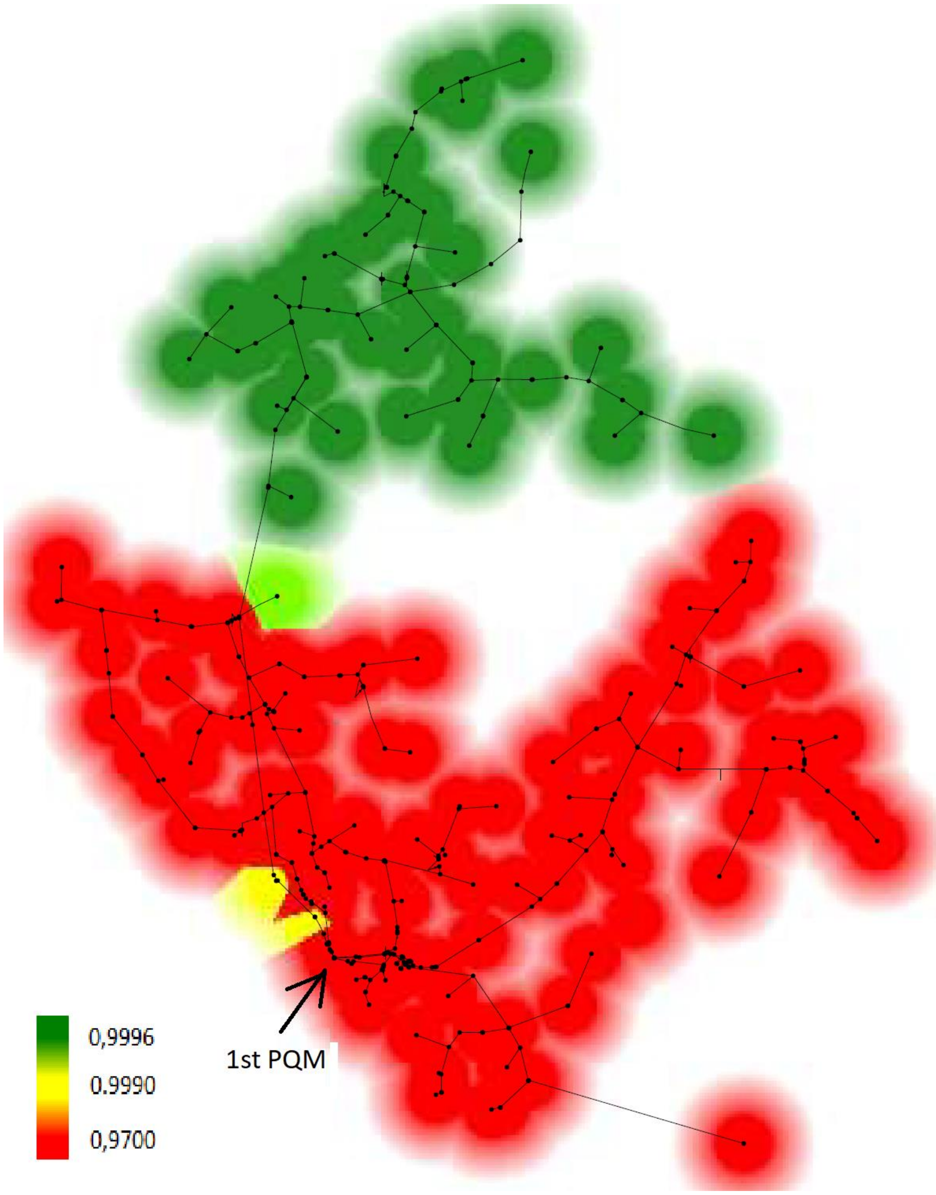

Fig. 6.5.5. *Heat map -1st location fixed (110/30 kV transformer substation), heat map represents results for 2nd choice of PQM location for $R^2_{average}$ as choice criteria*

Fig. 6.5.6. shows the choice criteria $R^2_{average}$ for the case where the 1st location is chosen by MVR, and heat map presents the results for 2nd choice of PQM location. We can see that the best result is achieved if the 2nd PQM is located in the upper part of the network, since the 1st PQM captures the behavior of the rest of the network. Again, there are a significant number of the nodes that give almost the same result. Since 1st PQM is located several nodes from the feeding transformer substation towards the longest upper feeder (red dot in the graphs), it captures some of the behaviour of the upper feeder also. Therefore, somewhat better solution than in Fig. 6.5.5. is

achieved if 2nd location is in the lower part of the network, since the upper part of the network can be captured partly by the first monitor.

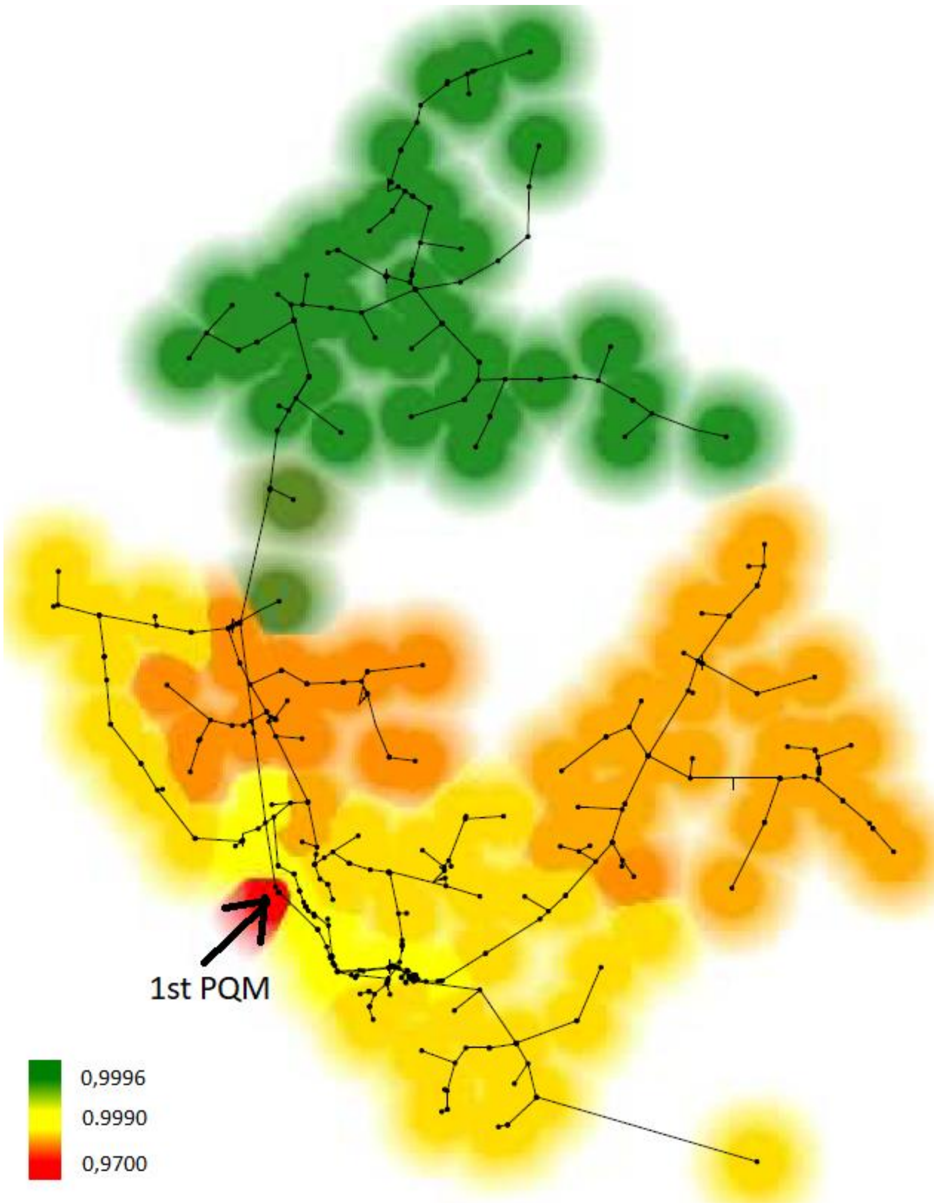

Fig. 6.5.6. *Heat map -1st location chosen by MVR, heat map represents results for 2nd choice of PQM location for $R^2_{average}$ as choice criteria*

<u>*State of Power Quality in All the Nodes Based on Regression Coefficients*</u>

As the best way to verify the validity of the regression model, using existing PQMs in the network, it has been proven that the state of PQ can be known based on only two PQMs. There are five existing PQMs in the analysed network, two of them have been in this test used as locations of PQMs, while the other three have been used to verify the MVR regression coefficients. In this way, it was proven that PQM configuration can be used to know the state of PQ in the whole network.

PQM configuration used in this test is shown in Fig. 6.5.5. PQM 5 and PQM 1 are used as locations of PQ monitors, i.e. predictors, explanatory, or independent variable. The rest of the available PQM measurements (PQM 2, PQM 3, PQM 4) were used as response, outcome, or dependent variables. After MVR calculation, explanatory variables (PQM 5, PQM 1) were multiplied by calculated regression coefficients to obtain the values of PQ parameters at the locations of response variables (PQM 2, PQM 3, PQM 4). This result has then been compared with the PQM measurements in the locations of response variables (PQM 2, PQM 3, PQM 4) to verify the MVR model. Results are shown for node of PQM 2, for 5^{th} harmonic (Fig. 6.5.6.), 7^{th} harmonic (Fig 6.5.7.) and flicker (Fig. 6.5.8.). Great similarity between the result of the MVR model and the measurements confirm the fact that the chosen PQM configuration can be used to monitor al the nodes in the network.

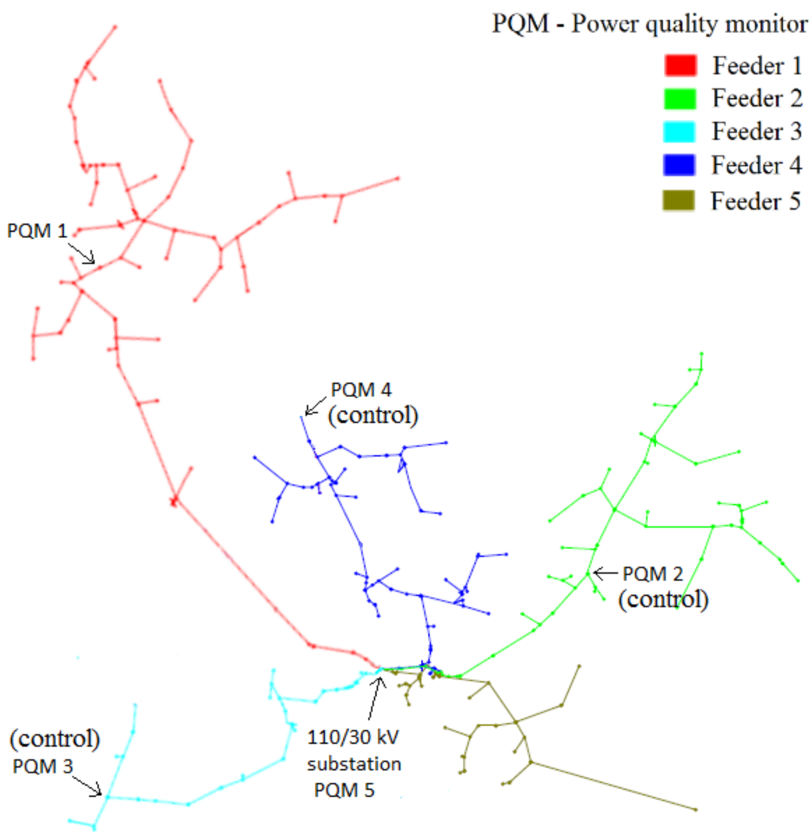

Fig. 6.5.5. *Modified geographical diagram of analysed MV network with feeder colouring and locations of PQMs used for verification of MVR*

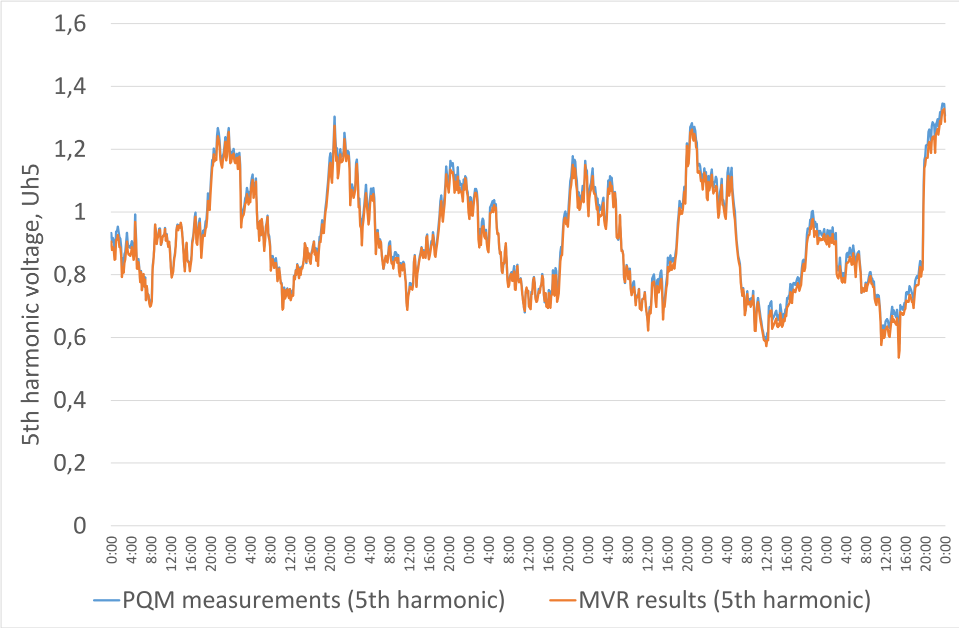

Fig. 6.5.6. *Comparison of PQ measurement and model results for 5th harmonic for PQM 2*

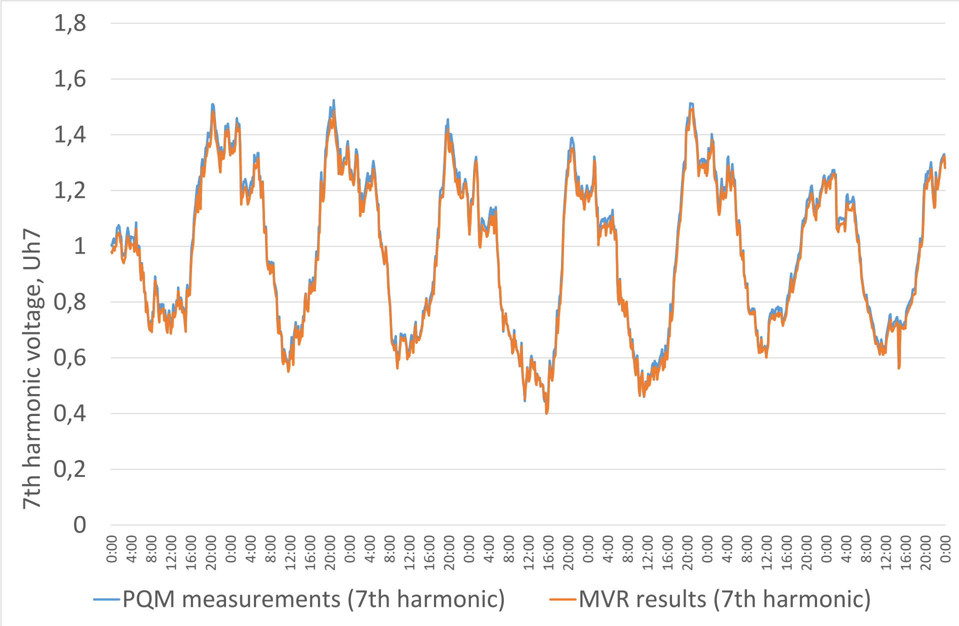

Fig. 6.5.7.. *Comparison of PQ measurement and model results for 7th harmonic for PQM 2*

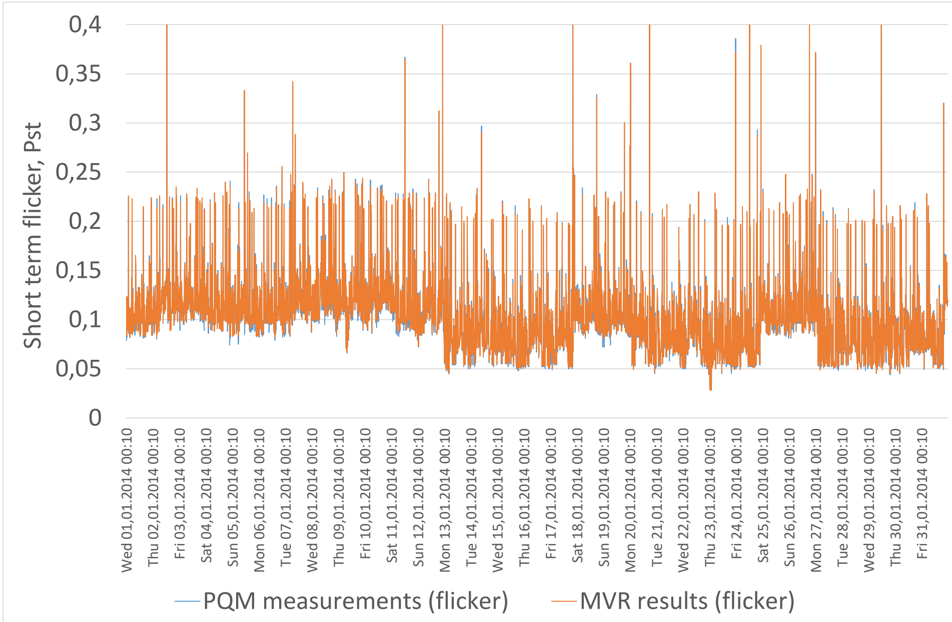

Fig. 6.5.8. *Comparison of PQ measurement and model results for flicker for PQM 2*

6.6 Sensitivity Analysis (Robustness)

In this subchapter, the robustness of the presented methodology is analysed. Mainly, it can be noted that the majority of the uncertainties come from the modelling of PQ parameters, while there are no significant uncertainties regarding the MVR part of the methodology. Analysis of the measurement data and different modelling approaches have shown that the harmonics are mostly deterministic, unbalance is both deterministic and stochastic, while the flicker is mostly stochastic in its behavior. Greatest uncertainties are in modelling flicker.

In order to test the robustness of the solution, a calculation of PQM placement locations was made, but with all the customers having same PQ emission coefficient (harmonic current, unbalance factor, flicker emission coefficient). The results are shown in Fig. 6.6.1. and it can be seen that only one PQM is chosen as

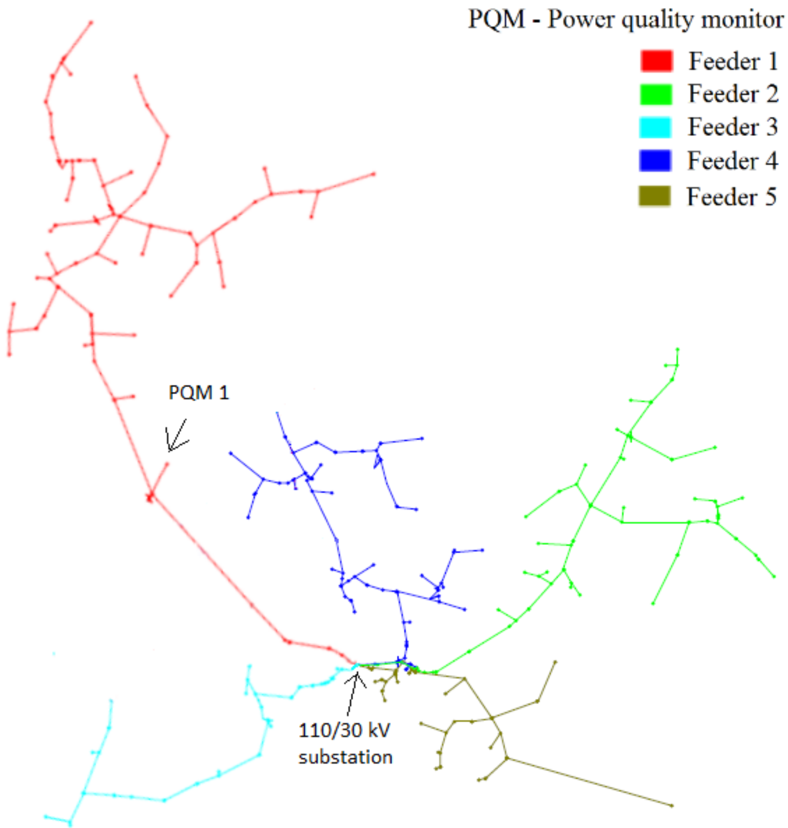

Fig. 6.6.1. *Geographical diagram of analysed MV network with locations of PQMs chosen for robustness testing*

The R^2_{avg} and R^2_{min} of the proposed solution are given below:

$$\mathbf{R^2_{avg}=0{,}9961,\ R^2_{min}=0{,}9810}$$

We can see that the algorithm was not proven to be robust, since only one PQM is suggested in the robustness test, while two PQM are the optimal configuration in the regular calculation. The reason behind this lays in the fact that large industrial customers have the same coefficients as the rest of the customers. Particularly important is the construction work company at the top Red feeder, which causes significant flicker disturbances, and therefore influences the algorithm to put 2nd PQM location in the upper Red feeder. Without this characteristic behaviour of the industrial customer, there is not enough of the characteristic behaviour in the feeders, and only one PQM is enough to capture the behaviour of the whole network.

6.7 Discussion of the Results

6.7.1 Modelling of Harmonics

From the results in Figs. 6.1.1. – 6.1.4. and Tables 6.1.1. and 6.1.2., it can be noticed that a perfect match between the simulation results and the measurements was not achieved, which is explained with the following facts:

- A large distribution network was modelled, with 12,347 customers and multiple times more harmonic sources,
- Deterministic models cannot reconstruct exactly all the variations in harmonic values (especially smaller ones), which happen due to the stochastic nature of the harmonic source emissions
- Aggregated harmonic current source models for several characteristic customer type categories were used, replacing the need for exact measurements of a large number of individual harmonic sources in the network
- Only exact background harmonic voltage source magnitudes were available and used for the analysed week, while the measurements of background harmonic voltage source phase angles were used from another week
- The harmonic current emission of rectifiers has an inherent uncertainty due to the load of the rectifier, pre- distorted harmonic voltages in the network and voltage unbalance, according to [84]
- The percentage of motors with VSDs in industry was estimated in this research, using available knowledge and experience

Despite all the uncertainties listed in the previous paragraph, the models provided good results.

Therefore, this research is the first research to achieve a good match, for a large real MV distribution network and for longer time period of one week, between the results of the harmonic model and the PQ measurements,. The only work with similar scope of analysed network is work [15], and in [15] probabilistic approach was used, while in this research deterministic approach was used. Probabilistic approach did not provide an exact match between the results of the model and the measurement, but rather gave a range of results influenced by the input parameter uncertainties. However, deterministic approach, used here in this research, provided a very good match between the results of the model and the measurements. The deterministic approach also provided a match between the weekly trends of the result of the model and the measurements (especially for the IEC 61000-3-6 method), which cannot be the objective of the probabilistic method.

In the proposed deterministic methodology, only a limited number of measurements were used to develop a model of aggregate harmonic source models of all major customer categories in the analysed network,. Therefore, the proposed methodology and easy to apply in multiple other MV networks. It must be stressed that it is necessary to have measurements of background harmonic voltages from the analysed network (usually at the feeding HV/MV transformer substation), due to their dominating impact on the total harmonic voltage levels [3].

The simulation method of modelling harmonic sources using complex phasors provided noticeably worse results than the method according to the IEC 61000-3-6 summation law. It can be discussed that the main reason for this is the robust formula of the IEC 61000-3-6 summation law and the lower number of input parameters and uncertainties in the IEC 61000-3-6 summation law method, compared to exact summation in the complex plain and the larger number of input parameters and uncertainties, as a result of modelling of the phase angles in the complex phasors method. The method according to the IEC 61000-3-6 is more robust, as shown by the sensitivity analysis. This is mostly due to the input data uncertainties, i.e. mostly due to lower number of input parameters of the model which needed to be tested for sensitivity. Of course, if the input parameters of the harmonic source models were perfectly known, the method using complex phasors would provide better results. But such quality of input data often is not the case in reality in large real distribution networks with a large number of harmonic sources, where significant uncertainties are more often to be expected. It can therefore be concluded that, for the applications in large distribution networks, the method according to the IEC 61000-3-6 summation law is a more practical method and is therefore recommended by the authors. Also, the method according to the IEC 61000-3-6 summation law is easier to implement due to the reduced modelling effort, since the phase angles are not modelled. Also, as another conclusion, the summation exponents from the IEC 61000-3-6 summation law have therefore proven to be suitable in the analysed case of a large number of harmonic sources in large real MV distribution network [3].

6.7.2 Modelling of Flicker

This research is the first work to model flicker in large real MV distribution network and achieve the match between the model and the measurements. Comparing to only similar work [28], this PhD thesis research calculated flicker based on real maximum power of all the customers, derived from measurements of yearly energy and synthetic load profiles, rather than on fictitious currents as applied in [28]. Also, in this PhD research work, PQ measurements were used both for developing the model and for verification of the results, which was not done in [28]. A good match was achieved despite the significant uncertainties related to number of customers and their flicker emission coefficients. It must be noted that the flicker emission coefficient values were roughly estimated in this research, in order to achieve the match between the model results and the PQ measurements. Special attention was given to flicker emission coefficients of the largest industry customers, since they dominantly impact the final result. Results of this methodology are highly dependent on the values of flicker emission coefficients, and there are no measurement-based flicker emission coefficients in the literature for the majority of customer categories. Therefore, this research presented a methodology for modelling flicker, and the methodology shall be improved in the future by measuring flicker emission coefficients of different customer categories, especially different types of large industries. Also, the measurements of flicker emission coefficients should provide a more reliable cdf distribution of flicker sources, which was in this research derived from voltage P_{st} measurements. Another uncertainty of the model is that the flicker summation law is not empirical, and cubic summation was used in this research since it is usually used for summation of flicker coming from many different flicker sources.

6.7.3 Modelling of Unbalance

This research answered the research gap recognized in the literature review (subchapter 3.3), that there is no published paper on modelling of unbalance in large real MV distribution networks, that is based on real measurements to develop a model. Comparing to only similar work [28], this PhD thesis research modelled unbalance based on measurements from LV networks, rather than on fictitious unbalance currents as applied in [28]. For this research, PQ measurements from different LV networks (residential, small commercial and industry) were used to develop a methodology for current unbalance factor determination. Only a limited number of customer categories were available and used, and these measurements were also used to model other similar customer categories. This is therefore definitely a space for improvement of the model, and additional measurement of current unbalance factor are needed to improve the methodology. Also, it would be useful to verify the model with PQ measurement results, which was not done in this research due to unavailability of correct voltage unbalance measurements. Another uncertainty of the model is that the general summation law for unbalance is not empirical, and α=1,4 was used in this research since it is usually used for summation of unbalance coming from many different unbalance sources.

6.7.4 Voltage Dips Consideration

In the results section 6.4 it was concluded that since the total information loss if no PQ monitors are installed in the MV feeders to monitor voltage dips is only 1,06%, there is no economic justification to install PQ monitor in the green feeder 2 to monitor voltage dips (Figure 5.6.1.). It can be discussed that if, however, the local DSO wants to monitor these 1,06% of voltage dips in its network, it can install a PQ monitor in the section of the green feeder 2 before the circuit breaker. Optimal location of PQ monitor in the green feeder 2 can be obtained by applying the algorithm from the literature [59], and integrating it with this PhD research as explained in the subchapter 5.6.

6.7.5 MVR Optimal Placement of PQ Monitors

This research is the first work to develop PQM placement algorithm for several key PQ parameters (harmonics, flicker, unbalance), while modelling the propagation of these PQ parameters based on real customer, consumption, load profile, network and PQ measurement data. The only previous work that took into account several PQ parameters [28], used fictitious currents without real customer, consumption and load profile data. Therefore, comparing to the research [28], the contribution of this thesis is that real customer, consumption, load profile, network and PQ measurement data were used to develop a model. Models for propagation of harmonics and flicker were validated using PQ measurements. These realistic models of propagation of harmonics, flicker and unbalance for longer time periods (e.g. week or month) are novelties of this research, which were not presented by other researchers, mostly testing their PQM placement algorithms on test networks. Also, MVR and R^2 as a choice criterion, based on standard approach applied in statistics were used, comparing to correlation and regression approach used in [28]. This research is also the first work to apply MVR for optimal PQM placement for harmonics, flicker and unbalance, where MVR was in earlier work [57] applied only to voltage dips. Also, multiple linear regression from multiple PQM's gives better estimates than simple linear regression from one PQM as implemented in [28]. Furthermore, method [28] provided only clusters of location from which PQM location shall be taken, without prioritisation among the nodes in the cluster, while method of this thesis gives a value of R^2 for all the nodes in the network, and therefore it can be prioritized which node is the best location for PQM. The MVR method presented in this thesis gives the result of only two monitors needed to cover the network, while the method of [28] gave the result of a total of 8 PQMs (4 PQMs in the MV feeders and 4 in feeding 110/30 kV transformer substation). This proves the superiority of the methodology presented in this research.

By analysing the final results, it can be noticed that many solutions are very close to the best one in terms of the choice criterion R^2. Therefore, many PQM configurations provide almost the same result. This is due to very high multicollinearity in the regression model, which comes from very high similarity of PQ parameter behaviour of the adjacent nodes. Network is electrically connected and inevitably neighbouring nodes have very similar behaviour, since it is impossible to change state of PQ in one node not affecting the other neighbouring nodes. Due to this reason, the R^2 values of the regression model are also very high, which corresponds with great multicollinearity and similarity of behaviour between the adjacent nodes in the network. This said, it must be noted that multicollinearity does not represent a problem for PQM location algorithm, since either one of the buses with high R^2 is taken, it provides a sufficient observability.

Linear regression and MVR rest on the mutual similarity in behaviour between different nodes. More similar behaviour means less PQMs at the end, and lower similarity of behaviour means mode PQMs needed to observe the network. One influence factor that influenced a lower number of PQMs needed for the analysed network is the similarity of behaviour between different nodes in the network, since the network is dominated by residential and small commercial customers, mainly having similar behaviour across the network. It was noticed that when higher impact is given to industry, as characteristic customer, lower similarity is obtained between the nodes and hence higher number of PQMs. This may be the reason why some of the other networks, dominated by characteristic industrial customers, will probably need more monitors to cover the whole network.

In order for the regression model to be accurate, correct representation of only the PQ parameter propagation is necessary. Exact recreation of time-series behaviour during the analysed longer periods of time is not necessary.

This research has proven that some PQ parameters have deterministic while others stochastic behaviour. Harmonics on one hand are mostly deterministic, flicker is mostly stochastic, while unbalance has both deterministic and stochastic behaviour. Therefore, PQ parameters of different nature, and using different modelling techniques were modelled in this research. Therefore, method previously discussed in Austria, based on purely stochastic approach to PQ parameters is not valid [95].

Mainly due to stochastic behaviour and modelling of flicker, different runs of the complete algorithm will at the end give different final results. However, solution that matches the PQ measurements best over different runs shall be taken.

In this research R^2_{min}=0,8 was set, which means that at least 80% of variability shall be explained for every node in the model. Different values of R^2_{min} can be set by the DSO in their project, since it is ultimately their decision, which has a crucial impact on number of PQMs. Higher values of R^2_{min} mean better observability and lead to higher number of PQM, while the lower values of R^2_{min} mean worse observability and lead to lower number of PQMs needed to cover the network with this criterion set.

Also, every DSO for their project should define a weighting factors for different PQ parameters, needed for choosing PQM locations when several PQ parameters are combined. The weighting factors in this thesis are adjusted for the analysed network, where flicker values are highest comparing to the EN 50160 norm, and hence the largest weighting factor is set for flicker. Other networks and other DSOs can have different weighting factors.

As the most important thing for the DSO, it has been proven that the PQM configuration of several PQMs can be used to cover the whole network. The state of PQ in other busses is known by the multiplication with regression coefficients, and this has been verified with PQM measurements in several nodes in the network. This observability is one of the key requirements for PQM placement algorithms. The presented great match between the regression model and the measurements proves also that there is no need for the complex state estimation algorithms for different PQ parameters, when a simple linear regression can be used for this purpose.

Most of the uncertainties of the MVR model come from the uncertainties in modelling PQ parameters, which are numerous as explained in other subchapters of this thesis. The MVR itself does not impose additional uncertainties, since linear regression is exact operation. Major uncertainties in PQ parameter modelling lead to uncertainties in the MVR model. Therefore, it is not possible to know if the global solution of PQM placement truly resembles the real state in the network, since the differences between many good solutions are so small and uncertainties can be larger than the difference between solutions.

This research focused only on 5th and 7th harmonic voltages, and it should be noted that if higher harmonics are taken into account the number of instruments will increase, since local resonances will result in higher diversity of harmonic levels.

Due to small number (two) of PQMs needed to cover the analysed network, the number of combinations of PQM locations was limited and the computing time for the global optimum solution was reasonable. Therefore, using of optimisation algorithms was not necessary for this network. The fact that there is only a slight difference between all the other best solutions presented and the global optimum is an argument that the optimisation algorithm is not needed for such a network. For larger networks with higher number of PQMs needed to cover the network, number of combinations of possible PQM locations will be much higher and the computing time might become quite long. Therefore, for these networks, optimisation algorithms as suggested in subchapter 5.7.4 should be used.

The arguments that for the analysed network optimisation was not necessary, and therefore this thesis did not include optimisation algorithms, are given below:

- Global optimum solution is very close in terms of choice criteria to other good solutions and therefore there is a question if the optimisation algorithm can find the global optimum solution
- Differences between many good solutions may be lower than the uncertainties brought in by the PQ parameter propagation models (harmonics, flicker, unbalance), therefore bringing the robustness of the optimal solution into question
- “Brute force” calculation of all the possible combinations lasts for several hours for network with 2 PQM monitors needed, with only small changes in the MATLAB code

Therefore, we can conclude that for small and medium sized grids optimisation is not necessary where 2 PQM monitors or less are needed to cover the network. For networks where 3 PQMs are needed, brute force calculation can last very long (150^3=3.375.000 solutions for the analysed grid, which equals cca. one week of calculations) Therefore, for larger grids, if necessary, optimisation procedure from the literature (genetic algorithm) can be used [10].

7 CONCLUSIONS AND THESIS CONTRIBUTION

7.1 Conclusions

This section gives the conclusions of this PhD thesis, organized according to the methodology sections of the research.

Modelling of Harmonics

This research work proposed a deterministic methodology for modelling harmonics in large real MV distribution networks. The methodology was verified by comparing the results of the model with the results of PQ measurements, for a longer time period of one week. This paper presents the deterministic approach of modelling harmonics, using aggregate harmonic source models parameterised based on measurements and results from the literature. This methodology gave good results, despite the fact that it was tested on a large real MV network with a large number of customers and harmonic sources. The methodology is practical and easy to apply in multiple other MV networks, since a limited number of measurements were used for developing a model.

Two commonly used methods for harmonic sources modelling were used and compared. The method of modelling harmonic sources according to the IEC 61000-3-6 summation law gave better results. The better results are due to its robustness in dealing with uncertainties regarding the harmonic source characteristics. This method is also more practical, since the measurement and pre-processing of the harmonic source phase angle data is not needed. The IEC 61000-3-6 method is therefore recommended by the authors in the case of analysing large MV distribution networks. In such networks, only a limited input data about customers and harmonic sources is available, or due to the large number of customers the effort for collecting and measuring all the required input data is not feasible. For the analysed case, this research also proves the suitability of the summation exponents recommended in the IEC 61000-3-6 standard.

One of the advantages of this methodology is that it can enable the reconstruction of harmonic voltage values in all the points in the MV network. Therefore, it is especially useful for Distribution Management Systems (DMS), where it can provide the network operators with information on instantaneous values of harmonic voltages in all the unmonitored nodes in the network. Also, this methodology can be used for different harmonic studies in MV distribution network, such as analysis of impacts of higher penetration of inverter-based DG’s as well as EV charging stations. Also, verification of the methodology for different networks, with different customer structures, and for different seasons in a year are possible topics for future work.

Modelling of Flicker

This research work has shown that it is possible to model flicker even in large MV distribution network and to verify the model with measurements. In order for the developed model to match the measurements, it must be noted that the flicker emission coefficients were assumed. This paper presented a methodology for modelling flicker, and the methodology shall be improved in the future by measuring flicker emission coefficients of different customer categories, especially different types of large industries. This is a topic for scientific community to work on in the future.

Modelling of Unbalance

This research has proven that it is possible to develop a model for unbalance studies even in large real MV distribution networks. The model was developed for a longer period of time (one month). It must be noted that current unbalance measurements were available only for key customer categories (households, small commercial and industry), and that the model can be improved in the future by additional measurements for other customer categories.

Voltage Dips Consideration

This PhD thesis presented a simple methodology of considering if additional PQ monitors are needed to monitor voltage dips in MV feeders. The methodology is especially useful for networks with no or low number of circuit breakers in the MV feeders, except the circuit breakers in the MV cabinets of feeding HV/MV transformer substations. For the analysed network, with only one circuit breaker in the MV feeders, this methodology showed that there is an information loss of 1,06% if no additional PQ monitors are installed to monitor voltage dips, Therefore, there is no economic justification to install additional PQ monitor, unless the local DSO wants otherwise.

MVR Optimal Placement of PQ Monitors

This research work proved that it is possible to develop a PQM placement algorithm, taking into account several key PQ parameters, and using real data to develop the model. The proposed approach uses novel modelling techniques for PQ parameter modelling, as well as MVR and R^2 choice criterion to decide the location of PQMs. The presented methodology is relatively easy and straightforward, and can be applied to multiple other networks. The proposed methodology is superior to other published approaches, since it takes into account several key PQ parameters simultaneously, comparing to only one PQ parameter taken in almost all other works. Comparing to only similar work [28], the approach of this thesis proposes only two PQM monitors to cover the whole network, comparing to eight PQ monitors proposed in [28].

7.2 Thesis Contribution and Answers to Research Questions

Thesis contribution

The contributions of this PhD research are listed below, organised according to the methodology sections of this research.

Modelling of harmonics

This research work solved all the three research gaps, related to harmonics modelling, presented in the literature review. This is the first research work to achieve the following scientific contributions:

- Develop a deterministic methodology for harmonic analysis in large real MV distribution networks.
- Achieve a very good match between the PQ measurements and the harmonic load flow model, for a large real MV distribution network, with the match in trend of results for longer time period of one week.
- Develop a comprehensive (deterministic) methodology for aggregate harmonic source modelling of all the major customer categories in electricity distribution networks, which is based on only a limited number of measurements needed to develop a model and is therefore relatively.
- Analyse, on an example of a large real MV distribution network, the implementation of two commonly used methods for harmonic source modelling,. This work has shown that the method according to the IEC 61000-3-6 summation law is more robust and suitable for large real MV distribution networks. At the same time, it is also the verification of the summation exponents for the 5th and 7th harmonic, given in the standard IEC 61000-3-6, for large real MV networks.

Modelling of flicker

The contribution of this work is that it is the first work to model flicker on an example of a large real MV distribution network. Real customer data and real PQ measurements were used to assume flicker emission coefficients. Also, the flicker model is developed for a longer time period of one whole month, and the model is validated using PQ measurements [6].

Modelling of unbalance

This PhD research is the first work to develop a model of unbalance for large real MV distribution networks, using real PQ measurements to develop a model. Model was developed for a longer time period of one month.

Voltage dip consideration

This work proposes a simple methodology to consider if additional PQ monitors are needed to monitor voltage dips, in the MV networks with no or low number of circuit breakers installed in the MV feeders (except the circuit breakers in the feeding HV/MV transformer substation).

MVR optimal placement of PQ monitors

This research answers the research gaps from the literature review, and it is the first work to develop a PQM placement algorithm, taking into account several key PQ parameters at the same time, using real data (network, customer, consumption and PQ measurements) to develop the model. Models of individual PQ parameter propagation are verified with the PQ measurements and are used as inputs to the MVR optimal monitor placement method, while majority of other works did not use real data and developed algorithms for test networks. This work is the first work to apply the MVR method to optimal placement of the following PQ parameters: harmonics, flicker, unbalance.

Answer to research questions

The answers to research questions posed at the beginning of this PhD thesis (subchapter 4.3) are given below, organized according to the methodology sections of this research:

Modelling of harmonics

1. Is it possible to develop a model for the harmonic load flow in a large real MV distribution network, and to verify the model with the measurements for a longer time period (e.g. one week)?

Answer: This thesis has proven that it is possible to develop a model for the harmonic load flow in a large real MV distribution network, and to verify the model with the measurements for a longer time period (e.g. one week). An example of a large real MV distribution network with different customer categories was used in the thesis and real PQ measurements from the same network were used for the validation.

2. Which method is more suitable for the harmonic studies in large real MV networks:
    a. Modelling according to the IEC 61000-3-6 summation law or
    b. Modelling using complex phasors

Answer: This thesis has proven that the method of modelling harmonics according to the IEC 61000-3-6 summation law is more suitable for the harmonic studies in large real MV networks, due to the robustness of the IEC 61000-3-6 summation law formula and due to less uncertainties related to lower number of input data in comparison to modelling method using complex phasors.

Modelling of flicker

3. Is it possible to model flicker in a large real MV distribution network, and to verify the model with the measurements for a longer time period (e.g. one month)?

Answer: This thesis has proven that it is possible to model flicker in a large real MV distribution network, and to verify the model with the measurements for a longer time period (e.g. one month). An example of a large real MV distribution network with different customer categories was used in the thesis and real PQ measurements from the same network were used for the validation.

Modelling of unbalance

4. Is it possible to model unbalance in a large real MV distribution network, and to verify the model with the measurements for a longer time period (e.g. one month)?

Answer: In this thesis, a model for unbalance in a large real MV distribution network was developed for a longer time period (e.g. one month), but unfortunately it was not verified with the measurements due to an unavailability of correct voltage unbalance measurements. An example of a large real MV distribution network with different customer categories was used in the thesis to develop the model.

Voltage Dips Consideration

5. What is the best way to consider voltage dips in the optimal PQ monitor placement algorithm if the MV network has no or low number of circuit breakers in the MV feeders, except the circuit breakers in the feeding HV/MV transformer substation?

Answer: For networks with no or low number of circuit breakers in the MV feeders, except the circuit breakers in the feeding HV/MV transformer substation, a simple methodology was presented in this research to assess if it is justifiable to install additional PQ monitors to monitor voltage dips in the MV feeders. For the analysed network, with only one circuit breaker in the MV feeder, due to very low information loss it was concluded that there is no need for additional PQ monitors in the MV feeders to monitor voltage dips, which simplified the overall PQ monitor placement algorithm.

MVR Optimal Placement of PQ Monitors

6. Which optimisation algorithm or statistical technique is the most appropriate for the problem of optimal placement of voltage quality monitoring devices in distribution networks?

Answer: This thesis has proven that the MVR is suitable for the problem of optimal PQM placement. The implementation is relatively easy and straightforward to apply and can be implemented for a large number of other distribution networks. Chosen criterion R^2 is easy to understand and comprehend, since it represents the variability explained by the model.

7. Is it possible to develop a model for voltage quality monitoring devices optimal placement that is verified with PQ measurements?

Answer: In this thesis, models of harmonics and flicker propagation in the network were verified with PQ measurements in the analysed network. As such, they were used as inputs to MVR optimal PQM placement algorithm and proved that it is possible to base the PQM placement algorithm on real PQ measurements.

8. Is it possible to optimise the number and location of voltage quality monitoring devices for different most important PQ parameters individually?

Answer: This PhD thesis has proven that it is possible to develop a PQM placement algorithm for several key PQ parameters: harmonics, flicker, unbalance, dips. Analogously, the method can be extended to other PQ parameters

9. Is it possible to optimise the number and location of voltage quality monitoring devices for several most important PQ parameters simultaneously?

Answer: This research work is the first work to develop PQM placement algorithm, which takes into account several PQ parameters simultaneously, by means of weighting factors for different PQ parameters.

10. How to develop an optimisation algorithm that is robust enough to take into account:
    - Possible connection of new customers/producers on the network

    Answer: The method is robust to take into account new smaller customers that do not change the state of PQ much in the network. However, for larger customers (e.g. industry) new model needs to be made.

    - Possible communication failure with some of the voltage quality monitoring devices

    Answer: MVR method provides the regression coefficients also when some of the PQMs are out of operation. Therefore, state of PQ in the network can be known without some of the monitors, but with reduced accuracy of course.

    - Existing devices that can measure some of the power quality parameters

    Answer: Existing devices that can measure some of the PQ parameters are taken into account when defining the list of parameters – e.g. voltage variations and interruptions already measured by AMI and SCADA.

    - Accuracy of measurement of voltage quality monitoring devices

Answer: It is suggested that the devices according to IEC 61000-4-30 are taken (class A or class S) so the error should be acceptable. Nevertheless, all the measurements provided should be scrutinized and examined for errors, since different measurement errors can happen in practice.

- Different configuration of distribution network as a result of reconfiguration after voltage interruption

Answer: Larger reconfigurations of the network can be modelled as variations of the network and the model before PQM placement configuration is defined, to tae into account all frequent network reconfigurations that can happen.

8 FUTURE WORK

Modelling of harmonics

Due to several uncertainties of the deterministic method for modelling harmonics, the perfect match between the model and the measurements was not achieved, as expected. There are several ways to improve the results of the model in the future [3]:

- Measurement of the background harmonic voltage phase angle variation in the week for which the model was developed
- Performing measurements of the weekly harmonic current emission of different types of industries
- Statistics on percentage of motors with VSDs in different industries
- Installing larger number of smart meters, with load profile measurement capabilities, to measure the consumption of customers that should replace the need for synthetic load profiles in the model
- Models for harmonic impedance of different customer configurations are needed, especially for analysing frequencies at which resonance effects occur.

Modelling of flicker

The methodology for modelling flicker can in the future be improved by measuring flicker emission coefficients of different customer categories, where measurements of different large industries is especially important. Models for flicker emission should be developed based on the measurements, for all the major customer categories [6].

Modelling of unbalance

Methodology for modelling unbalance presented in this PhD thesis can be in future improved by additional measurements of unbalance current factors and developing models for unbalance emission, for all the customer categories present in the distribution networks. In this thesis, measurements only for residential, small commercial and industry customer groups were available. Also, it would be useful to verify the methodology by PQ measurement results, which was not done in this thesis due to unavailability of such correct PQ measurement data.

Voltage dips consideration

For larger distribution networks with higher number of CBs, the methodology of this thesis can be supplemented to include modelling of voltage dips, as presented in the literature [57].

MVR Optimal Placement of PQ Monitors

For larger distribution networks, where more than two PQMs are needed to cover the network, optimisation algorithm from [10] based on genetic algorithm should be used in combination with the methodology of this research.

Disturbance Location Detection

Future work for researchers is to try to develop an algorithms for disturbance location detection based on linear regression and MVR. Authors of [94] managed to develop an algorithm for locating of voltage sags using genetic algorithm and MVR. Similar works should be done for other PQ parameters.

Including other parameters in MVR

Other parameters may be included in the MVR such as voltage levels, length and type of lines, customer structure, distributed generation. Based on this data, it then may be possible to define number of PQMs needed in the network in an easier and more straightforward method. This can be done after the MVR algorithm has been applied on a larger number of networks, which would serve as a sample for such calculation. Soma machine learning techniques might need to be applied, to take into account the mentioned other parameters.

PQ and Smart Grids

Future work for other researchers would be to include in the algorithm PQ measurements from other smart devices (smart meters, protective relays etc.) in Smart Grids. These devices do not measure PQ according to EN 50160 and IEC 61000-4-30, but they can be good indicators of PQ problems as presented in IPQMS system. In such case, quantity of PQ measurement data is present and not quality. Large number of measurement devices and large number of PQ parameters, which should be analysed, create a Big Data problem. This thesis dealt with PQ monitors in MV networks, but with installation of smart devices in LV networks, the analysis of the propagation of some of the PQ parameters becomes possible.

9 REFERENCES

[1] "IEC 61000-4-30: Electromagnetic compatibility (EMC) – part 4–30: testing and measurement techniques – power quality measurement methods," IEC, 2003.

[2] "EN 50160: Voltage characteristics of electricity supplied by public electricity networks," 2003.

[3] A. Bosovic, H. Renner, A. Abart, E. Traxler, J. Meyer, M. Domagk and M. Music, "Deterministic Aggregated Harmonic Source Models for Harmonic Analysis of Large Medium Voltage Distribution Networks," *IET Generation, Transmission & Distribution,* vol. 13, no. 19, pp. 4421-4430, 2019.

[4] A. Bosovic, H. Renner, A. Abart, E. Traxler, J. Meyer, M. Domagk and M. Music, "Validation of aggregated harmonic current source models based on different customer type configurations," in *10th Electric Power Quality and Supply Reliability Conference (PQ 2016)*, Tallin, Estonia, 2016.

[5] A. Bosovic, H. Renner, A. Abart, E. Traxler, J. Meyer, M. Domagk and M. Music, "Modelling the propagation of harmonic voltages in large medium voltage distribution networks," in *25th International Conference on Electricity Distribution (CIRED 2019)*, Madrid, Spain, 2019.

[6] A. Bosovic, H. Renner, A. Abart, E. Traxler and M. Music, "Modelling of flicker in large real medium voltage electricity distribution networks," in *26th International Conference on Electricity Distribution (CIRED 2021)*, Geneva, 2021.

[7] C. Mirra, "Connection of fluctuating loads," International Union for Electroheat WG Disturbances, 1988.

[8] "IEC 61000-4-15: Testing and measurement techniques - Flickermeter - Functional and design specifications," IEC, 2010.

[9] L. Simon and R. Heckard, "Statistics Online STAT 501: Regression Methods," The Pennsylvania State University, Eberly Collage of Science, [Online]. Available: https://online.stat.psu.edu/stat501/lesson/1/1.1. [Accessed 2 7 2021].

[10] A. Kazemi, A. Mohamed, H. Shareef and H. Zayandehroodi, "Optimal power quality monitor placement using genetic algorithm and Mallow's Cp," *Electrical Power and Energy Systems,* vol. 53, p. 564–575, 2013.

[11] L. Simon and R. Heckard, "1.5 - The Coefficient of Determination, r2," The Pennsylvania State University - Eberly College of Science, [Online]. Available: https://online.stat.psu.edu/stat501/lesson/1/1.5. [Accessed 7 7 2021].

[12] S. Williams, G. Brownfield and J. Duffus, "Harmonic propagation on an electric distribution system: field measurements compared with computer simulation," *IEEE Transactions on Power Delivery,* vol. 8, no. 2, p. 547–552, 1993.

[13] C. Venkatesh, D. Srikanth Kumar, D. Siva Sarma and M. Sydulu, "Modelling of nonlinear loads and estimation of harmonics in industrial distribution system," in *Proceedings 15th NPSC 2008 Conference*, Bombay, India, 2008.

[14] S. Middlekauf, A. Ebel and C. Jensen, "Using harmonic simulation to evaluate facility-wide harmonic mitigation," in *Proceedings 2000 PES Summer Meeting*, Seattle, USA, 2000.

[15] M. Au and J. Milanovic, "Establishing harmonic distortion level of distribution network based on stochastic aggregate harmonic load models," *IEEE Transactions on Power Delivery,* vol. 22, no. 2, p. 1086–1092, 2007.

[16] M. Au and J. Milanovic, "Development of stochastic aggregate harmonic load model based on field measurements," *IEEE Transactions on Power Delivery,* vol. 22, no. 1, p. 323–330, 2007.

[17] A. Collin, G. Tsagarakis, A. Kiprakis and S. McLaughlin, "Simulating the time-varying harmonics of the residential load sector," in *16th International Conerence on Harmonics and Quality of Power (ICHQP 2014)*, Bucharest, Romania, 2014.

[18] A. Castañeda, Stochastic harmonic emission model of aggregate residential customers, PhD thesis, Technische Universitaet Dresden, 2017.

[19] D. Salles, C. Jiang, W. Xu, W. Freitas and H. Mazin, "Assessing the Collective Harmonic Impact of Modern Residential Loads—Part I: Methodology," *IEEE Transactions on Power Delivery,* vol. 27, no. 4, p. 1937–1946, 2012.

[20] L. Miègeville, P. Guérin and R. Le Doeuff, "Identification of the harmonic currents drawn by an institutional building: application of a stochastic approach," in *9th International Conference on Harmonics and Quality of Power (ICHQP 2000)*, Orlando, USA, 2000.

[21] A. Collin, J. Acosta, B. Hayes and S. Djokic, "Component-based aggregate load models for combined power flow and harmonic analysis," in *7th Mediterranean Conf. and Exhibition on Power Generation, Transmission, Distribution and Energy Conversion (MedPower 2010),* Agia Napa, Cyprus, 2010.

[22] X. Xie, S. Y. Q. Wang, Y. Li, Y. Zhang and L. Zhang, "A Piecewise Probabilistic Harmonic Model of Aggregate Residential Loads," *IEEE Transactions on Power Delivery,* vol. 36, no. 2, pp. 841-852, 2021.

[23] CIGRE WG B4.19.,, "Static synchronous compensator (STATCOM) for arc furnace and flicker compensation," CIGRE, 2003.

[24] D. Giacosa, D. Bentancur, I. Lussich, G. Abal, L. Valevici and A. Pardo, "Power Quality Analysis for a PV Plant in Uruguay," in *International Conference on Renewable Energies and Power Quality (ICREPQ'16)*, Madrid, Spain, 2016.

[25] N. Golovanov, G. Lazaroiu, M. Roscia and D. Zaninelli, "Power Quality Assessment in Small Scale Renewable Energy Sources Supplying Distribution Systems," *Energies,* vol. 6, pp. 634-645, 2013.

[26] Å. Larsson, "Flicker Emission of Wind Turbines Caused by Switching Operations," *IEEE Transactions on Energy Conversion,* vol. 17, no. 1, pp. 119-123, 2002.

[27] T. Thiringer, J. MacEnri and M. Reed, "Flciker Evaluation of the SeaGen Tidal Power Plant," *IEEE Transactions on Sustainable Energy,* vol. 2, no. 4, pp. 414-422, 2011.

[28] C. Ammer and H. Renner, "Determination of the optimum measuring positions for power quality monitoring," in *11th International Conference on Harmonics and Quality of Power*, Lake Placid, USA, 2004.

[29] F. Möller and J. Meyer, "Probabilistic household load model for unbalance studies based on measurements," in *2016 Electric Power Quality and Supply Reliability (PQ 2016),* Tallin, Estonia, 2016.

[30] F. Möller, J. Meyer and P. Schegner, "Load model of electric vehicles chargers for load flow and unbalance studies," in *2014 Electric Power Quality and Supply Reliability Conference (PQ 2014)*, Rakverre, Estonia, 2014.

[31] D. Perera, P. Ciufo, L. Meegahapola and S. Perera, "Attenuation and propagation of voltage unbalance in radial distribution networks," *International Transactions on Electrical Energy System*, vol. 25, no. 12, pp. 3738-3752, 2015.

[32] J. M. C. Filho, R. C. Leborgne, P. M. da Silveira and M. H. Bollen, "Voltage sag index calculation: Comparison between time-domain simulation and short-circuit calculation," *Electric Power Systems Research*, vol. 78, p. 676–682, 2008.

[33] J. M. C. Filho, R. C. Leborgne, J. P. G. de Abreu, E. G. C. Novaes and M. H. J. Bollen, "Validation of Voltage Sag Simulation Tools: ATP and Short-Circuit Calculation Versus Field Measurements," *IEEE Transactions on Power Delivery*, vol. 23, no. 3, pp. 1472-1480, 2008.

[34] A. Kazemi, A. Mohamed, H. Shareef and H. Zayandehroodi, "A Review of Power Quality Monitor Placement Methods in Transmission and Distribution Systems," *Przeglad Elektrotechniczny*, vol. 89, no. 3a, pp. 185-188, 2013.

[35] G. Olguin and M. Bollen, "Optimal Dips Monitoring Program for Characterization of Transmission System," in *IEEE Power Engineering Society General Meeting*, Toronto, Canada, 2003.

[36] G. Olguin, "An Optimal Trade-off Between Monitoring and Simulation for Voltage Dip Characterization of Transmission Systems," in *IEEE/PES Transmission & Distribution*, Dalian, China, 2005.

[37] D. C. S. Reis, P. R. C. Villela, C. A. Duque and P. Ribeiro, "Transmission Systems Power Quality Monitors Allocation," in *IEEE Power and Energy Society General Meeting*, Pittsburgh, USA, 2008.

[38] G. Olguin and M. Bollen, "Stochastic Assessment of Unbalanced Voltage Dips in Large Transmission Systems," in *IEEE Power Tech*, Bologna, Italy, 2003.

[39] K. Mazlumi, H. Abyaneh, Y. Gerivani and I. Pordanjani, "A New Optimal Meter Placement Method for Obtaining a Transmission System Indices," in *IEEE Power Tech*, Lausanne, Switzerland, 2007.

[40] M. Haghbin and E. Farjah, "Optimal Placement of Monitors in Transmission Systems using Fuzzy Boundaries for Voltage Sag Assessment," in *IEEE Power Tech*, Bucharest, Romania, 2009.

[41] E. Espinosa-Juarez and A. Hernandez, "Neural Networks Applied to Solve the Voltage Sag State Estimation Problem: An Approach Based on the Fault Positions Concept," in *Electronics, Robotics and Automotive Mechanics Conference (CERMA)*, Cuernavaca, Mexico, 2009.

[42] A. Ibrahim, A. Mohamed and H. Shareef, "Optimal Placement of Voltage Sag Monitors Based on Monitor Reach Area and Sag Severity Index," in *IEEE Student Conference on Research and Development (SCOReD)*, Putrajaya, Malaysia, 2010.

[43] A. Ibrahim, A. Mohamed and H. Shareef, "Optimal Power Quality Monitor Placement in Power Systems Based on Particle Swarm Optimization and Artificial Immune System," in *IEEE Data Mining & Optimization*, Selangor, Malaysia, 2011.

[44] M. Avendano-Mora, N. Woolley and J. Milanovic, "On Improvement of Accuracy of Optimal Voltage Sag Monitoring Programmes," in *IEEE International Conference Harmonics and Quality of Power*, Bergamo, Italy, 2010.

[45] W. Cai and H. Huimin, "A Study on Optimal Placement of Voltage Sag Monitors," in *International Conference on Electricity Distribution (ICED)*, Nanjing, China, 2010.

[46] M. Eldery, E. El-Saadany, M. Salama and A. Vannelli, "A Novel Power Quality Monitoring Allocation Algorithm," *IEEE Transactions on Power Delivery,* vol. 21, no. 2, pp. 768 - 777, 2006.

[47] N. Kuzjurin, "Combinatorial Problems of Packing and Covering and Related Problems of Integer Linear Programming," *Journal of Mathematical Sciences,* vol. 108, no. 1, pp. 1-6, 2002.

[48] S. Arazm., J. Rouhi and R. Ahmadi, "New Algorithm for Optimal Placement of Power Quality Monitors in Multi Voltage Level Power Systems," in *International Power System Conference (PSC),* Tehran, Iran, 2007.

[49] D. J. Won and S. I. Moon, "Optimal Number and Location of Power Quality Monitors Considering System Topology," *IEEE Transactions on Power Delivery,* vol. 23, no. 1, pp. 288-295, 2008.

[50] G. Stagg and A. EL-Abiad, Computer Methods in Power Systems Analysis, New York, USA: McGraw-Hill, 1968.

[51] M. Weiss, Data Structures & Problem Solving Using JAVA, Boston, USA: Addison-Wesley, 2002.

[52] D. J. Won and S.-I. Moon, "Topological Locating of Power Quality Event Source," *Journal of Electrical Engineering & Technology,* vol. 1, no. 2, pp. 170 - 176, 2006.

[53] K. Kyoung-Nam, P. Jin-Woo, L. Jong-Hoon, A. Seon-Ju and M. Seung-Il, "A Method to Determine the Relative Location of Voltage Sag Source for PQ Diagnosis," in *8th IEEE International Conference on Electrical Machines and Systems*, Nanjing, China, 2005.

[54] S. Ahn, D. Won, D. Chung and S. Moon, "Determination of the Relative Location of Voltage Sag Source According to Event cause," in *IEEE Power Engineering Socirey General Meeting*, Denver, USA, 2004.

[55] D.-J. Won, I.-Y. Chung, J.-M. Kim, S.-I. Moon, J.-C. Seo and J.-W. Choe, "A New Algorithm to Locate Power Quality Event Source with Improved Realization of Distributed Monitoring Scheme," *IEEE Transaction on Power Delivery,* vol. 21, no. 3, pp. 1641-1647, 2006.

[56] A. Kazemi, M. A. and H. Shareef, "A New Method for Determining Voltage Sag Source Locations by Using Multivariable Regression Coefficients," *Journal of Applied Sciences,* vol. 11, no. 15, pp. 2734- 2743, 2011.

[57] A. Kazemi, A. Mohamed and H. Shareef, "A New Power Quality Monitor Placement Method Using the Multivariable Regression Model and Statistical Indices," *International Review of Electrical Engineering (IREE),* vol. 6, no. 5, pp. 2530- 2536, 2011.

[58] A. Kazemi, A. Mohamed and H. Shareef, "Tracking the Voltage Sag Source Location Using Multivariable Regression Model," *International Review of Electrical Engineering (IREE),* vol. 6, no. 4, pp. 1853-1861, 2011.

[59] A. Kazemi, A. Mohamed and H. Shareef, "A Novel PQM Placement Method Using Cp and Rp Statistical Indices for Power Transmission and Distribution Networks," in *IEEE International Power Engineering and Optimization Conference (PEOCO)*, Malaka, Malaysia, 2012.

[60] A. Kazemi, A. Mohamed and H. Shareef, "An Improved Power Quality Monitor Placement Method Using MVR Model and Combine Cp and Rp Statistical Indices," *Journal of Electrical Review,* vol. 88, pp. 205-209, 2012.

[61] Y. Hong and Y. Chen, "Placement of power quality monitors using enhanced genetic algorithm and wavelet transform," *IET Generation, Transmission & Distribution,* vol. 5, no. 4, p. 461–466, 2011.

[62] C. Almeida and N. Kagan, "Harmonic State Estimation Through Optimal Monitoring Systems," *IEEE Transactions on Smart Grids,* vol. 4, no. 1, pp. 467-478, 2013.

[63] A. Kumar, B. Das and J. Sharma, "Genetic Algorithm-Based Meter Placement for Static Estimation of Harmonic Sources," *IEEE Transactions on Power Delivery,* vol. 20, no. 2, pp. 1088-1096, 2005.

[64] C. Madtharad, S. Premrudeepreechacharn, N. Watson and R. Saeng-Udom, "An Optimal Measurement Placement Method for Power System Harmonic State Estimation," *IEEE Transactions on Power Delivery,* vol. 20, no. 2, pp. 1514-1521, 2005.

[65] M. Music, A. Bosovic, N. Hasanspahic, S. Avdakovic and E. Becirovic, "Integrated power quality monitoring systems in smart distribution grids," in *Conference Proceedings IEEE International Energy Conference and Exhibition (ENERGYCON),* Florence, 2012.

[66] M. Music, A. Bosovic, N. Hasanspahic, S. Avdakovic and E. Becirovic, "Integrated power quality monitoring system and the benefits of integrating smart meters," in *Conference Proceedings 8th International Conference on Compatibility and Power Electronics (CPE),* Ljubljana, 2013.

[67] M. Music, A. Bosovic, N. Hasanspahic, D. Aganovic and S. Avdakovic, "Upgrading smart meters as key components of Integated Power Quality Monitoring System," in *2016 IEEE 16th International Conference on Environment and Electrical Engineering (EEEIC)*, Florence, 2016.

[68] "SIMEAS Q80 Power Quality Recorded, Energy automation, SR 10.2.1 2009," Siemens, 2009.

[69] "Encore Series 61STD DataNode®, Power Quality, Demand & Energy Monitoring," Dranetz.

[70] "ION7550 / ION7650 Functions and characteristics," Schneider Electric, 2013.

[71] "Iskraemeco mx38y – Technical description v1.00," Iskraemeco, 2011.

[72] "Iskraemeco MT830 - MT831 - Technical description, V1.7," Iskraemeco, 2013.

[73] Siemens, "Phasor Measurement Unit (PMU) - Features & functions," Siemens, [Online]. Available: https://new.siemens.com/global/en/products/energy/energy-automation-and-smart-grid/protection-relays-and-control/general-protection/phasor-measurement-unit-pmu.html. [Accessed 10 6 2021].

[74] CIGRE/CIRED JWG C4.112, "Guidelines for Power Quality Monitoring – Measurement locations, processing and presentation of data," CIGRE/CIRED, 2014.

[75] "IEC 61000-4-7: Electromagnetic compatibility (EMC) – part 4–7: testing and measurement techniques – general guide on harmonics and interharmonics measurements and instrumentation, for power supply systems and equipment connected thereto," IEC, 2002.

[76] G. Funk and T. Hantel, "Frequenzabhängigkeit der betriebsmittel von drehstromnetzen," *EtzArchiv Bd., 9, H. 11,* p. 349–35, 1987.

[77] H. Renner, Beitrag zur Problematik der Oberschwingungsimpedanz- und Oberschwingungsemissionsermittlung in elektrischen Energieversorgungsnetzen, PhD thesis, Graz University of Technology, 1994.

[78] J. Meyer, R. Stiegler, P. Schegner, I. Roder and A. Belger, "Harmonic resonances in residential low-voltage networks caused by consumer electronics," *CIRED – Open Access Proceedings Journal*, p. 672–676, 2017.

[79] DIgSILENT GmbH, "DIgSILENT PowerFactory 2018 user manual," DIgSILENT GmbH, 2018.

[80] "IEC 61000-3-6: Electromagnetic compatibility (EMC) – part 3–6: limits – assessment of emission limits for the connection of distorting installations to MV, HV and EHV power systems," IEC, 2008.

[81] R. Stiegler, J. Meyer, M. Elst, E. Sperling and K. M., "Accuracy of harmonic voltage measurements in the frequency range up to 5 kHz using conventional instrument transformers," in *21st International Conference on Electricity Distribution (CIRED 2011)*, Frankfurt am Main, Germany, 2011.

[82] "APCS power clearing and settlement AG - synthetic load profiles for 2014," [Online]. Available: https://www.apcs.at/en/clearing/physical-clearing/synthetic-loadprofiles. [Accessed 2015].

[83] J. Meyer, A. M. Blanco, M. Domagk and P. Schegner, "Assessment of prevailing harmonic current emission in public low voltage networks," *IEEE Transactions on Power Delivery*, vol. 32, no. 2, p. 962–970, 2017.

[84] S. Hanssen, Harmonic Distortion of Rectifier Topologies for Adjustable Speed Drives, PhD thesis, Aalborg University, 2000.

[85] S. Hanssen, P. Nielsen and F. Blaabjerg, "Harmonic cancellation by mixing nonlinear single-phase and three-phase loads," *IEEE Transactions on Industrial Applications,* vol. 36, no. 1, p. 152–159, 2000.

[86] U.S. Department of Energy, "United States industrial electric motor systems market opportunities assessment," U.S. Department of Energy, Office of Energy Efficiency and Renewable Energy, Washington, DC, USA, 1998.

[87] ABB, "ABB review motors and drives," ABB Ltd,, 2004.

[88] DIgSILENT GmbH, "DIgSILENT PowerFactory 2018 technical reference documentation – general load," DIgSILENT GmbH, 2017.

[89] DIgSILENT GmbH, "DIgSILENT PowerFactory advanced tutorial – DIgSILENT programming language (DPL)," DIgSILENT GmbH, 2017.

[90] "IEC 60909-0: Short-circuit currents in three-phase a.c. systems - Part 0: Calculation of currents," IEC, 2016.

[91] H. Renner and M. Sekulin, "Flicker propagation in meshed high voltage network," in *Proceedings of 9th International Conference on Harmonics and Quality of Power*, Orlando, 2000.

[92] H. Renner, "Voltage Unbalance Emission Assessment," in *2013 IEEE Power & Energy Society General Meeting*, Vancouver, Canada, 2013.

[93] "Electromagnetic compatibility (EMC) – Part 3-13: Limits – Assessment of emission limits for the connection of unbalanced installations to MV, HV and EHV power systems," IEC, 2008.

[94] A. Kazemi, A. Mohamed, H. Shareef and H. Raihi, "Accurate voltage sag-source location technique for power systems using GACp and multivariable regression methods," *Electrical Power and Energy Systems*, vol. 56, p. 97–109, 2014.

[95] H. Renner and M. Sakulin, Power Quality (scriptum), Graz: Graz University of Technology.